1-1-2019

Side-to-Side Comparison of Total Shoulder Arthroplasty and Intact Function in Individuals

Sarah Rose Walden
University of Denver

Side-to-Side Comparison of Total Shoulder Arthroplasty and Intact Function in Individuals

Abstract

Total Shoulder Arthroplasty (TSA) is a surgery which replaces the shoulder joint, or the interface between the humerus and the scapula glenoid. To test TSA success, most prior research compares patients with TSA to healthy controls. However, the shoulder anthropometry, motion, and musculature of individuals varies widely across the population making it important to assess TSA performance in individuals. The overall goal of this study is to determine if patients with one of two TSA implant designs on one side achieve the same range of motion as their intact side, and if so to find if they compensate using increased scapula rotation over normal humeral motion. Six TSA subjects performed for each shoulder abduction, forward flexion, and internal/external (I/E) humerus rotation with their arm abducted to 0° and 90°, captured as x-ray videos with a Radiography System. Glenohumeral and scapulothoracic kinematics were calculated. Results show that TSA shoulder trends for abduction and flexion lie within the range of healthy standard deviation for both glenohumeral and scapulothoracic elevation. No substantial differences were observed between TSA and healthy shoulders' overall motion but that the scapula exhibits some compensation in elevation for TSA shoulders, especially in flexion. I/E implanted shoulder results additionally show a deficit compared to intact shoulders, with scapula retraction compensation presenting more strongly with the arm abducted to 0° than at 90°.

Document Type

Thesis

Degree Name

M.S.

Department

Mechanical Engineering

First Advisor

Kevin B. Shelburne, Ph.D.

Second Advisor

Peter Laz, Ph.D.

Third Advisor

Bradley Davidson, Ph.D.

Keywords

Anatomic total shoulder arthroplasty, Biplane radiography, Individuals, Kinematics, Reverse total shoulder arthroplasty

Subject Categories

Biomechanical Engineering | Engineering | Mechanical Engineering

Side-to-Side Comparison of Total Shoulder Arthroplasty and

Intact Function in Individuals

A Thesis

Presented to

the Faculty of the Daniel Felix Ritchie School of Engineering and Computer Science

University of Denver

In Partial Fulfillment

of the Requirements for the Degree

Master of Science

by

Sarah Walden

August 2019

Advisor: Dr. Kevin Shelburne

Author: Sarah Walden
Title: Side-to-Side Comparison of Total Shoulder Arthroplasty and Intact Function in Individuals
Advisor: Dr. Kevin Shelburne
Degree Date: August 2019

Abstract

Total Shoulder Arthroplasty (TSA) is a surgery which replaces the shoulder joint, or the interface between the humerus and the scapula glenoid. To test TSA success, most prior research compares patients with TSA to healthy controls. However, the shoulder anthropometry, motion, and musculature of individuals varies widely across the population making it important to assess TSA performance in individuals. The overall goal of this study is to determine if patients with one of two TSA implant designs on one side achieve the same range of motion as their intact side, and if so to find if they compensate using increased scapula rotation over normal humeral motion. Six TSA subjects performed for each shoulder abduction, forward flexion, and internal/external (I/E) humerus rotation with their arm abducted to 0° and 90°, captured as x-ray videos with a Radiography System. Glenohumeral and scapulothoracic kinematics were calculated. Results show that TSA shoulder trends for abduction and flexion lie within the range of healthy standard deviation for both glenohumeral and scapulothoracic elevation. No substantial differences were observed between TSA and healthy shoulders' overall motion but that the scapula exhibits some compensation in elevation for TSA shoulders, especially in flexion. I/E implanted shoulder results additionally show a deficit compared to intact shoulders, with scapula retraction compensation presenting more strongly with the arm abducted to 0° than at 90°.

Acknowledgements

I would like to thank everyone who made completing this thesis and overall endeavor possible and a success. My advisor Dr. Kevin Shelburne is at the top of the list for his teaching and mentorship. My thanks to Drs. Laz and Davidson for not only participating on my defense committee but for all I've learned from them in their courses over the last few years. I'd like to extend my gratitude to Drs. Hume and Meyers as well as to Vasiliki Kefala for their discussions with me over many kinematics questions during this process. For my family, friends, and fellow DU students thank you for the support you are always ready to give. Thank you to the University of Denver Department of Orthopaedic Biomechanics for support and the Knoebel Institute for Healthy Aging for funding this work.

Table of Contents

List of Figures

Chapter 1 Introduction

1.1 Introduction

Knee and hip replacement surgeries are both common practice (~900,000+ surgeries in the knee and hip each year [1]), and have become relatively routine; in comparison, shoulder replacement surgery is performed less frequently (~50,000 surgeries [1]) even though injury of the knee, hip, and shoulder are equally common [1]. There is still information to be learned about joint replacement surgery overall and specifically how Total Shoulder Arthroplasty (TSA) restores or limits patient’s motion post-surgery and how to best facilitate rehabilitation in TSA patients. Common practice is to study TSA in comparison to separate healthy cohorts but there are advantageous comparisons to be made between an individual’s implanted and healthy shoulder. The overall goal of this study is to determine if patients with one of two TSA implant designs on one side achieve the same range of motion as their intact side, and if so do they compensate using increased scapula over normal humeral motion?

Solutions to injuries, including rotator cuff tears, osteoarthritis, and acute fracture, that lead to TSA are in high demand, but shoulder joint reconstruction poses a challenge of complexity. The joint depends on the interaction between the humerus, scapula, clavicle, and thorax. Stability of the ball and socket joint is dependent on soft tissue much more than bone geometry. Most TSA patients' soft tissue and bone are degraded to a degree. Various stages of bone and soft tissue degradation as well as unique shoulder anthropometry, motion, and musculature in individuals makes variability high and therefore studying and comparing range of motion to the contralateral control crucial.

Two TSA common designs exist: 1) anatomic total shoulder arthroplasty (ATSA) and 2) reverse total shoulder arthroplasty (RTSA). ATSA implant designs mimic human anatomy where the scapula and glenoid act as a socket to the ball of the humerus. RTSA has emerged as an alternative option, mostly commonly for patients with significant rotator cuff tears, where the glenoid implant acts as the ball to the reconstructed humeral socket. Among other impacts, this design changes the center of glenohumeral rotation and muscle lines of action. Learning more about differences between the effect of each design on post-surgery range of motion, kinematics, and patient function could offer way to improve treating shoulder pathology and improve specific rehabilitation for each design type.

Total Shoulder Arthroplasty restores mobility and relieves pain in patients suffering from shoulder pathology, but more can be learned on its impact on restoring healthy range of motion. This study aims to quantify side-to-side shoulder function by presenting in-vivo kinematics data with patients implanted with either ATSA or RTSA performing four motions: abduction, forward flexion, I/E with the arm at the side, and I/E with the arm abducted to 90°.

1.2 Objectives

The research objectives of this thesis are to:

1) Determine if TSA restores individual's intact arm elevation and internal/external rotation in six patients each with an intact and an implanted shoulder.

2) Determine if implanted shoulders in an individual utilize compensation from increased scapulothoracic rotation to achieve maximum arm elevation and internal/external rotation.

3) Determine differences in arm elevation and internal/external rotation range of motion and differences in scapulothoracic compensation between ATSA and RTSA implanted shoulders within a sample of three ATSA and three RTSA patients.

4) Determine if comparing side-to-side differences in individuals better reveal how TSA changes normal function?

Chapter 2 Literature Review and Background

2.1 Introduction

A large breadth of both engineering and medical anatomy knowledge is required to conduct such a study into TSA surgery and so this literature review will outline both. A description is provided of shoulder anatomy and TSA design, existing methods for bone tracking are outlined, with their respective advantages and disadvantages, and existing literature on joint tracking and glenohumeral kinematics is reviewed to be clear where this study fits in with the whole.

2.2 Shoulder Anatomy

The shoulder is a complex series of interactions of bone, muscle, ligament, and tendon. The first step in understanding TSA surgery requires familiarity with shoulder anatomy. The three primary shoulder bones are the *scapula*, the shoulder blade, the *humerus*, the upper arm bone, and *clavicle*, the bony protrusion at the top anterior portion of the shoulder (*Figure 2-1*). Note that the glenoid is the distal portion of the scapula that forms the socket of that bone, in which the humerus rests. These are connected by four joints: of primary interest is the *glenohumeral joint*, which is the interaction between the ball of the humerus and the socket of the scapula; the interaction between the clavicle and the top curve of the scapula is named the *acromioclavicular (AC) joint*; next, the *sternoclavicular (SC) joint* connects the shoulder bones to the skeletal torso; and finally, the *scapulothoracic joint* has a similar function in that it controls alignment between the scapula and the rib cage. *Figure 2-2* shows a diagram of these joints.

Shoulder stabilization comes largely from muscle and therefore it is important to consider those muscles that span the joint. The rotator cuff tendons and muscles surround the glenohumeral joint and help raise and rotate the arm. See *Figure 2-3* for a posterior diagram of shoulder muscles and *Figure 2-4* for an anterior view. The anterior, middle, and posterior deltoid muscles are the primary lifters during arm elevation. Careful attachment of the deltoid muscle in TSA surgery can change the moment arm of humerus bone rotation about the glenohumeral joint, and therefore change the torque or strength possible in a patient's shoulder, which has great effect on the success of the surgery.

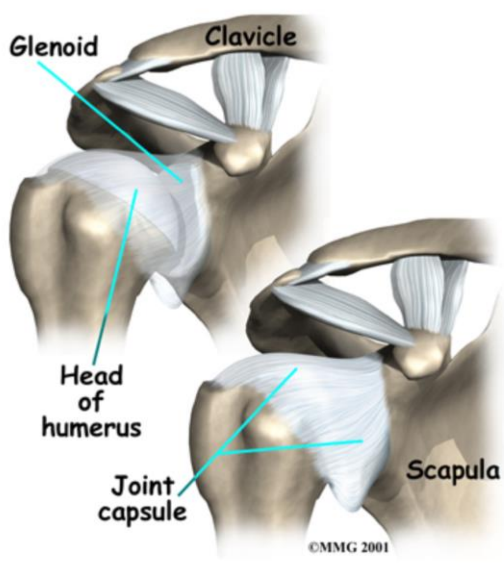

Figure 2-1 Shoulder Bone and Ligament Anatomy [6]

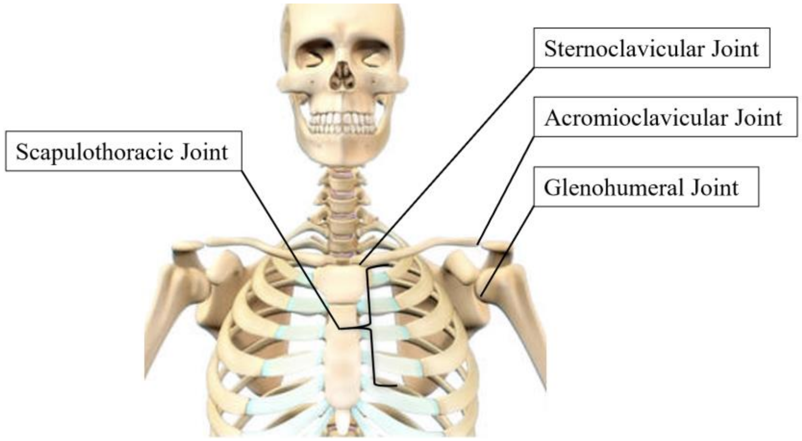

Figure 2-2 Glenohumeral Joints [2]

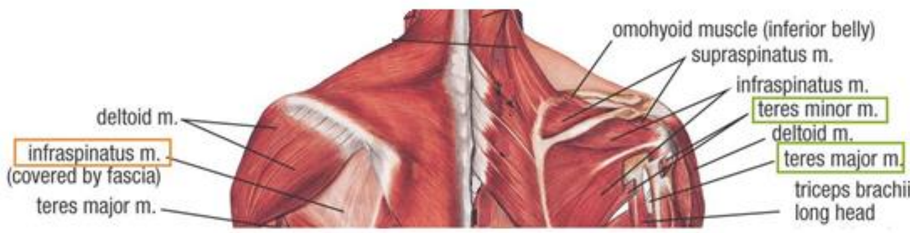

Figure 2-3 Posterior View of the Shoulder Muscles [3]

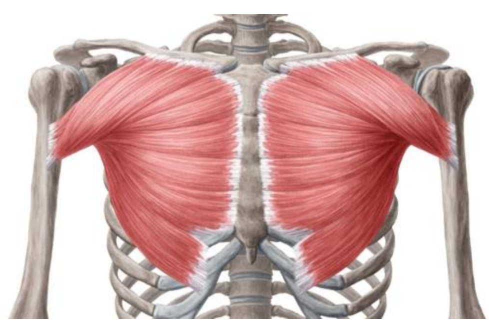

Figure 2-4 Anterior View of Pectoral Muscles [4]

2.3 TSA Surgery Background

2.3.1 Overview

TSA is a surgery for shoulder pathology (*Figure 2-5*) and is particularly common with the elderly with osteoarthritis, rotator cuff tears, or humeral head fracture. TSA replaces the glenohumeral joint with metal alloy and variations of polyethylene and has a 90% success rate [1]. In general, design solutions for TSA fall into two categories: 1) Anatomic Total Shoulder Arthroplasty (ATSA), which mimics original anatomy and 2) Reverse Total Shoulder Arthroplasty (RTSA), which reverses original anatomy so that the scapula glenoid becomes the ball and the humerus becomes the socket of the joint (*Figure 2-6*).

Reversing normal shoulder anatomy through RTSA was approved in 2004 in the United States. RTSA was introduced as a beneficial surgery over ATSA for cases with severe rotator cuff deficiency or significant bone loss at the interface between the glenoid and the humeral head. Roberts et al. describes the advantages of this surgery: that the patient's glenohumeral joint center of rotation is moved "distally and medially", which allows for more motion control. In this position, the deltoid muscles have more leverage over humerus bone motion, giving patients a larger range of motion and less pain [5].

The differences in patient results between standard total shoulder arthroplasty and reverse total shoulder arthroplasty are of interest. Variables that effect patient results include variation in patient-specific joint anatomy, the large degree of glenohumeral joint freedom, the fact that the joint is stabilized primarily through muscle rather than bone, and the complex biomechanics of the joint where multiple joints are considered besides the glenohumeral joint. This complexity requires in depth study of the differences between anatomic and reverse TSA designs.

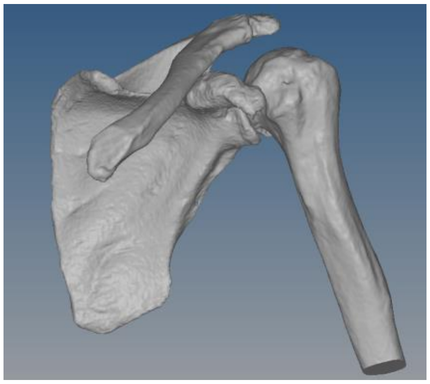

Figure 2-5 Natural Glenohumeral Joint Model

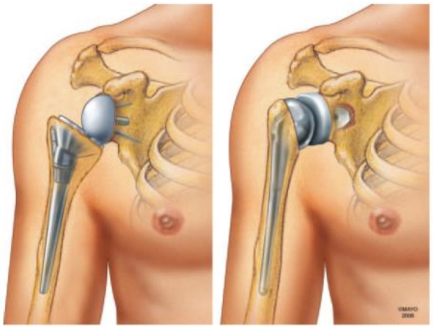

Figure 2-6 Reverse TSA (left) and Anatomic TSA (right) [5]

2.3.2 Indications for Shoulder Arthroplasty

Causes to perform TSA are varied. Most forms of arthritis can necessitate TSA. Osteoarthritis, where bone cartilage wears down, is common form of arthritis where patients experience pain and decreased range of motion, particularly "trouble performing overhead activities" [6]. Rotator cuff arthropathy is a condition which exhibits rotator cuff degeneration, superior migration of the humeral head, and arthritis.

Other pathologies which commonly lead to TSA are inflammatory arthritides and acute trauma, for example, humeral head fracture.

2.3.3 Development & History of Shoulder Arthroplasty

The first shoulder orthopaedic surgery in 1995 by Charles S Neer replaced only "articular surface" of the humeral head "with little disturbance to the anatomy of the tuberosities and their muscular attachments" [6]. Testing was performed on twelve patients, where eleven reported no pain in post-surgery checkups. The second-generation model was the first unconstrained shoulder system, which is one of the most common modern concepts. Neer also fabricated the first reverse ball-and-socket shoulder system, which is the other most common modern design. Failures did occur with these models and later designs, mostly through component loosening.

The Delta 3 reverse shoulder model was developed in 1985 and tested on fifty-eight patients with rotator cuff tear injuries. Out of these fifty-eight patients, twenty-one complications occurred; causes included hematomas, dislocations, glenoid loosening, humeral stem loosening, and one dislocation of the polyethylene layer [6].

Three main philosophies on shoulder arthroplasty design developed: *unconstrained*, *semi-constrained*, and *constrained*. These three philosophies outline the tradeoff between prioritizing stability (constrained) or range of motion (unconstrained). The glenohumeral joint is primarily stabilized through soft tissue. Therefore, natural shoulder anatomy relies on soft tissue stabilization and offers a large range of motion. Replacing the glenohumeral joint with a similar unconstrained style of implant, where there is degenerated soft tissue and bone, is difficult because of potential dislocation failure. Choosing a constrained replacement might avoid failure through dislocation but can lead to a decrease in joint mobility.

TSA design problems have become more solvable as technology improved. Unconstrained ATSA has become the standard arthroplasty option. The best results eliminate patient pain and restores range of motion to the glenohumeral joint. The overall design of TSA has not drastically changed since the Neer designs but features such as materials and material layering have improved. The reverse ball-and-socket design has developed for use when a patient has severe rotator cuff deficiency or significant bone loss at the glenohumeral interface.

2.3.4 The Value of RTSA

RTSA has developed alongside TSA for when TSA is no longer a dependable solution for specific patient conditions. These conditions are summarized in ‘Shoulder Arthroplasty’ by Fealy et al. [6]:

- Rotator cuff tear arthropathy
- Osteoarthritis associated with massive cuff tear
- Massive, irreparable cuff tear with chronic pseudo-paralytic shoulder
- Failed, painful rotator cuff repair
- Static shoulder instability with severe glenoid erosion
- Chronic fixed dislocations
- Rheumatoid arthritis with rotator cuff tear

- Acute fracture in an older patient
- Tumor reconstruction

RTSA is most often indicated for severe rotator cuff deficiency or significant humeral and/or glenoid bone loss. “In rotator cuff-deficient shoulders,” Fealy et al. states, “the forces that normally counteract the upward force of the deltoid and stabilize the center of rotation of the shoulder are lost.” In this case RTSA is a more reliable solution. RTSA is more specifically reported as successful when the following conditions occur: “(1) the rotator cuff-deficient shoulder in paralytic shoulder with arthritis… (2) the scarred proximal humerus fracture sequelae (FS) with severe tuberosity malunion or non-union… (3) the rotator cuff-deficient shoulder in which a previous unconstrained arthroplasty has failed” [6].

2.3.5 Common Causes of Revision of Shoulder Arthroplasty

Shoulder arthroplasty requires the study and understanding of its post-surgery complications for improvement. The primary of these long-term failures has been found to be glenoid loosening, or instability [6]. In general, instability is the most common failure mode for this surgery, primarily due to the unconstrained design of the reconstruction. An instability review cited in Fealy et al. found that 5.2% of 1496 surveyed TSA patients experienced instability post-surgery.

Instability is categorized by location of that instability. Inferior instability is usually caused by failure to restore humeral length when treating humeral fracture [6]. Superior instability occurs with a deficient rotator cuff or coracoacromial arch (often muscle tear problems). Anterior and posterior instabilities are not well reported but often are the cause of incorrect glenoid component placement or are a combination of implant mispositioning and soft tissue damage [6]. Finally, incorrect humeral component placement can cause instability in any of the mentioned directions.

Soft tissues complications post-TSA surgery are the topic of many studies. Soft tissue complications include: rotator cuff tears, impingement syndromes, and lesions of the long head of the biceps tendon (LHB) [6]. These damages have serious impact on patient pain and range of motion post-surgery, but most authors recommend early repair of all soft tissue damage post-surgery to avoid this failure. TSA is still the best and most cost-effective solution for treating patients with osteoarthritis or other shoulder pathologies.

2.3.6 Compensation in TSA Shoulders and in Common Pathologies

Scapula compensation is a documented pattern of increased scapula rotation where there is impinged glenohumeral rotation. In elevation motions compensation can be visualized as an additional upward shoulder shrug to increase elevation. Baumgarten et al. defines compensation as “scapular substitution” and in a data review of participants who have had rotator cuff surgery found significant substitution during abduction and flexion [7]. Fayad et al. found an increase in osteoarthritis shoulders’ scapulothoracic compensation in the form of elevation during abduction and flexion compared to the intact side [8]. This pattern of compensation has also been found in TSA shoulders.

Walker et al. in 2015 found RTSA shoulders to have an increase in scapulothoracic elevation compared to glenohumeral elevation, and that the compensation occurs most clearly near the end of the motion [9].

Compensation also has been documented during external rotation in shoulder pathology and TSA [7]. The deficit between injured or TSA and intact shoulders during internal/external (I/E) rotation is commonly reported as larger than in elevation motions. Glenohumeral Internal Rotation Deficit is a similar shoulder injury that explains this deficit, which is the limitation of internal rotation common in baseball pitchers, where damage is done to the rotator cuff [10]. Rotator cuff tears or arthropathy are common injuries that lead to TSA surgery and therefore TSA patients show a deficit in I/E rotation. Compensation occurs in external rotation rather than internal rotation due to physical bounds of the joint.

2.4 Methods for Measuring Motion of Shoulder Bones

Measurement of shoulder bone motion is important because it allows for study of range of motion and comparison between motion of different shoulder types. For example, range of motion can be compared between anatomic and reverse TSA shoulders. There are several well established methods for collecting human motion data, with the intent of recreating the 3D positions and relationships of bones. Each has advantages and disadvantages most importantly related to either precision in tracking and patient comfort and safety.

These pros and cons will be discussed in the following section and how they eventually effected the final decision for which method to use for this study.

2.4.1 Motion Capture

Marker-based motion capture systems are common because of their ease of use and human safety. This passive-optical system functions by 3D positioning small reflective makers using multiple calibrated infrared cameras. The markers are easily affixed with adhesive and placed on boney landmarks; this method has no safety concerns. The location of these landmarks in 3D space allows the subject's motion to be virtually recreated for kinematics analysis. The disadvantage to this system is that the markers are placed on the subject's skin which decreases precision compared to tracking actual bone. For example, using skin-level landmarks to track the scapula is difficult using motion capture because a large portion of the bone is moves beneath overlying tissue. Karduna et al. performed a validation with eight healthy participants of a skin-level magnetic scapula tracker compared to the highly accurate bone pin method and found root mean square errors ranging between 1.1° - 10° [11]. In comparison, tracking the knee joint is more accurate useful landmarks are more easily accessible. Beniot et al. completed a knee kinematics study with eight subjects comparing the precision of motion capture against the highly accurate bone pin method. Rotational error was found to be between 4.4° and 13.1° for the walking and cut motions completed in the study, respectively, and 13.0 mm and 16.1 mm translational error [12].

2.4.2 Bone Pins

Bone pins are the “gold standard” of bone tracking. To use this method, a subject will have “surgically implanted intra-cortical bone-pins” [12] inserted into relevant landmarks in a bone before data collection, and then removed after testing. Radiography images of the bone where the bone pins are used can establish the relationship between the bones, pins, and markers placed on the pins. The disadvantage to this method is the invasiveness and discomfort to the subject in having them undergo a surgical procedure.

2.4.3 Biplane Radiography

Biplane radiography is a method where two x-ray systems are used to collect images at different angles at a subject’s joint of interest. CT or MR scans are collected to create 3D bone models that are matched to both 2D x-ray images to recreate the 3D motion of those real bones in space. This is a more accurate method of bone tracking than motion capture: Mozingo et al. found errors of 0.22-0.32 mm (translational) and 0.12-0.45 ° (rotational) for dynamic glenohumeral motion while comparing biplane radiography to the “gold standard” implanted beads in a cadaver torso [13]. The disadvantage to this method is the computational time to process data; 3D bone models are commonly tracked to the x-ray images manually with some aid from automated interpolation. This makes for a slower computational process than marker-based motion capture. Biplane radiography is still more accurate, which is important when studying the glenohumeral joint where the scapula moves under overlying tissue.

2.5 Rotations of the Shoulder Complex

The most common features for study of shoulder kinematics are crucial to understand when implementing any new research. The ability to compare results, by replicating some basic procedures and calculations, to previous research is essential. This holds true for understanding similar procedures for other joint research, including knee and hip. The following section of this literature review will condense previous joint study in such a way that shows how the procedure of this TSA study was chosen.

2.5.1 Describing Relative Bone Motion

The research standard for describing relative bone kinematics was first described for the knee by the 1983 Grood and Suntay paper, 'A Joint Coordinate System for the Clinical Description of Three-Dimensional Motions: Application to the Knee' [14]. This paper introduced a new way to understand the engineer-minded relative rotation and displacement of local bone coordinate systems so that it could be clinically understandable. It is "three-dimensional joint motion in a way which facilitates the communication between biomechanician and physician" [14]. While Grood and Suntay kinematics are not calculated in this study, their method of forming the transformation matrix between two bones is still applicable.

In the definition from Grood and Suntay et al., each bone is defined by a Cartesian coordinate system, as seen in *Figure 2-7*. Each bone has an origin, three axes (e_i) about which rotations occur and can be broken down to; two of these axes are *body fixed* and the third is the *floating axis* (F) which acts as the common perpendicular axis between the two bodies. The three angular coordinates labeled in *Figure 2-7*, (α, β, γ) are Euler angles, the angels which are used to describe joint kinematics. The vector H which connects the two bodies can be decomposed into medial/lateral, anterior/posterior, and joint distraction/compression translations as seen in *Equation 2-1*.

Equation 2-1 Grood & Suntay et al. Translations [14]

$$
\begin{aligned}
q_1 &= \mathbf{H} \cdot \mathbf{e}_1 \\
q_2 &= \mathbf{H} \cdot \mathbf{e}_2 \\
q_3 &= -\mathbf{H} \cdot \mathbf{e}_3
\end{aligned}
$$

Grood and Suntay then outline how to describe coordinate transformations for any bone motion. Given a body coordinate system position (see *Equation 2-2*), which is comprised of translations and a rotation matrix (*R*) of the femur with respect to the tibia, inverse kinematic calculations are required to determine the angles and positions of the bones relative to each other. *Equation 2-3* shows the rotation matrix *R*, or the direction cosine matrix, from *Equation 2-2* as a series of dot products of the femoral body axes onto the tibial body axes. Flexion, external, and abduction rotations can be extracted.

Equation 2-2 Grood & Suntay et al. Transformation Matrix [14]

$$\mathrm{R} = [B]\mathbf{r}$$

where

$$
[B] = \left[\begin{array}{c|ccc}
1 & 0 & 0 & 0 \\
\hline
(S_1 + S_3 \cos\beta) & & & \\
(S_2 \cos\alpha + S_3 \sin\alpha \sin\beta) & & [R] & \\
(-S_2 \sin\alpha + S_3 \cos\alpha \sin\beta) & & &
\end{array}\right]
$$

Equation 2-3 Grood & Suntay et al. Rotation Matrix [14]

$$[R]^T = \begin{bmatrix} \mathbf{I}\cdot\mathbf{i} & \mathbf{J}\cdot\mathbf{i} & \mathbf{K}\cdot\mathbf{i} \\ \mathbf{I}\cdot\mathbf{j} & \mathbf{J}\cdot\mathbf{j} & \mathbf{K}\cdot\mathbf{j} \\ \mathbf{I}\cdot\mathbf{k} & \mathbf{J}\cdot\mathbf{k} & \mathbf{K}\cdot\mathbf{k} \end{bmatrix}$$

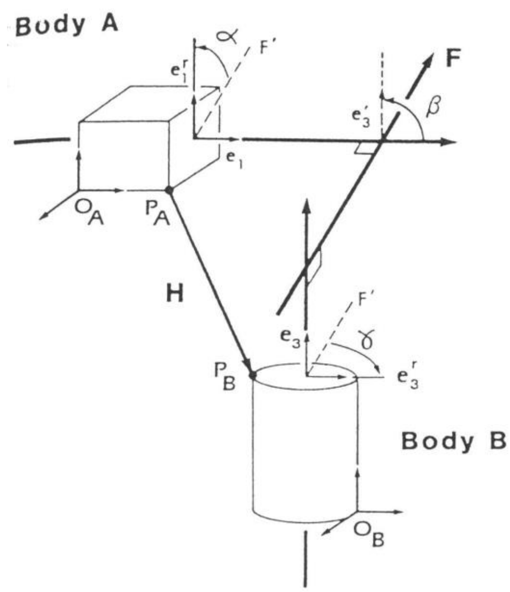

Figure 2-7 Grood & Suntay Coordinate System Definition [14]

2.5.2 ISB Recommended Frames for the Shoulder

The International Society of Biomechanics (ISB) recommendation on definitions of joint coordinate systems of various joints for the reporting of human joint motion – Part 2' by Wu et al. [15] is the standard for defining glenohumeral and scapulothoracic local coordinate systems. The paper follows the coordinate systems approach of Grood and Suntay [14]. For each bone combination, an approach was taken to assign the local coordinate system to each bone and providing a recommended Euler angle sequence. Clinical definitions of flexion and abduction were not used for the shoulder joint as with the knee, because “flexion followed by abduction would give radically different results than abduction followed by flexion” [15]. Therefore, the Euler rotations recommended are Y-X-Y for the glenohumeral joint and Y-X-Z for the scapulothoracic joint.

Figure 2-8 shows images taken from Wu et al. describing bony landmarks used for the assignment of coordinate systems for the thorax, scapula, and humerus in *Figure 2-9, Figure 2-10,* and *Figure 2-11*.

The Euler angle sequence for glenohumeral kinematics suggested by Wu et al. was the following: Y (plane of elevation) – X (arm elevation) – Y (internal/external rotation). See *Figure 2-12 f*or visuals of this Euler sequence. The first angle, plane of elevation, describes the position of the humerus with respect to the scapula relative to the Y axis, discounting axial rotation. The second angle corresponds to humerus elevation with respect to scapula elevation about the X axis. The third angle describes axial humerus rotation with respect to the scapula. For the glenohumeral sequence it is important to include both Y rotations, because of the distinction between axial rotation and plane of elevation. The potential challenge is that the two Y axis rotations can become convoluted with one another, or in other words, the math to decompose the Euler angles does not always separate these two angles when the arm is at the side. When the arm is at the side, the elevation angle is zero or nearly zero, so that the first Y rotation and the third Y rotation are aligned. This may yield a singularity and an infinite number of possible solutions.

The recommended Euler angle sequence for scapulothoracic kinematics was the following: Y (protraction/retraction) – X (elevation/depression) – Z (anterior/posterior tilt). See *Figure 2-16* for visuals of this Euler sequence. The first Euler angle is an internal or external rotation about the local Y axis of the scapula with respect to the local Y axis of the thorax. This rotation is commonly referred to as scapula winging. The second angle is an X axis rotation, which corresponds to scapula elevation with respect to the thorax. The rotation about the Z axis of the scapula with respect to the thorax, which corresponds to anterior or posterior tilting of the scapula.

Final definitions of Euler sequences and coordinate system definitions used in this study can be found in the Methods section of this document. Changes have been made in some cases to better represent the data and shoulder function.

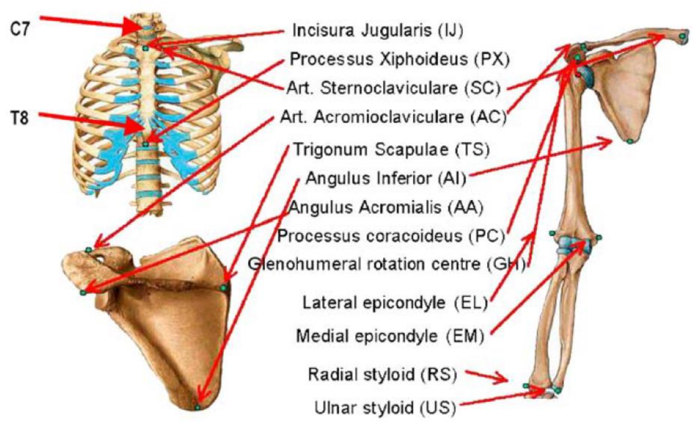

Figure 2-8 Bony Landmarks Used for Coordinate System Definitions Wu et al. [15]

O_t: The origin coincident with IJ.
Y_t: The line connecting the midpoint between PX and T8 and the midpoint between IJ and C7, pointing upward.
Z_t: The line perpendicular to the plane formed by IJ, C7, and the midpoint between PX and T8, pointing to the right.
X_t: The common line perpendicular to the Z_t- and Y_t-axis, pointing forwards.

Figure 2-9 Thorax Coordinate System Wu et al. [15]

O_s: The origin coincident with AA.
Z_s: The line connecting TS and AA, pointing to AA.
X_s: The line perpendicular to the plane formed by AI, AA, and TS, pointing forward. Note that because of the use of AA instead of AC, this plane is not the same as the visual plane of the scapula bone.
Y_s: The common line perpendicular to the X_s- and Z_s-axis, pointing upward.

Figure 2-10 Scapula Coordinate System Wu et al. [15]

O_{h1}: The origin coincident with GH.
Y_{h1}: The line connecting GH and the midpoint of EL and EM, pointing to GH.
X_{h1}: The line perpendicular to the plane formed by EL, EM, and GH, pointing forward.
Z_{h1}: The common line perpendicular to the Y_{h1}- and Z_{h1}-axis, pointing to the right.

Figure 2-11 Humerus Coordinate System Wu et al. [15]

2.6 Prior Measurement of Shoulder Kinematics

Prior measurement of glenohumeral and scapulothoracic kinematics are vital to this literature review because they offer a comparison for the results found in this study. Variation in patient populations, in vivo or in vitro studies, differently assigned local coordinate systems, and other variables do not allow for perfect results comparison but validation of overall excursions and trends. In the next sections, prior measurements of glenohumeral kinematics, scapulothoracic kinematics, and scapulohumeral rhythm will be provided from different sources.

2.6.1 Glenohumeral Kinematics

Prior data on glenohumeral kinematics is commonly decomposed into a Y-X-Y Euler sequence. The first set of kinematics data that will be discussed are scapulohumeral kinematics, which are broken down into a Y-X-Y Euler angle sequence. This sequence is visualized as *Figure 2-12*.

Giphart et al. [16] is a primary source for comparative glenohumeral kinematics for abduction and forward flexion motions; the paper follows standard local coordinate system assignments (*Figure 2-13*). In the study, data was collected from thirteen shoulders from patients who did not have any pathologic shoulder condition. Euler rotations can be found in *Figure 2-14* as reported by Giphart et al. Maximum glenohumeral values are reported to be 100.8º ± 7.9º for abduction and 92.2º ± 10.6º for flexion. Plane of glenohumeral elevation remains slightly posterior to the scapula plane in abduction and flexion; finally, abduction shows an external glenohumeral rotation and flexion shows an internal glenohumeral rotation. Giphart et al. additionally finds that "forward flexion was associated with a greater scapular contribution via upward rotation and relatively less glenohumeral elevation compared with abduction" [16]. This suggests that forward flexion might be a better method for studying abnormality because they are more apparent in this motion.

In 2019 Sahara et al. studied axial glenohumeral rotation by using a Y-Z-X Euler sequence to emphasize the rotation about the Y axis (internal / external rotation) [17]. This method prevents confusion between the two Y axis rotations in the Y-X-Y glenohumeral Euler sequence. The study enrolled fourteen healthy volunteers. Participants held both a maximum external and maximum internal rotation position for arm abduction angles of 0°, 90°, 135°, and maximum possible abduction. *Figure 2-15* shows average Y rotation angles where at 0° abduction an excursion of 113.3° ± 13.9° was recorded and at 90° abduction 119.0° ± 15.2° was recorded.

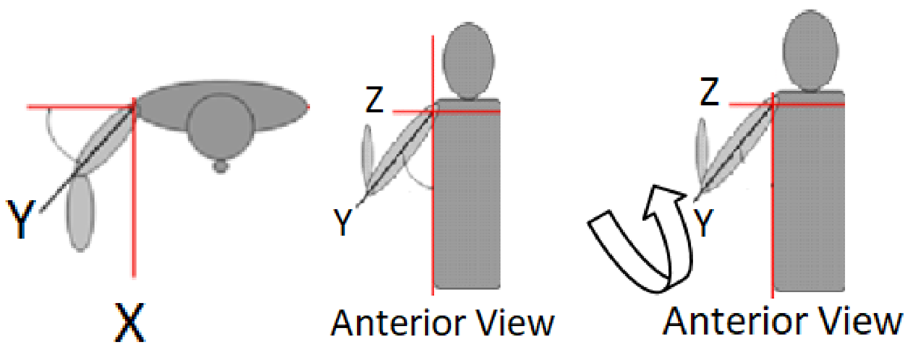

Figure 2-12 YXY Euler Decomposition Rotations: Plane of Elevation (left), Arm Elevation (middle), I/E Rotation (right)

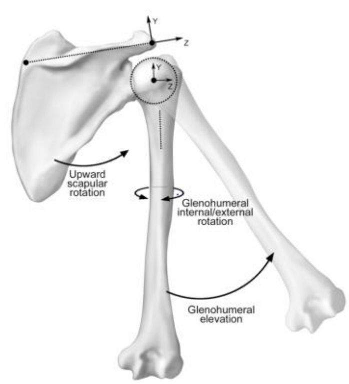

Figure 2-13 Coordinate System from Giphart et al. [16]

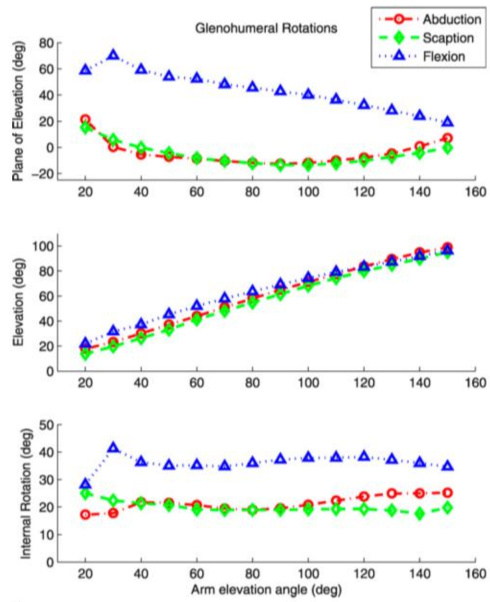

Figure 2-14 Glenohumeral Rotations from Giphart et al. [16]

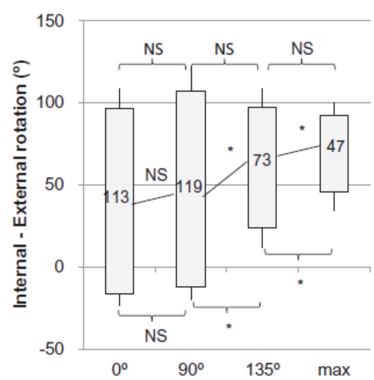

Figure 2-15 Humerus Axial Y Rotations at Various Abduction Angles from Sahara et al. [17]

2.6.2 <u>Scapulothoracic Kinematics</u>

The standard Euler angle sequence for scapulothoracic motion decomposition is Y-X-Z. See *Figure 2-16* for visualization of these three rotations.

Karduna et al. examines differences in scapulothoracic results for different Euler sequences. The study included eight healthy subjects and used a magnetic tracking device to capture motion of the scapula, humerus, and thorax during an arm elevation motion. See the plotted “EUP” (proposed standard) plotted lines in the kinematics results, *Figure 2-17*. Karduna et al. found significant differences in results when the Euler angle sequence was altered for decomposing the three scapula rotations [18].

Seth et al. developed a “rigid-body model of a scapulothoracic joint to describe the kinematics of the scapula relative to the thorax,” which was compared, “to “gold standard” bone-pin kinematics collected during three shoulder tasks” [19]. By comparison to bone-pin kinematics data, Seth et al. found that the model was accurate to within 2mm root-mean-squared error for individual bone-pin markers for all motions performed. The local coordinate systems differed between Seth et al. and this study: their “joint origin is located at the centroid of the anatomic markers used to define the joint frame instead of the Angulus Acromialis,” and the scapula coordinate system axes “are rotated -90° about Y (to enable positive upward rotation about Z)” [19]. The change of the coordinate system axes flips the X and Z axes compared to the current study. See *Figure 2-18* for Seth et al. kinematics for flexion (top) and abduction (bottom). Results found that both flexion and abduction motions were “dominated by the upward rotation of the scapula” reaching a peak of 27° for the flexion task [19], in agreement with Karduna et al. [18] and others.

McClure et al. collected bone-pin data from eight healthy patients who completed three motions: scapular plane elevation, flexion, and internal-to-external rotation with the arm elevated to 90°. The local coordinate systems differ from that in the current study: Z, Y, and X axes correspond to the current study's Y, X, and Z axes, respectively. See *Figure 2-19* for McClure et al. scapulothoracic kinematics. Results find that "During scapular plane elevation of the arm, there was a consistent pattern of scapular upward rotation, posterior tilting, and external rotation…" and that "the results of sagittal plane elevation (flexion)… do not differ substantially from the motions observed during scapular plane elevation" ; for the motion of external/internal humeral rotation, "relatively little scapular rotation occurred except at the end-range of external rotation" [20].

In a series of papers, Banks et al. [21] [22] [23] [24] [9] described scapula kinematics for the healthy and implanted shoulder. Local coordinate systems in these papers switch the X and Z axes compared to the current study, with no Y axis change. Additionally, scapula rotations were reported relative to the starting neutral pose of the scapula, with the origin relocated to the thorax. This avoided the challenge of interpretation of scapula rotations relative to the trunk, which made results more comparable between sitting subjects. This method for scapulothoracic calculations was used in the current study.

In 2011 Matsuki et al. studied the differences between dominant and nondominant shoulder kinematics in twelve healthy males performing elevation in the scapular plane. Scapulothoracic kinematics were calculated with respect to a neutral scapula frame. Results found the mean change in upward rotation, posterior tilt, and external rotation to be 43°, 25°, and 6°, respectively (*Figure 2-20*) [23].

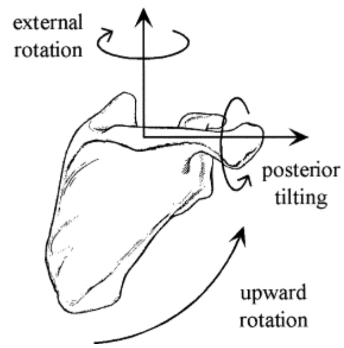

Figure 2-16 Scapulothoracic Euler Decomposition [18]

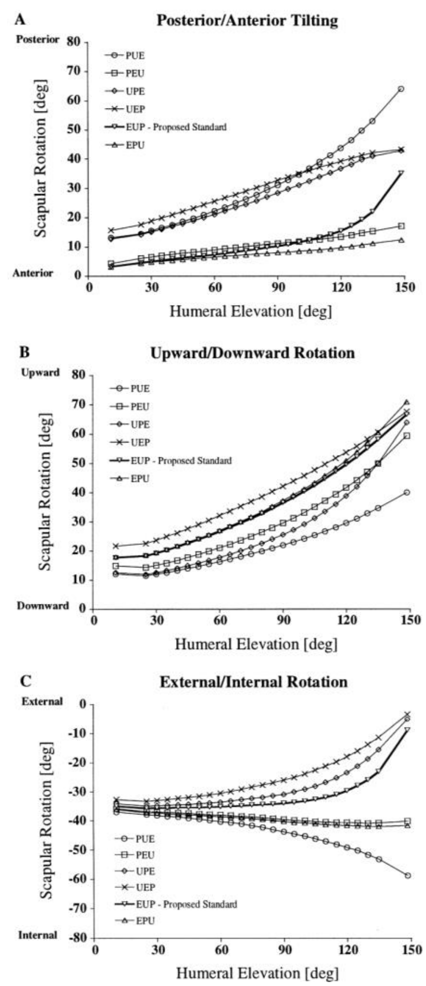

Figure 2-17 Scapulothoracic Kinematics from Karduna et al. [18]

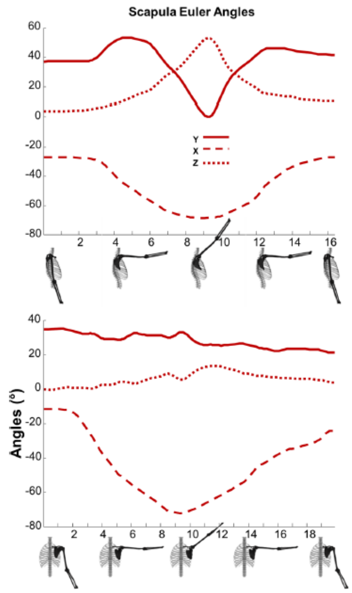

Figure 2-18 Scapulothoracic Kinematics from Seth et al. [19]

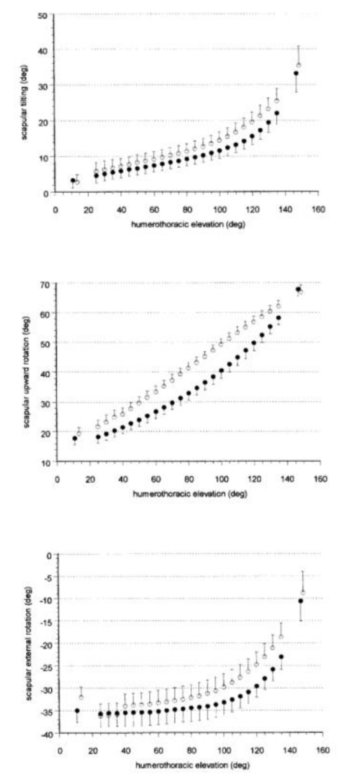

Figure 2-19 Scapulothoracic Kinematics from McClure et al. [20]

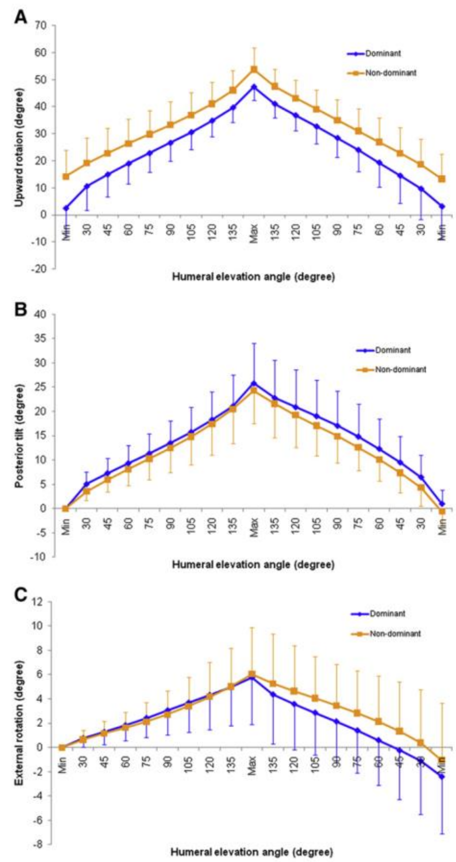

Figure 2-20 Scapula Kinematics Comparing Dominant and Non-Dominant Shoulders from Matsuki et al. [23]

2.6.3 <u>Scapulohumeral Rhythm</u>

A common parameter for quantifying humeral elevation kinematics is scapulohumeral rhythm, which is the ratio of glenohumeral elevation and scapulothoracic elevation and describes the relative contribution of scapula and humeral upward rotation needed to elevate the arm. The higher the ratio, the less the arm elevation motion depends on scapula elevation and vice versa.

Giphart et al. reported scapulohumeral rhythm ratios as 2.0 +/- 0.4:1 for abduction and 1.1 +/- 0.3:1 for forward flexion in healthy subjects [16].

In 2008, Kon et al. published scapulohumeral rhythm results for ten healthy shoulders, with and without handheld weights. *Figure 2-21* shows reported mean ratios of scapulohumeral rhythm at different arm elevation values [22].

In 2015, Walker et al. studied scapulohumeral rhythm in shoulders with RTSA. Twenty-eight subjects performed arm elevation in the coronal plane, repeated while holding weights. The data were compared to healthy, young shoulders from separate subjects. The results found that subjects with RTSA had a scapulohumeral rhythm of 1.3:1 for that motion, compared to a healthy 3:1 ratio. Therefore, it was found that RTSA subjects used more scapula upward rotation than normal shoulders [9].

With eight healthy subjects, Karduna et al. validated scapulothoracic results by calculating scapulohumeral rhythm for comparison to prior measurements. A ratio of 2.0:1 for flexion and 1.7:1 for scapular plane elevation was reported.

Matsuki et al., studying differences between dominant and non-dominant shoulders, found ratios to be 2.6° ± 0.7° for the dominant shoulder and 2.7° ± 0.6° for nondominant. No significant difference between dominant and nondominant shoulders was found.

In summary, these papers report a variety of ratios from 1.7:1 to 3.0:1 for abduction and similar variation for flexion. Giphart et al. notes that “ratios ranging from 1.25:1 to 5.3:1 have been… reported” [16]. While these results captured a wide range, the ratio of 2:1 will be used as a common value for comparison.

GH angle	GH/ST ratio (mean ± SD) 0 kg	3 kg
15°	3.0 ± 4.2	3.7 ± 5.7
25°	2.0 ± 1.8	2.5 ± 2.5
35°	1.4 ± 1.1	5.0 ± 4.4
45°	1.3 ± 0.9	1.9 ± 1.4

Figure 2-21 Kon et al. Scapulohumeral Ratios [22]

2.7 Musculoskeletal Modelling

Combining accurate kinematics with musculoskeletal models of the shoulder enable investigation of how TSA implant geometries effect natural muscle function. - Ackland et al. in the paper "Moment arms of the muscles crossing the anatomical shoulder" provided a detailed description for the moment arms of the "18 major muscle sub-regions of the rotator-cuff, teres major, deltoid, pectoralis major and latissimus dorsi in elevation of the humerus" [25]. A comprehensive study was created of glenohumeral moment arms in a cadaver joint; a comparative study in vivo could give information more relevant to creating better TSA or RTSA implants, perhaps on a patient by patient basis.

Musculoskeletal modeling of TSA subjects could describe which muscles are used and which neglected with the new implant geometries. RTSA especially is of interest because part of the procedure is to relocate the center of rotation of the glenohumeral joint to better employ the deltoid muscles. Walker et al. partially answers this question in the paper "How do deltoid muscle moment arms change after reverse total shoulder arthroplasty?" [24]. A twelve-degree musculoskeletal model was employed to recreate the abduction motion of fourteen RTSA patients, compared to twelve healthy shoulders. Muscle moment arms of the anterior, lateral, and posterior deltoid muscle were calculated. Findings highlighted the importance of the deltoid muscles as a primary lifter for RTSA patients. This suggests the possibility for improving deltoid muscle moment arms through patient-specific surgery. A more medial, inferior, anterior glenohumeral RTSA center of rotation was found to produce a larger moment arm [24]. A more lateral, superior, posterior center of rotation resulted in a smaller muscle moment arm [24]. See *Figure 2-22* for Walker et al. results.

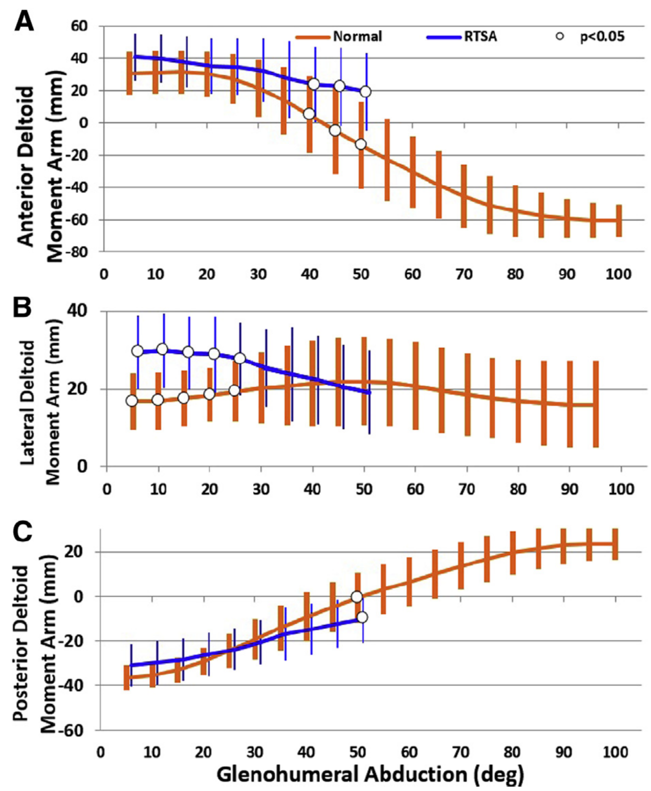

Figure 2-22 Walker et al. Deltoid Muscle Moment Arms for RTSA and Normal Shoulders [24]

2.8 Finite Element Modelling

Biplane radiography data and kinematics for the shoulder have applications in finite element modelling, which can assess contact mechanics and bone strains. Belvedere et al. measured knee arthroplasty joint kinematics during daily living activities and calculated contact mechanics of tibial-femoral articular surfaces using fluoroscopy-driven finite element analysis [26]. The study reported kinematics “not only in terms of standard joint motion along the three anatomical planes, but also in terms of articular surface contacts” [26]. This method applied to shoulder arthroplasty would be equally useful for building a better finite element model of TSA using in vivo fluoroscopy kinematics.

Chapter 3 Methods

3.1 Introduction

The methods of this study involved collecting biplane radiography data for six subjects, each having one reconstructed shoulder, to draw comparisons between subject's intact and implanted shoulders as well as between ATSA and RTSA function. This chapter of the thesis will provide a description of methods for data collection and data processing, which required a complex integration of different systems and software. *Figure 3-1* shows a work flow diagram visually representing this process.

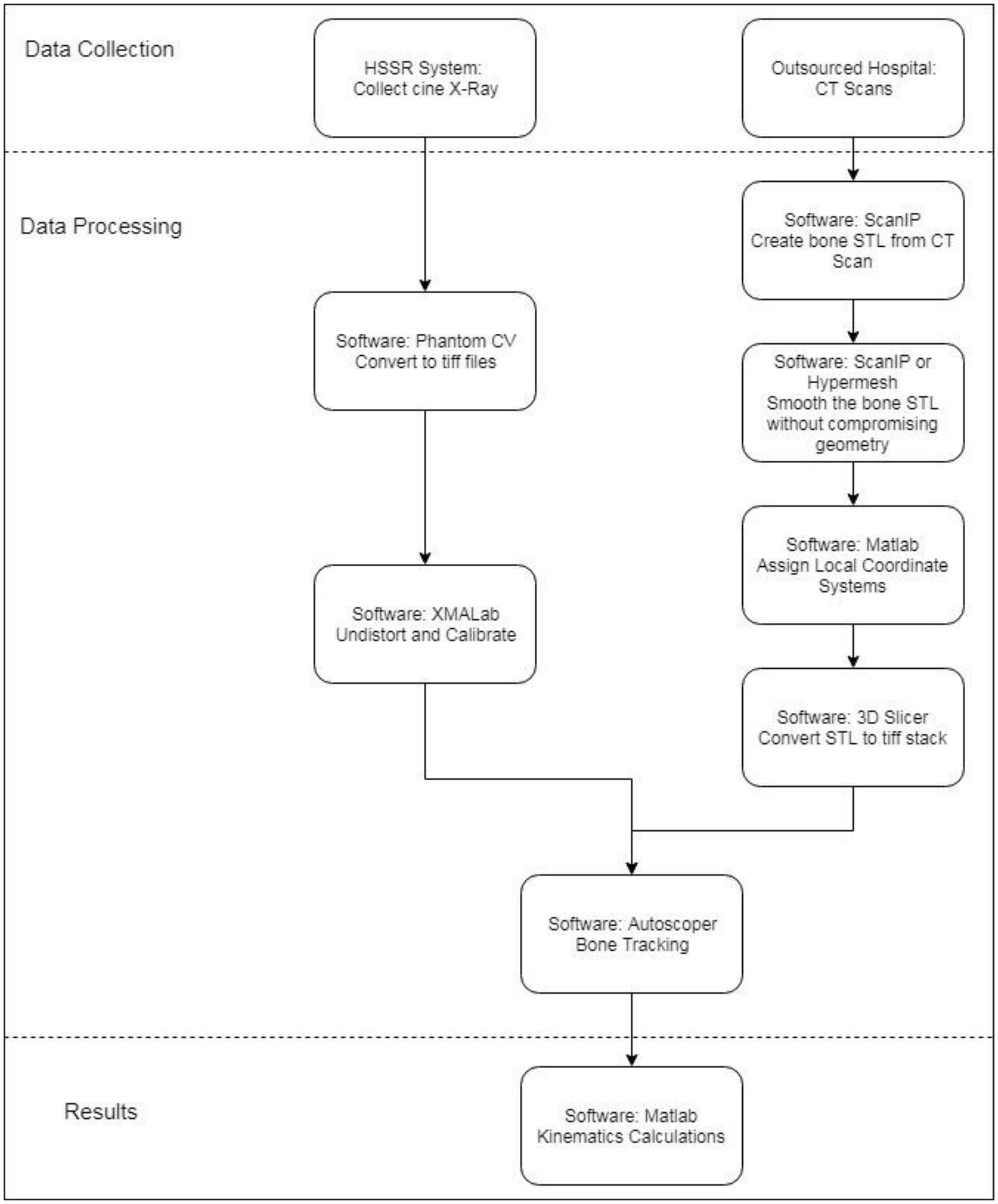

Figure 3-1 Workflow Diagram of Data Collection and Processing

3.2 Data Collection with Human Subjects

Data collection for calculating kinematics at the University of Denver (DU) requires two parts: 1) collecting x-ray videos with the DU High Speed-Stereo Radiography (HSSR) system, or biplane radiography, and 2) obtaining CT scans of the same subject. Both processes will be discussed in the following sections. Subject specifications for the six participants can be found in *Table 3-1* (means ± standard deviations: height = 173.10 ± 8.65 cm, weight = 97.72 ± 15.81 kg, and age = 74.60 ± 5.18 years).

The TSA study consisted of six subjects between the ages of 18 to 85 years of age, each with one ATSA or RTSA shoulder and one healthy shoulder. The study was IRB approved for studying human subjects. Following informed consent, subject data was deidentified. The amount of x-ray the HSSR system emits is 7% of the maximum dose allowed by the Food and Drug Administration per year. Subjects wore a neck shield for added safety. Each collection followed the same test protocol as described in the paragraphs below. A Vicon (Vicon Hauppauge, NY, USA) motion capture system was employed throughout testing to gather data for future comparison to the biplane radiography kinematics.

Each part of the biplane system has three components: The x-ray source, the image intensifier, and a high definition camera which records the images taken by the image intensifier [27]. See *Figure 3-2* for a diagram of the HSSR System setup. Subjects sat in a chair between the two x-ray sources and the two image intensifiers to position first the right shoulder in camera frame (*Figure 3-2)*. The first camera recorded motions from an anterior view and the second camera recorded from a anterior-medial view. Two static images were collected, one neutral relaxed pose with arms at the side and one T-pose with arms abducted 90º. Four dynamic trials were collected, at a frequency of 25 Hz [27]. These motions were repeated for the left shoulder. Dynamic motions performed by the subject were 1) abduction, 2) forward flexion (cross-body), 3) internal/external (I/E) rotation with arm at the side, 4) and I/E rotation with the arm abducted to 90º (see *Figure 3-3*). All trials were collected with the HSSR system set to 85 kilovolts, 80 milliamps, a shutter speed of 1.8 milliseconds [27]. These methods yielded an x-ray video for each trial recorded, for each of the two cameras of the HSSR system. After the HSSR data collection, each subject was then taken to an outsourced medical imaging center to obtain CT scans of each shoulder, in the form of a series of DICOM images.

Calculating bone kinematics requires a high level of accuracy, which biplane radiography achieves. Mozingo et al. reported accuracy of a biplane radiography system for the knee [13]. Kefala et al. in 2015 performed validation tests of the University of Denver biplane fluoroscopy system compared to the ‘gold standard’ bead tracking, as well as implant and bone tracking for the knee with that system [27]. Giphart et al. with a biplane fluoroscopy system performed a validation study for glenohumeral bone tracking by tracking a cadaver performing elevation and comparing to inserted tantalum beads [16]. See *Table 3-2* for a summary of associated error with biplane radiography.

Table 3-1 Subject Specifications

Subjects	Implant Type and Shoulder	Gender	Height (cm)	Weight (kg)	Age (years)
TSA01	Right ATSA	Male	174	91.3	71
TSA02	Right TSA	Male	163	*Not Recorded*	71
TSA03	Right RTSA	Male	177	102.5	73
TSA04	Right RTSA	Female	158	74.8	81
TSA05	Left ATSA	Male	178	102.5	79
TSA06	Left RTSA	Male	179	117.5	69

Table 3-2 Study Errors

	Type of Error	Translation	Rotation
Kefala et al.	Bead Tracking	0.2 ± 0.1 mm (Average)	0.11° ± 0.03°
	Knee Implant Tracking	0.9 ± 0.7 mm (Average)	0.62° ± 0.59°
	Knee Bone Tracking	0.15 ± 0.1 mm (Average)	0.41° ± 0.30°
Giphart et al.	Shoulder Bone Tracking	0.3 ± 0.3 mm (Superior/Inferior)	0.60 ± 0.73° (Average)
Mozingo et al.	Knee Bone Tracking	0.22 mm - 0.32 mm	0.12° - 0.45°

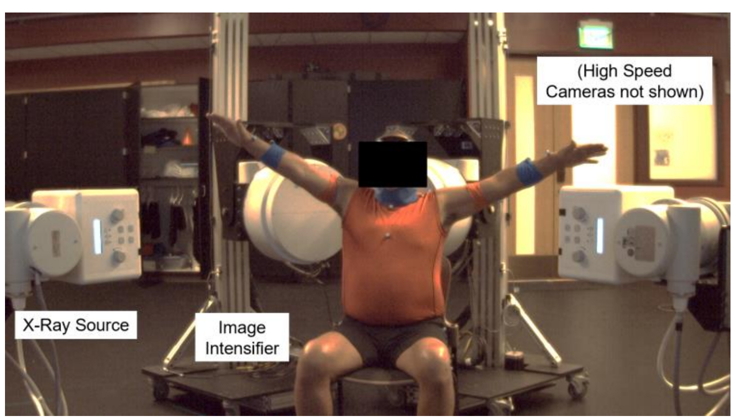

Figure 3-2 DU HSSR System with a Subject Performing an Abduction Motion

Figure 3-3 The Four Dynamic Motions for Study from Left to Right: Abduction, Forward Flexion, I/E with Arm at Side, and I/E with Arm Abducted 90°

3.3 Data Processing

The following sections describe the methods for obtaining kinematics data.

3.3.1 Image Processing

- Convert:

First x-ray images were converted from .cine files to .tiff, or a ‘tiff stack’, which breaks the trial into a series of single frames using Phantom Cine Viewer (Phantom Camera Control software, Phantom, NJ, USA).

- Undistort:

During HSSR system data collection, un-distortion images were obtained by hanging a panel with a grid pattern of circles over the front of the image intensifier. The known diameter of each circle can be used to undistort the curvature of the camera lens. XMALab (XROMM XMALab software, Brown University, Providence, RI, USA) performs the undistortion automatically once given the undistortion images.

- Calibrate:

Calibration images were obtained for each data collection. Images of a radio-translucent calibration cube were used to orient the placement of the two image frames in 3D space. The cube has three levels embedded with a total of fifty-two tantalum beads, whose spacing relative to one another is known to establish position in 3D space. For image processing in XMALab (XROMM XMALab, Brown University, Providence, RI, USA) the user selected four predetermined beads on the cube in both frames so that the location of the other forty-eight beads were automatically located, with an associated error. Any beads with an outlier error were deleted and improved the overall 3D positioning. Calibration data in the form of a CSV file was exported for use in bone motion measurement. All collected trial images were imported into XMALab and undistorted for bone motion measurement.

3.3.2 STL Generation

The following section describes the process for obtaining bone and implant geometries from CT scans, to ultimately compare healthy to ATSA shoulders and healthy to RTSA shoulders within the same subjects. See *Figure 3-4* and *Figure 3-5* for images of CT scouts with examples of side-by-side healthy and implanted shoulders.

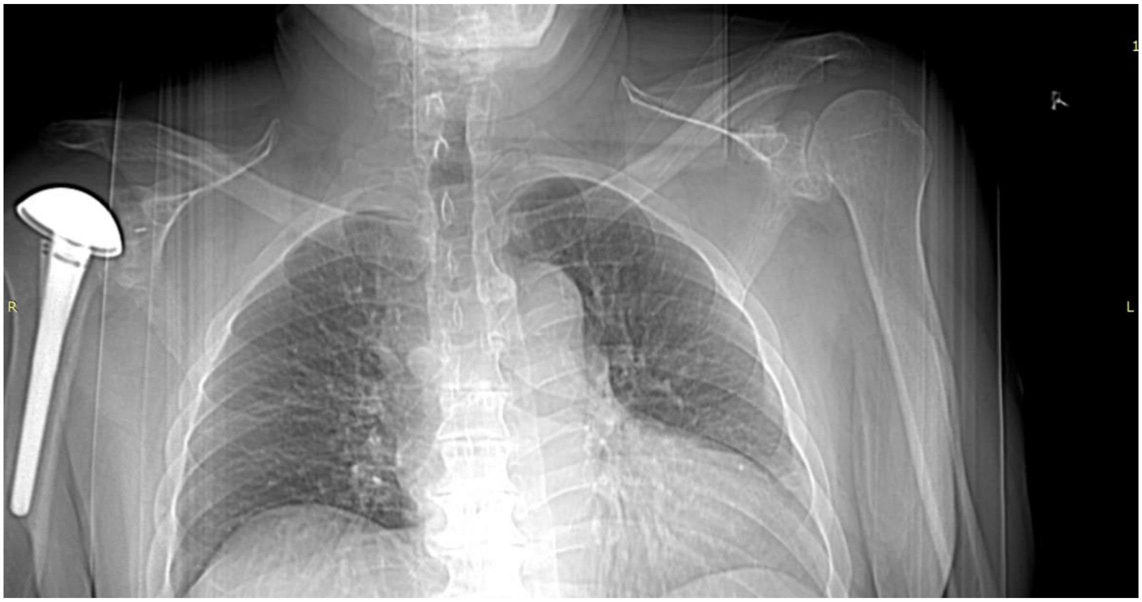

Figure 3-4 TSA01 CT Scout Showing Healthy and ATSA Implanted Shoulders

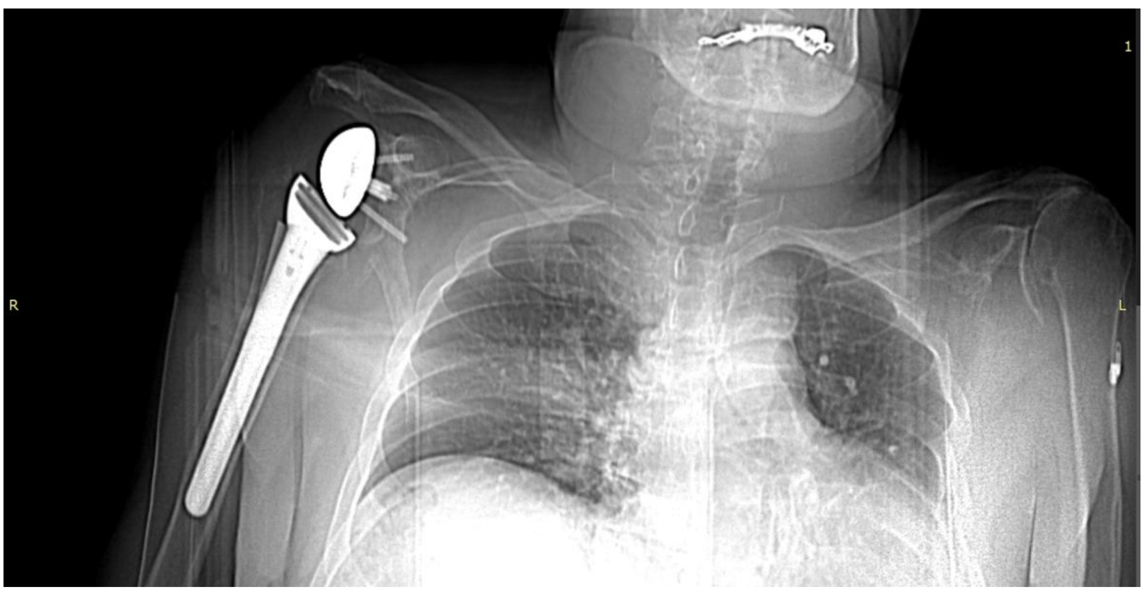

Figure 3-5 TSA03 CT Scout Showing Healthy and RTSA Implanted Shoulders

- Bone:

CT images for each shoulder were imported into ScanIP (Simpleware Synopsys Mountain View, CA, USA) for ‘segmentation’. For three different views of each shoulder, the geometry of each bone of interest was identified and highlighted either manually or using computational tools. Each layer of outlined bone, in each of three views, compiled to create a 3D bone model. ScanIP (Simpleware Synopsys Mountain View, CA, USA) supports smoothing tools that were used to make the bone model surfaces a better representation of the real bone, but often this would erode the geometry too much. In these cases, a triangle meshed stereolithography (STL) model of each bone was exported from ScanIP, and re-meshed and smoothed in the finite element preprocessing software, Hypermesh (Altair Hypermesh MI, USA).

- Implants:

TSA implants were segmented in ScanIP rather than using implant geometries from DePuy (DePuy Synthes Raynham, MA, USA) and merged with segmented subject bones. Bone motion measurement with implant geometries from DePuy might have been more accurate, but segmented implants were used because of delays in receiving permission to use the DePuy implant geometries.

- Convert STL:

The STL bone models were converted to a tiff stack for bone motion measurement. 3D Slicer (3D Slicer open source software, Slicer) was used to slice the

STL models into a pixel thickness of 0.2 for satisfactory image quality. This was done after local coordinate systems were assigned as described below. This process relocates the model origin to the most positive X and Z and most negative Y position of the new tiff stack, which was corrected during kinematics calculations.

3.3.3 Assign Local Coordinate Systems

An STL file is a series of nodes, specified by X, Y, and Z locations. Anatomic coordinate systems were assigned to each bone in this study to generate meaningful kinematics descriptions.

- Humerus:

The humeral coordinate system has its origin at the glenohumeral rotation center (GH). A sphere was fit to the humeral head to find the origin of the humeral local coordinate system (*Figure 3-6*). The Y axis is assigned as the line connecting GH and the midpoint between the most caudal point on the lateral epicondyle (EL) and the most caudal point on the medial epicondyle (EM); this axis points towards GH. The Matlab (Matlab, Simulink software Natick, MA, USA) code finds this line by fitting a cylinder shape to the stem of the humerus. The X axis is the line perpendicular to the plane formed by EL, EM, and GH, and points anterior. Finally, the Z axis is perpendicular to the Y and X axes and points right [15]. *Figure 3-7* shows an assigned humerus coordinate system.

- Scapula:

The origin of the scapula local coordinate system is at the Angulus Acromialis (AA), which is the most laterodorsal point of the scapula. The Z axis connects the Trigonum Spinae Scapulae with the AA and points towards the AA. The X axis is the line perpendicular to the plain formed by AA, TS, and the Angulus inferior, and points anterior. Finally, the Y axis the line perpendicular to the X and Z axes and points cranially [15]. See *Figure 3-7* for an example of an assigned scapula coordinate system in Matlab (Matlab, Simulink software Natick, MA, USA).

- Implants:

There are some differences in assigning coordinate systems to an implanted bone. ATSA implants have a sphere fit to the implanted humeral head to find the GH as with a normal humerus. For RTSA implants the sphere can still be matched to the concave humeral head, but this no longer represents the center of rotation of the joint. This is because rotation of the humerus now occurs about the glenoid implant in the scapula. *Figure 3-8* shows an example of that glenoid implant center of rotation for RTSA subject TSA03 performing abduction. The start frame from the motion is superposed onto the end frame, and the glenoid implants of the start and end frames have been aligned to represent a fixed center of rotation. The visual representation of the error between the assigned center of rotation and the actual center of rotation is the difference between the crosshairs of the circle and the “+” at the center of the circle. The crosshairs show the assigned center of rotation at the center of the humeral head and the “+” shows the approximate center of the radius of curvature of the glenoid implant, the actual center of rotation. This is a limitation of assigning coordinate systems to RTSA shoulders.

- Thorax:

Two different methods were tested to find the best method of calculating scapulothoracic kinematics. Wu et al. proposes a method for creating a thorax coordinate system to calculate scapulothoracic kinematics [15]. Dynamic radiography images of subjects' thorax were not collected so a coordinate system could not be assigned in the same way as the humerus and scapula.

1) First, a thorax coordinate system was built from motion capture markers in Vicon Nexus (Vicon Hauppauge, NY, USA) and transformed into radiography space. The transformation matrix was obtained by finding the locations of three markers placed on the calibration cube in both Vicon and radiography space. The thorax coordinate system followed Wu et al. using the motion capture markers available: the T10 thoracic vertebra, the C7 cervical vertebra, and the most inferior point on the sternum [15]. These markers were sometimes blocked and so were not present in the Vicon data which added inaccuracy to constructing the thorax coordinate systems. This method accounts for patient-specific posture but makes kinematic comparisons between subjects more difficult because of the added variation.
2) Second, a substitution for a thorax coordinate system was created from the neutral scapula coordinate system pose from each subject's abduction trial. The origin was moved to be coincident to the sternal notch, at the most superior point on the

sternum. The disadvantage to this method is the loss of accounting for patient posture. This method provides more comparable kinematics data between subjects because using neutral scapula positions as a comparison for scapula rotations is a more common baseline between subjects; therefore, this method was used. Prior literature has employed this method [22] [21] [9].

- Translations:

To calculate glenohumeral translations, the scapula local coordinate system was moved to the glenoid. The X axis of the glenoid coordinate system was assigned as the vector from the most posterior to the most anterior point of the glenoid; the Y axis was the vector from the most superior to the most anterior point of the glenoid; the Z axis was the vector perpendicular to the X and Y axes; the origin lies at the center of the glenoid (*Figure 3-10*, left*)*. An RTSA implanted scapula glenoid coordinate system was similarly created (*Figure 3-10*). This method was used in Giphart et al. for calculating glenohumeral translations [16].

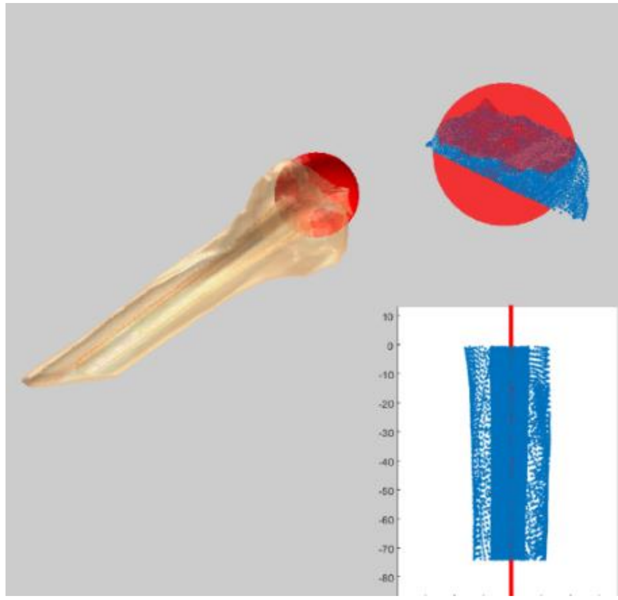

Figure 3-6 Matching a Sphere to Humeral Head for Local Coordinate System Assignment (The origin is located at center of the sphere matched to the humeral head.)

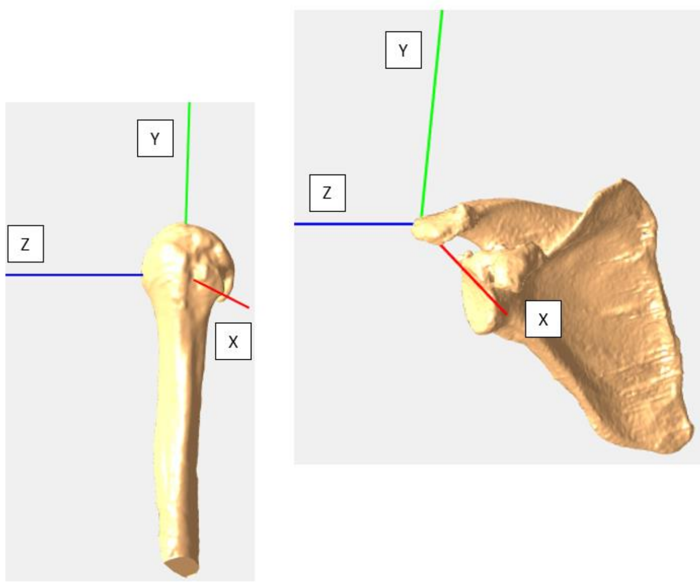

Figure 3-7 Assigned Local Healthy Humerus and Scapula Coordinate System (Red – X Axis; Green – Y Axis; Blue – Z Axis; the humerus origin is at the center of the humeral head and the scapula origin is at the Angulus Acromialis.)

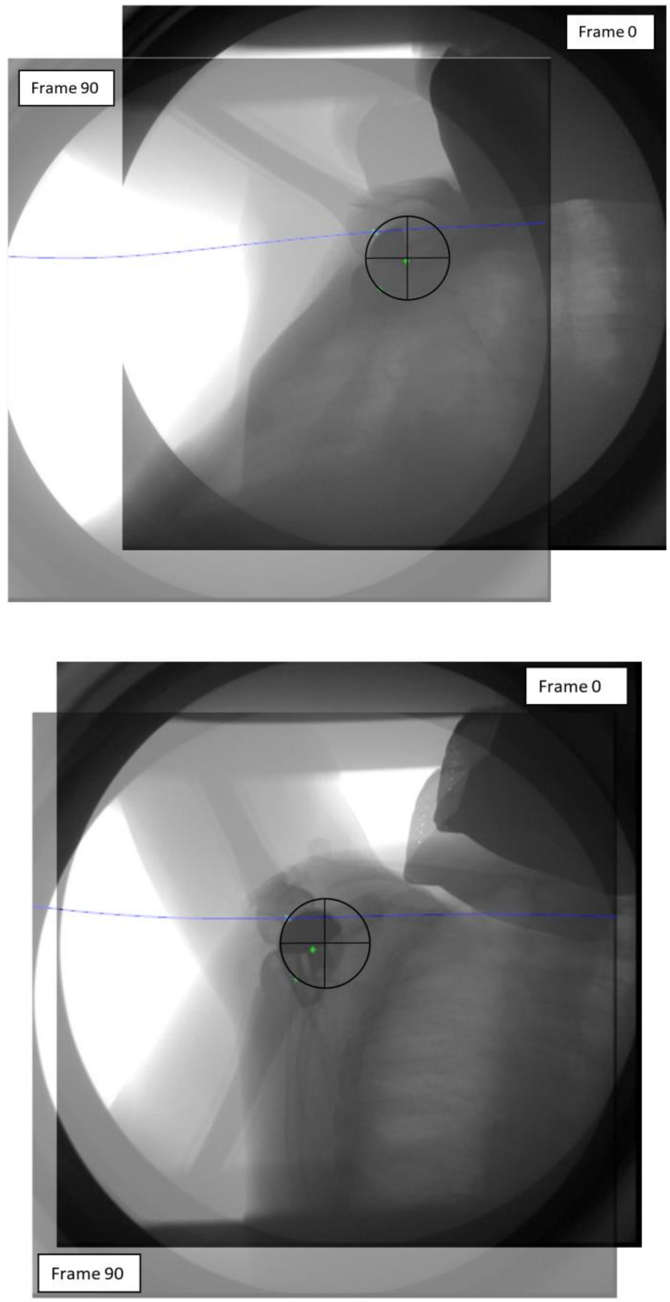

Figure 3-8 Error in Assigned RTSA Center of Rotation: The actual center of rotation (CoR) should be at the crosshairs but the assigned CoR is at the green cross. Camera A (top), Camera B (bottom), each with overlapped first and last frames of motion.

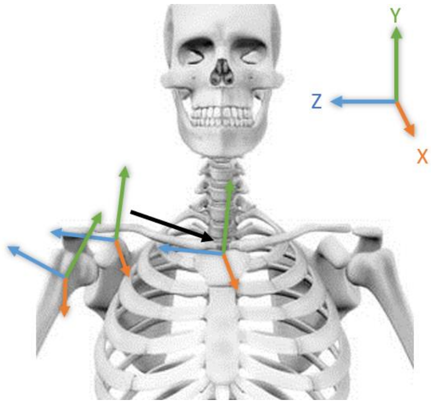

Figure 3-9 Humerus, Scapula, and Thorax Coordinate Systems [2]

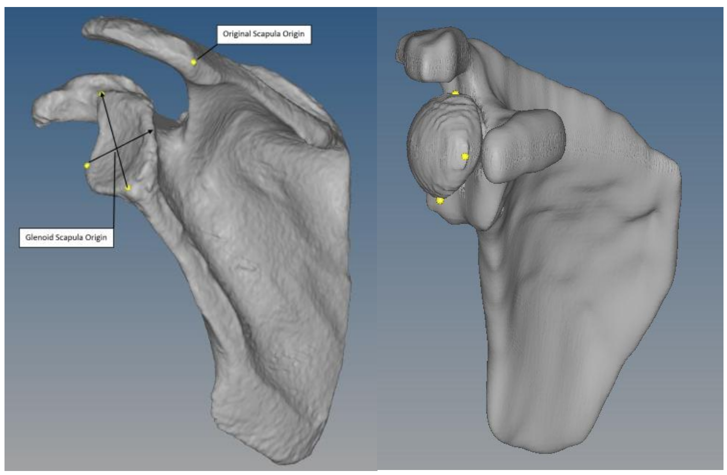

Figure 3-10 Glenoid Coordinate System: Scapula (left), RTSA Scapula (right)

3.3.4 <u>Bone Motion Measurement / Tracking</u>

Measuring bone motion was done by 'tracking' the tiff stack bone models to x-ray images using the software Autoscoper.

- Configuration Files:

A configuration file was made for each bone in each trial. It is a series of file paths on calibration information, the undistorted x-ray trial images from XMALab (XROMM XMALab software, Brown University, Providence, RI, USA), and the tiff stack bone model.

- Tracking:

A calibration file was loaded so that both undistorted trial images appeared in the background with the bone geometry displayed in the foreground of each view. The bone geometry was manually matched to the undistorted trial images by manipulating position and rotation. Smoothing was manually performed, and untracked frames were filled with an interpolation tool. A tracking file, containing transformation matrices frame to frame, was saved. There is an associated human error related to manual tracking, and between different people performing the tracking, but this was minimized as much as possible through checking and correcting the results of each individual tracked motion.These transformation matrices, containing both translation and rotation information, describe the motion of the bone through the motion. See *Figure 3-11* for an example of how the bone geometry (orange) is matched to the trial images (blue). *Figure 3-12* shows animation images of an abduction.

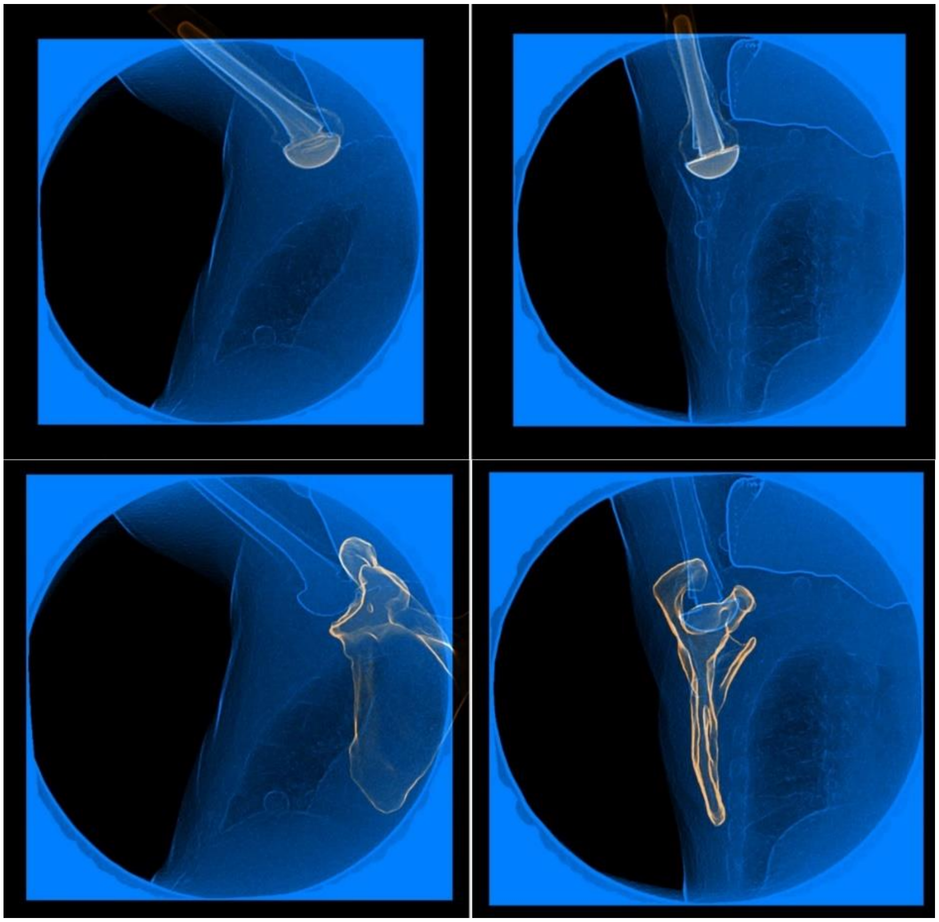

Figure 3-11 Autoscoper Bone Tracking: Implanted TSA Humerus (top), Scapula (bottom)

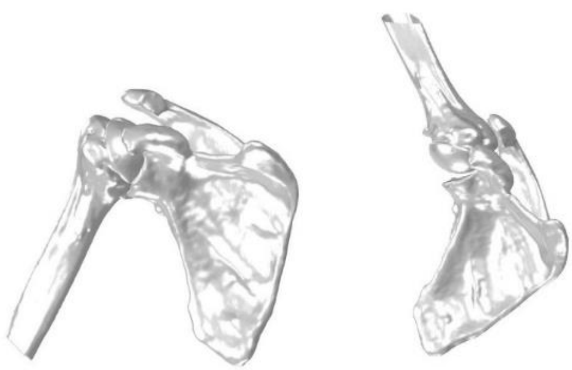

Figure 3-12 Images from an animated Humerus (TSA Implanted) and Scapula Trial

3.3.5 Kinematics Calculation

Kinematics are calculated by extracting changes in rotation and translation between two bones, or two assigned local coordinate frames. See the full kinematics Matlab (Matlab, Simulink software Natick, MA, USA) script in the Appendix D.

The code requires the tracking files from Autoscoper, the bone geometries with local coordinate systems assigned, the subject numbers, with associated trial numbers and trial frame ranges. Tracking files were reformatted into 4x4 transformation matrices in the format of *Equation 3-1*. The rotation matrix is stored in rows and columns $2 \rightarrow 4$ of the transformation matrices. Each element of a rotation matrix is the projection, or dot product, of the one coordinate system axis onto another. Column one of the transformation matrix stores a placeholder "1" and then the x, y, and z translations.

Equation 3-1

$$T = \begin{pmatrix} 1 & 0 & 0 & 0 \\ T_i & R_{I\cdot i} & R_{J\cdot i} & R_{K\cdot i} \\ T_j & R_{I\cdot j} & R_{J\cdot j} & R_{K\cdot j} \\ T_k & R_{I\cdot k} & R_{J\cdot k} & R_{K\cdot k} \end{pmatrix}$$

Commonly the neutral position of each bone would be removed in kinematics calculations; this was not done in this study because differences in neutral positions of all bones were decided to be negligible. See *Figure 3-13* for a diagram of all subjects' bones superposed based on assigned coordinate systems to show that the differences between neutral positions are negligible by visual examination.

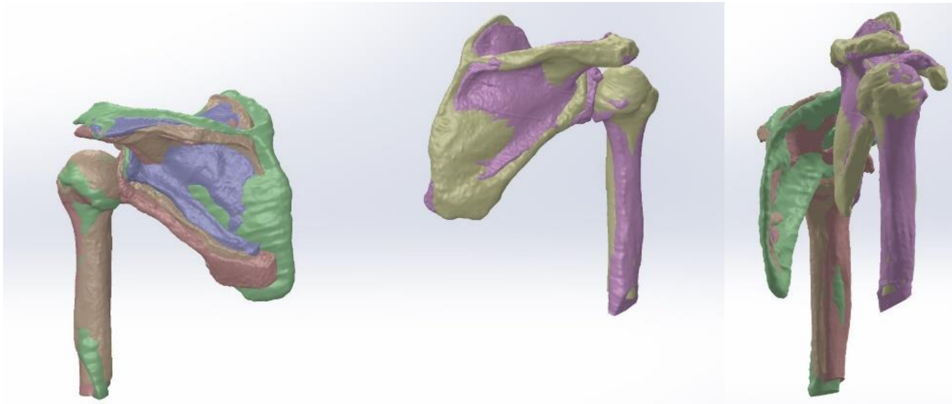

Figure 3-13 Neutral Scapula and Humerus Positions of All Intact Shoulders: Posterior View (left), Side View (right)

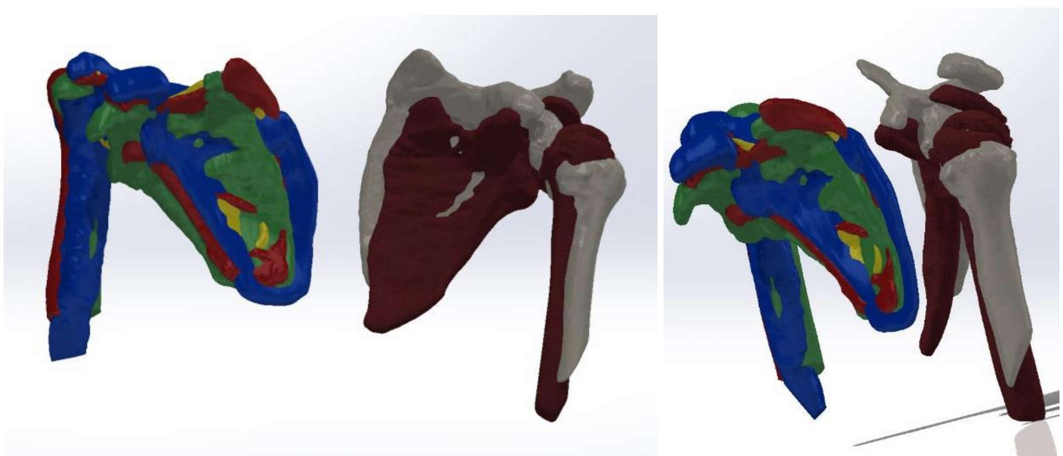

Figure 3-14 Neutral Scapula and Humerus Positions of All TSA Shoulders: Anterior View (left), Side View (right)

Equation 3-2 shows the glenohumeral kinematics calculation. This equation has two parts: the proximal (scapula) and the distal (humerus) bone. Distal bone positions are compared to proximal bone position.

The calculation includes the tracking file transformation matrices of each bone, $T_{scapula}$ and $T_{humerus}$ (*Equation 3-1*), a Z axis flip to account for the flip Autoscoper introduces, and the incorrect bone tiff stack origin that must be subtracted out.

Equation 3-2

$$Glenohumeral\ Transformation\ Matrix =$$

$$\left[\frac{Z_{flip}}{(Scapula\ Tiff\ Origin) * T_{scapula}}\right] * [(Humerus\ Tiff\ Origin) * Z_{flip} * T_{humerus}]$$

$$where\ Z_{flip} = \begin{pmatrix} 1 & 0 & 0 & 0 \\ 0 & 1 & 0 & 0 \\ 0 & 0 & 1 & 0 \\ 0 & 0 & 0 & -1 \end{pmatrix}$$

Scapulothoracic kinematics were calculated as shown in *Equation 3-3*. Scapula motion is compared to a static neutral scapula pose, with its origin relocated to the sternal notch of the thorax.

Equation 3-3

$$Scapulothoracic\ Transformation\ Matrix =$$

$$\left[\frac{1}{T_{neutral\ scapula}}\right] * [(Scapula\ Origin) * Z_{flip} * T_{scapula}]$$

$$where\ Z_{flip} = \begin{pmatrix} 1 & 0 & 0 & 0 \\ 0 & 1 & 0 & 0 \\ 0 & 0 & 1 & 0 \\ 0 & 0 & 0 & -1 \end{pmatrix}$$

Glenohumeral kinematics decompose into a Y-X-Y Euler sequence for abduction and flexion motions (*Equation 3-4*). For internal/external motions the decomposition is Y-Z-X (*Equation 3-8*). Cosine of angle *x* is written as *c1* and Sine of angle *x* is written as *s1*. *Equation 3-5*, *Equation 3-6*, and *Equation 3-7* were used to solve for the Euler angles for the Y-X-Y sequence. *Equation 3-9*, *Equation 3-10,* and *Equation 3-11* were used to solve for the Euler angles for the Y-Z-X sequence.

Equation 3-4

$$R_{YXY} = \begin{pmatrix} c1c3 - c2s1s3 & s2s3 & c3s1 + c1c2s3 \\ s1s2 & c2 & -c1s2 \\ -c2c3s1 - c1s3 & c3s3 & c1c3 - c2s1s3 \end{pmatrix}$$

Equation 3-5

$$Euler\ Angle\ 2 = X = \operatorname{acos}\big(R_{YXY}(2,2)\big)$$

Equation 3-6

$$Euler\ Angle\ 1 = Y = \operatorname{atan}\frac{\big(R_{YXY}(2,1)\big)}{\big(-R_{YXY}(2,3)\big)}$$

Equation 3-7

$$Euler\ Angle\ 3 = Y = \operatorname{atan}\frac{\big(R_{YXY}(1,2)\big)}{\big(R_{YXY}(3,2)\big)}$$

Equation 3-8

$$R_{YZX} = \begin{pmatrix} c1c2 & -s2 & c2s1 \\ c1c3s2 + s1s3 & c2c3 & c3s1s2 - c1s3 \\ s1s2s3 - c3s1 & c2s3 & c1c3 + s1s2s3 \end{pmatrix}$$

Equation 3-9

$$Euler\ Angle\ 2 = Z = \operatorname{asin}\big(-R_{YZX}(1,2)\big)$$

Equation 3-10

$$Euler\ Angle\ 1 = Y = \operatorname{atan}\frac{\big(R_{YZX}(1,3)\big)}{\big(R_{YZX}(1,1)\big)}$$

Equation 3-11

$$Euler\ Angle\ 3 = X = \operatorname{atan}\frac{\left(R_{YZX}(3,2)\right)}{\left(R_{YZX}(2,2)\right)}$$

Scapulothoracic kinematics decompose into a Y-X-Z Euler sequence (*Equation 3-12*). *Equation 3-13*, *Equation 3-14*, and *Equation 3-15* were used to solve for the Euler angles for the Y-X-Z sequence.

Equation 3-12

$$R_{YXZ} = \begin{pmatrix} c1c3 - s1s2s3 & -c2s3 & c3s1 + c1s2s3 \\ c3s1s2 + c1s3 & c2c3 & s1s3 - c1c3s2 \\ -c2s1 & s2 & c1c2 \end{pmatrix}$$

Equation 3-13

$$Euler\ Angle\ 2 = X = \operatorname{asin}\left(R_{YXZ}(3,2)\right)$$

Equation 3-14

$$Euler\ Angle\ 1 = \mathrm{Y} = \operatorname{atan}\frac{\left(-R_{YXZ}(3,1)\right)}{\left(R_{YXZ}(3,3)\right)}$$

Equation 3-15

$$Euler\ Angle\ 3 = Z = \operatorname{atan}\frac{\left(-R_{YXZ}(1,2)\right)}{\left(R_{YXZ}(2,2)\right)}$$

Sign flips occur whenever a rotation with a tangent calculation passes 90°; if a rotation decreases past -90° it will incorrectly change to +90° and vice versa. Whenever this occurred, the flip was qualitatively assessed and fixed.

Any left shoulder was corrected in the Z axis direction to match right shoulder orientation.

All abduction and flexion Euler angles were plotted against total arm elevation. Internal/external motions were plotted against time because arm elevation remains relatively constant. Total arm elevation is calculated with *Equation 3-16* as an addition of glenohumeral elevation and scapulothoracic elevation.

Equation 3-16

$$Arm\ Elevation = R_{YXY}\ Euler\ Angle\ 2\ +\ R_{YXZ}\ Euler\ Angle\ 2$$

X, Y, and Z translations come from either the rows/columns *Glenohumeral Transformation Matrix (2:4,1)* or *Scapulothoracic Transformation Matrix (2:4,1)* from those transformation matrices. Each element represents the distance between the bones' origins. To calculate glenohumeral translations, this calculation was done with the glenoid scapula coordinate system, not the original located at the Angulus Acromialis.

All rotations and translations were passed through a digital Butterworth filter, with a 2^{nd} order coefficient and a normalized cutoff frequency of 4/50 as a method of smoothing and removing human bone tracking error.

3.3.6 Effect of Coordinate System Position

Two sensitivity studies were completed to assess the effect on kinematics of moving and changing a local coordinate system on a bone. First it was found that moving the origin of the humerus from the center of the humeral head to the center of the humeral shaft produced the same kinematics rotations without differences. If the local coordinate system remains on the same bone, no change will occur in rotational kinematics.

Second, a sensitivity study tests the effect on kinematics of two different coordinate systems of the scapula. The difference between the Angulus Acromialis (AA) and the glenoid coordinate systems was calculated; there is a displacement of the origin as with the first study but also a change in axes orientation. Examples of plotted rotation and translation error between the AA and glenoid scapula coordinate systems can be found in *Figure 3-15* and *Figure 3-16*. Average rotational and translation difference was calculated to be 5.16° ± 3.53° and 2.21 ± 2.06 mm respectively.

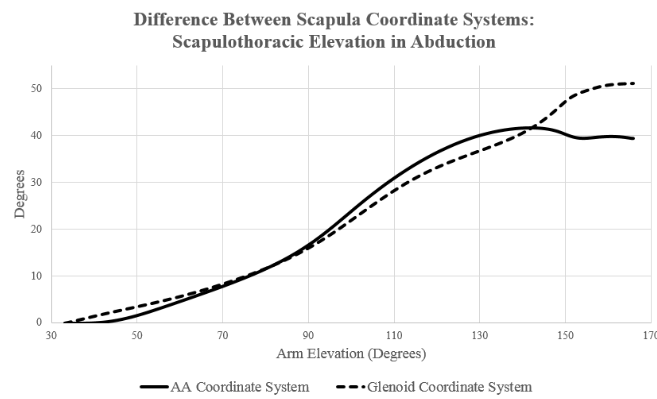

Figure 3-15 Difference Between AA and Glenoid Scapula Coordinate Systems in Scapulothoracic Abduction Elevation

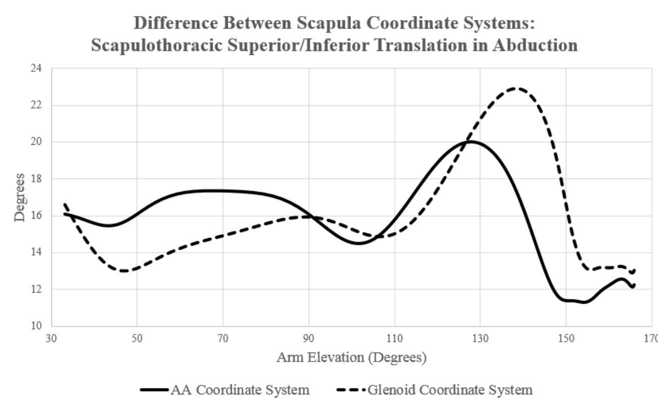

Figure 3-16 Difference Between AA and Glenoid Scapula Coordinate Systems in Scapulothoracic Abduction Superior/Inferior Translation

3.3.7 Effect of Static Neutral Scapula as Thorax Frame

As described in the Methods section a transition was made from using a thorax coordinate system as defined by Vicon (Vicon Hauppauge, NY, USA) motion capture markers to a thorax frame whose orientation was coincident with a static neutral scapula frame with its origin located at the sternal notch. The effect on results of this transition was evaluated in two aspects: 1) the effect of using a static over a dynamic frame, and 2) the effect of using the neutral scapula frame over the true thorax frame.

First, it was found that the amount of thorax or trunk translation is negligible and justifies using a static thorax coordinate system. *Figure 3-17* shows an example of subject TSA01 performing abduction, and the amount of change in position in thorax motion capture markers.

Second, it was determined that using a neutral scapula coordinate system was a good substitute for the thorax coordinate system because this is a method used by previous literature and because the two different methods result in the same maximum value, as evidenced by *Figure 3-18*, which shows subject TSA01 scapulothoracic elevation.

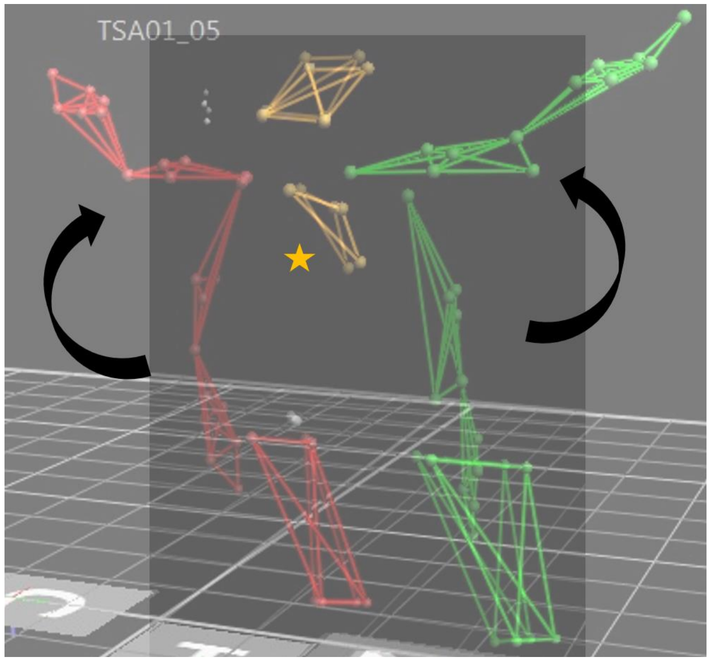

Figure 3-17 Example of Translation of Trunk Motion Capture Markers (TSA01 Abduction)

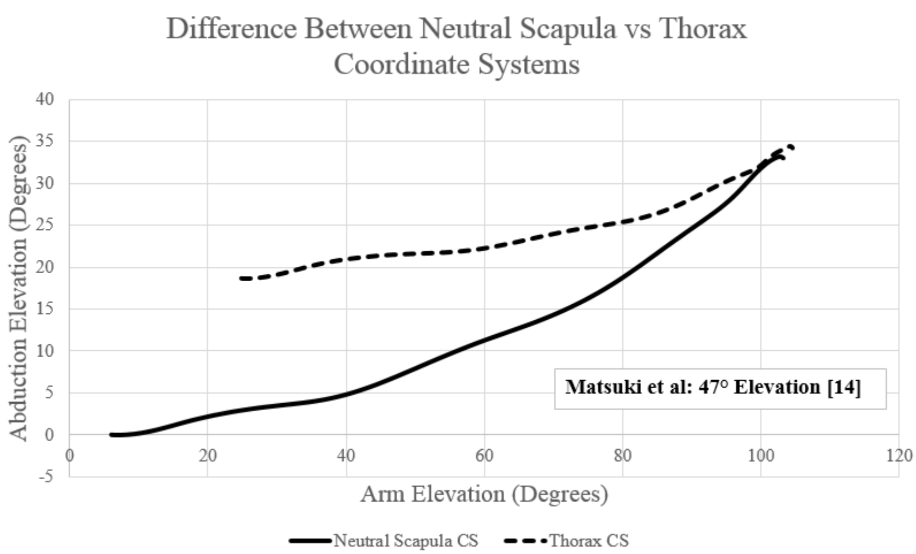

Figure 3-18 Difference Between Neutral Scapula Frame over the Thorax Frame

Chapter 4 Results

Relevant results which answer the following research questions will be the focus of this section and the Discussion.

1) Does TSA restore individual's intact arm elevation in abduction and flexion and in internal/external rotation?
2) Do implanted shoulders utilize compensation from increased scapulothoracic rotation to achieve maximum range of motion?
3) Do differences exist between ATSA and RTSA implanted shoulder kinematics?
4) Does comparing side-to-side differences in individuals over healthy controls better reveal how TSA changes normal function?

For abduction and flexion, humerus with respect to scapula (HS) and scapula (S) elevation comparisons will be made between intact and implanted shoulders as well as RTSA versus ATSA shoulders. Additionally, average scapulohumeral rhythm data will be provided as a commonly reported measure of shoulder function. The motions of internal/external (I/E) rotation with the subject's arm at their side and I/E rotation with the arm abducted to 90° target studying axial humerus rotation with respect to the scapula and therefore valuable results are comparisons of I/E rotation between intact and implanted shoulder I/E rotation and between RTSA and ATSA shoulder I/E rotation.

Finally, a summary of translation results will be presented in the context of intact, RTSA, and an ATSA conditions. Note that the asymptomatic contralateral shoulder will be referred to as the intact shoulder. Raw data recorded and processed for this study can be found in Appendix C. Standard deviation values for each rotation and translation per trial as well as confidence intervals of standard deviations can be found in Appendix A. Upper bound confidence intervals are large, but trends seen in individual data points (which match previous literature) lend confidence to averages and standard deviations.

4.1 Comparison to Prior Literature

Favorable comparison of the results of this study to prior published kinematics of the healthy shoulder provides confidence in the measurements and analysis, and in most cases provides comparison of intact older subject data from the current study with younger participants in prior literature [16] [23] [17]. See Table 4-1 for a side-by-side comparison of results found in this study and prior published results.

Giphart et al. used biplane fluoroscopy to measure the glenohumeral rotations and scapulohumeral rhythm of young healthy participants as they performed abduction and flexion without weight. Authors found a 100 ± 7.9° average maximum glenohumeral elevation (an 80º excursion) in healthy shoulders for both abduction and flexion and reported scapulohumeral (SH) ratios of 2.0 ± 0.4:1 for abduction and 1.1 ± 0.3:1 for forward flexion [16]. This study found maximum intact glenohumeral elevation to be 90.94° ± 15.85º for abduction and 92.21° ± 12.41° for flexion; results found SH ratios of 1.95:1 ± 0.24:1 and 1.95 ± 0.36:1 for abduction and flexion respectively, which are in range of Giphart et al. abduction standard deviation. The mean age of participants of this study was 75 ± 5 years whereas the subjects from Giphart et al. had a mean age of 27±6 years. Doriot et al. published a study comparing shoulder range of motion in a young and an elderly population using marker motion capture and found in an elderly population a loss of 42% for external rotation, of 25% for flexion, and of 10% for adduction [28]. It is therefore reasonable that healthy 'young' subjects will reach a higher glenohumeral elevation compared to intact 'old' subjects. See *Figure 4-1* for data from the current study plotted against Giphart et al. data in abduction and flexion.

Sahara et al. used biplane fluoroscopy to take images at maximum internal and external glenohumeral rotations at several different angles of abduction with a population of healthy volunteers with a mean age of 26.9 ± 5.9 years. The authors found an average range of axial glenohumeral motion ± standard deviation to be 113.3º ± 13.9º with the arm abducted to 0º and 119.0º ± 15.2º with the arm abducted to 90º [17]. Corresponding values in this study found 79.21º ± 20.63º with arm abducted to 0º and 80.62º ± 12.41º with the arm abducted to 90º [17]. Again, it is hypothesized that the roughly 30º difference in values between Sahara et al. and this study comes from the age difference in participants, supported by Doriot et al. [28]. See *Figure 4-2* for data from the current study plotted next to Sahara et al. data in I/E rotation with the arm abducted to 0º and 90º.

Matsuki et al. collected data on scapulothoracic elevation to investigate differences between dominant and non-dominant shoulders in twelve healthy males of a mean age of 32 years. The average of dominant and non-dominant upward scapulothoracic rotation was found to be 42º ± 7.5º [23]. This result agrees with other papers such as McClure et al. [20]. The current study finds a mean intact scapulothoracic upward rotation excursion of 47.11º ± 16.30º; when the outlier TSA06_R is excluded from that mean it drops to be 43.89º, agreeing with Matsuki et al. and McClure et al.

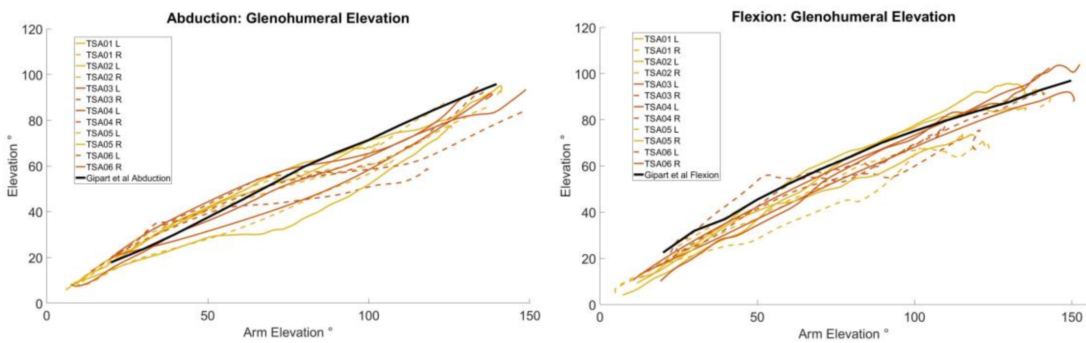

Figure 4-1 Comparison of Abduction (left) and Flexion (right) to Giphart et al. [16]

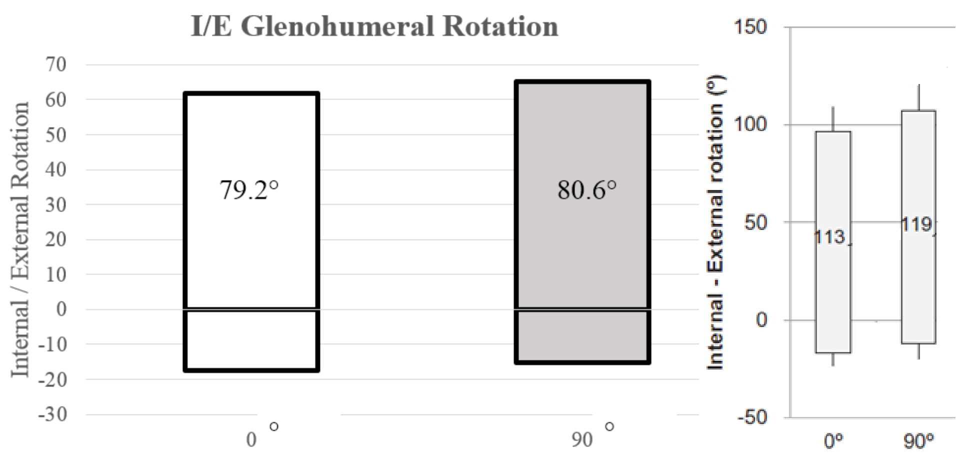

Figure 4-2 Comparison of I/E Rotation (left) to Sahara et al. (right) [17]

Table 4-1 Comparison to Literature Results

Kinematic Measure	Current Study Result	Literature Result
Maximum Abduction/Flexion Glenohumeral Elevation	91.6º ± 14.1°	Giphart et al. 100º ± 7.9° [16]
Abduction Scapulohumeral Rhythm	1.95:1 ± 0.24:1	Giphart et al. 2.0 ± 0.4:1 [16]
Flexion Scapulohumeral Rhythm	1.95 ± 0.36:1	Giphart et al. 1.1 ± 0.3:1 [16]
Maximum Abduction Scapulothoracic Elevation	47.11º ± 16.30º (43.89º ± 16.30º without outlier)	Matsuki et al. 42º ± 7.5º [23]
I/E with Arm Abducted 0° Glenohumeral Rotation	79.21º ± 20.63º	Sahara et al. 113.3º ± 13.9º [17]
I/E with Arm Abducted 90° Glenohumeral Rotation	80.62º ± 12.41º	Sahara et al. 119.0º ± 15.2º

4.2 <u>Comparison of Shoulder Kinematics During Abduction</u>

The first question this section addresses is: 1) Does TSA restore intact shoulder elevation motion in abduction? This can be answered by finding if the six subjects on average reach the same elevation angle (glenohumeral elevation + scapulothoracic elevation) with their implanted shoulder as they do with their intact, while accounting for standard deviation.

Results show no notable deviation of implanted glenohumeral elevation from intact during abduction and remain within intact standard deviation. This is true for the entire abduction motion; comparison across the entire motion is important so as not to make incorrect assumptions solely based on maximum values. However, in this case implanted and intact motion remain similar across the entire motion.

Figure 4-3 shows implanted shoulder glenohumeral elevation across the entire abduction motion for each implanted shoulder plotted against mean intact elevation and an area of intact standard deviation (the gray band surrounding the dark grey intact mean).

The second question addressed is: 2) If subjects achieve intact elevation, are they using compensation as hypothesized with scapula rotation? Scapulothoracic compensation means an increase in scapula movement to compensate for a decrease in glenohumeral movement. Abduction shows evidence of increased scapula compensation in *Figure 4-4*, where implanted scapulothoracic elevation data is plotted for the entire motion against an intact mean trend and standard deviation area.

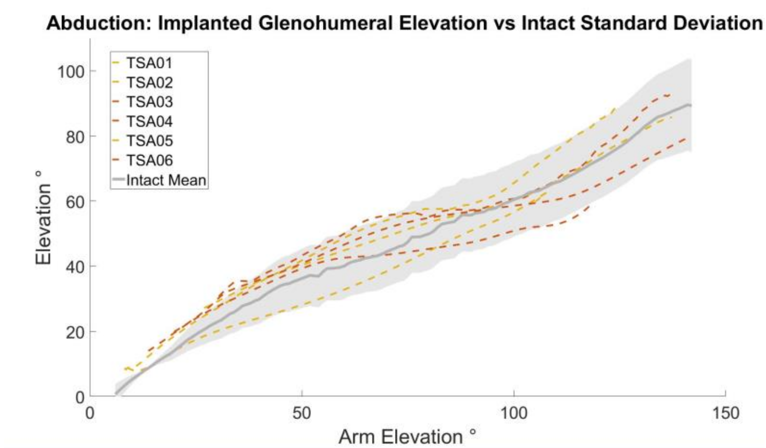

Figure 4-3 Abduction: Implanted Glenohumeral Elevation Trends Plotted Against Intact Mean (Dark Gray) and Standard Deviation (Gray Band)

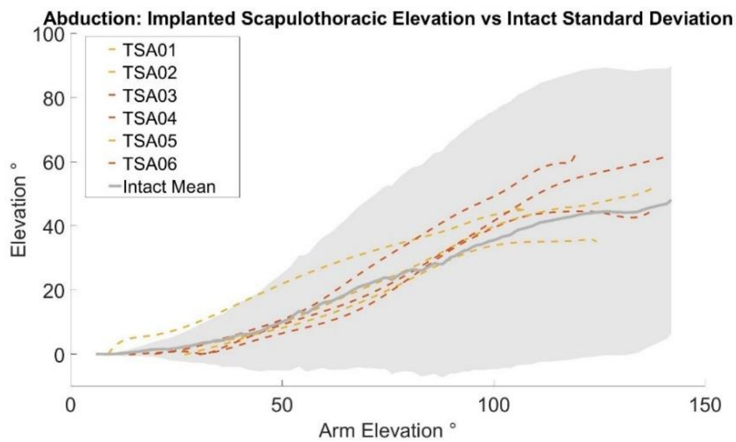

Figure 4-4 Abduction: Implanted Scapulothoracic Elevation Trends Mean (Dark Gray) and Standard Deviation (Gray Band)

Comparing maximum abduction elevation values supports the answers to the first two research questions discussed above: TSA does restore intact abduction elevation, but implanted shoulders show a trend of more scapula compensation over intact. The bar chart in *Figure 4-5* (left) shows that the majority of healthy glenohumeral elevation values exceed the implanted values, but not outside of intact standard deviation. Averages in the same figure (right) supports that fact. *Figure 4-6* (left) shows scapulothoracic maximum elevation; two-thirds of subjects showed implanted scapula elevation values as equal or larger than intact. Averages in the same figure (right) confirm this statement. The box and whisker plots in *Figure 4-7* support the findings: glenohumeral implanted mean (*x*) shows a deficit compared to the intact, and the range of values (data range bars) agree. Comparing scapulothoracic elevation as box and whisker plots reveal that although on average intact shoulders show a deficit compared to implanted, there is no such trend between the range of values shown by the data range bars. There is less evidence of a trend of scapula compensation in abduction than in flexion (as will be shown).

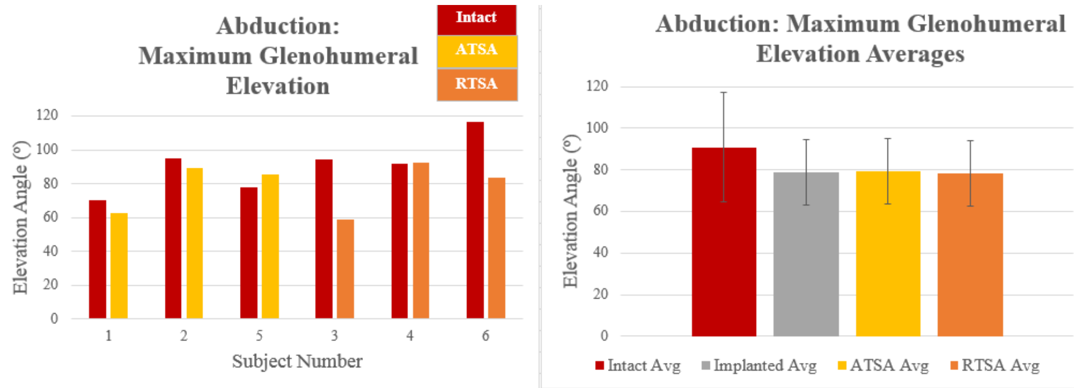

Figure 4-5 Abduction Maximum Glenohumeral Elevation Comparison: in Individuals (left) and on Average (right)

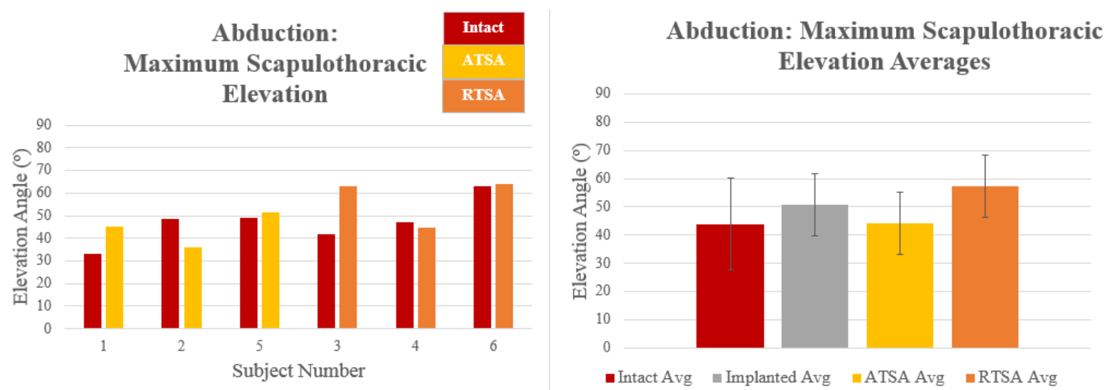

Figure 4-6 Abduction Maximum Scapulothoracic Elevation Comparison in Individuals (left) and on Average (right)

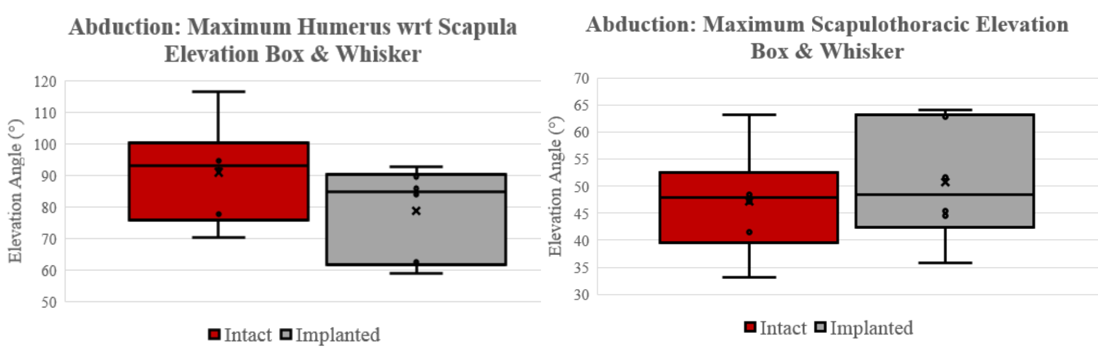

Figure 4-7 Abduction Maximum Glenohumeral (left) and Scapulothoracic (right) Elevation Comparison: Box & Whisker Plots

Calculating scapulohumeral (SH) rhythm, which combines into a ratio glenohumeral elevation divided by scapulothoracic elevation, supports the findings that implanted shoulders compensate with scapulothoracic elevation during abduction. *Figure 4-8* shows this measure at the end of the motion, in individuals and on average. Rhythm ratios were found to be 1.95:1 ± 0.24:1 in intact and 1.64:1 ± 0.57:1 in implanted shoulders, respectively. There is a higher proportion of scapulothoracic to glenohumeral elevation in implanted shoulders on than intact on average.

Most individuals show the pattern of deficits in glenohumeral elevation combined with greater scapulothoracic elevation. Some differences in SH ratio between intact and implanted shoulders are more pronounced, as with TSA03, where the implanted SH ratio nearly doubles. The visual validation of this difference, which shows the right and left TSA03 shoulders at the same arm elevation, *Figure 4-10* is striking. The scapula on the implanted side is at a much higher upward rotation compared to the intact scapula. TSA03 kinematics confirm this in *Figure 4-11* and *Figure 4-12* shows that TSA03 reaches nearly the same humerus with respect to thorax elevation in both shoulders. There is clear scapulothoracic compensation.

Scapula compensation occurs throughout the majority of abduction elevation in this population, in all shoulders, as seen in *Figure 4-9*. Roughly the first 30º of elevation can be attributed to the glenohumeral joint in intact, ATSA, and RTSA shoulders. The next phase of elevation shows a 1.3:1 ratio of glenohumeral to scapulothoracic contribution to elevation in intact and ATSA shoulders.

In contrast, RTSA shows a 0.6:1 glenohumeral to scapulothoracic contribution of elevation and therefore trends towards using more scapula compensation through the motion.

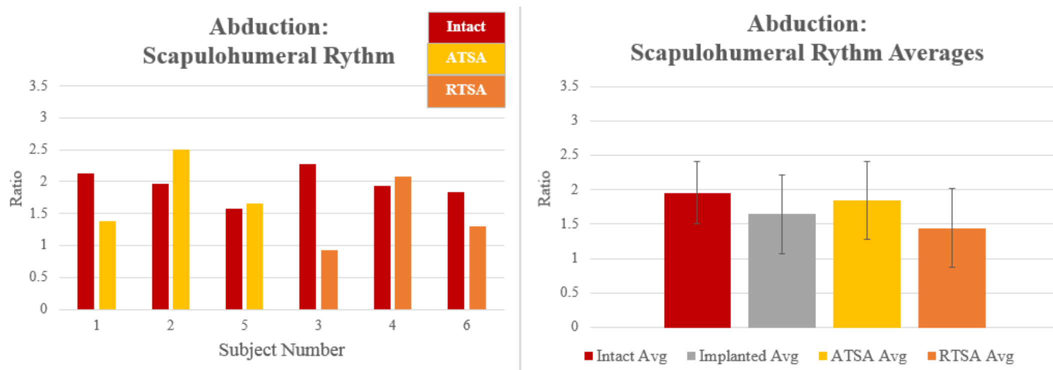

Figure 4-8 Abduction Scapulohumeral Rhythm at Full Extension Pose: In Individuals (left) and on Average (right)

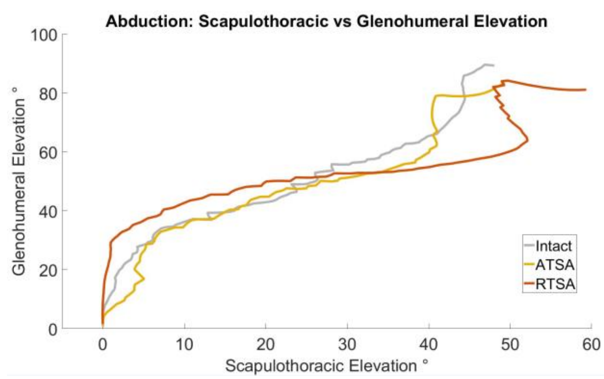

Figure 4-9 Abduction Scapulohumeral Rhythm Trajectory: Relative Contributions of Humerus vs Scapula Elevation

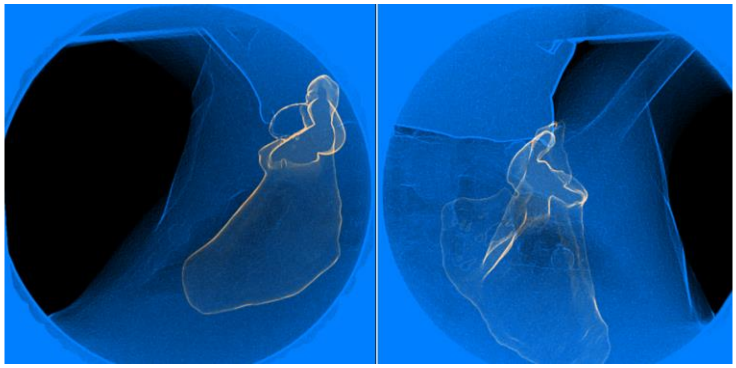

Figure 4-10 Differences observed in scapular position at equal arm elevation for intact (right) and TSA implanted (left) in subject TSA03

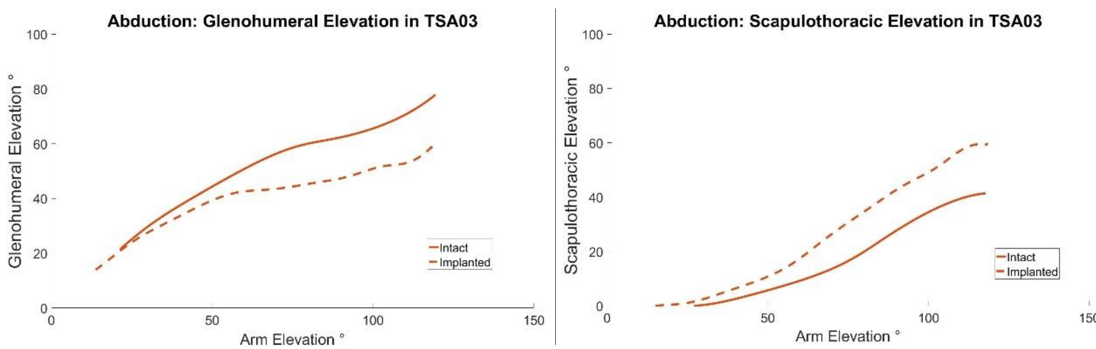

Figure 4-11 TSA03 Intact (Solid Line) vs Implanted (Dashed) Elevation: Glenohumeral (left), Scapulothoracic (right)

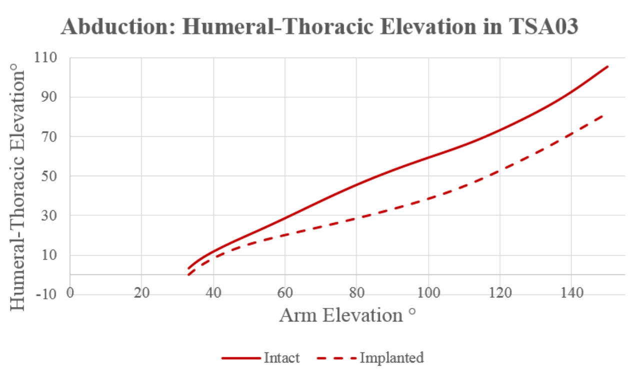

Figure 4-12 TSA03 Intact vs Implanted Elevation: Humeral-Thoracic

The third question this section addresses is: 3) Do any differences present between ATSA and RTSA kinematics in abduction?

The bar charts, *Figure 4-5* and *Figure 4-6*, do not show considerable differences between ATSA and RTSA average maximum elevation values. In abduction, glenohumeral averages agree between ATSA and RTSA but RTSA does exceed the maximum ATSA scapulothoracic value. The next section describing flexion shows a different result, suggesting the difference might by activity dependent.

Looking at differences across the entire abduction motion only show a notable difference at the end of the motion. *Figure 4-13 and Figure 4-14* show RTSA glenohumeral or scapulothoracic elevation, respectively, plotted against the intact mean and standard deviation area. RTSA subjects completed the motion at a lower glenohumeral elevation value than the average of the ATSA subjects. In contrast RTSA subjects completed abduction at a higher scapulothoracic elevation value than the average of the ATSA subjects. This suggests that RTSA shoulders compensate with scapula elevation over humeral elevation more so than ATSA shoulders.

However, this was only true for the last 20° of abduction and RTSA trends all remained within ATSA standard deviation, suggesting no notable differences between the two design types.

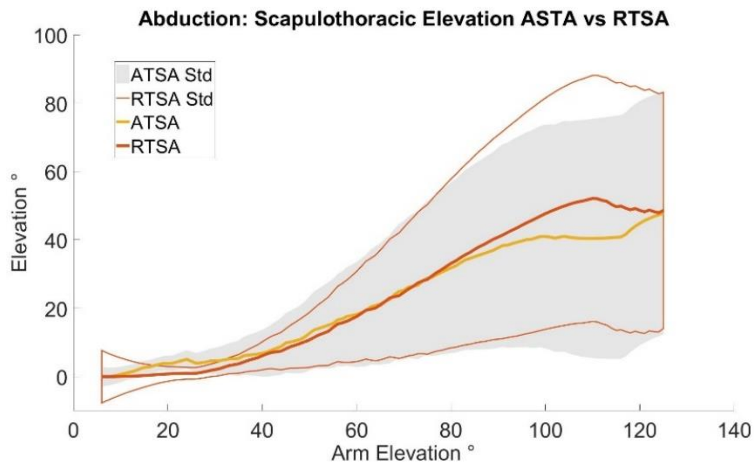

Figure 4-13 Abduction: RTSA Glenohumeral Elevation Mean (Orange) Plotted Against ATSA Mean (Yellow) and Standard Deviation (Gray Band)

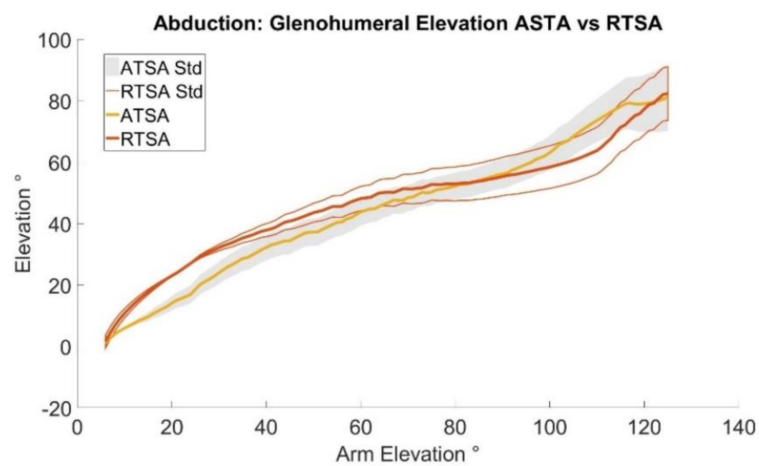

Figure 4-14 Abduction: RTSA Scapulothoracic Elevation (Orange) Plotted Against ATSA Mean (Yellow) and Standard Deviation (Gray Band)

The fourth research question this section answers is: 4) Does comparing side-to-side differences in individuals over healthy controls better reveal how TSA changes normal function?

Calculating root mean squared difference (RMSD) between individual's implanted and intact sides revealed the importance of comparing side-to-side in individuals. (See *Equation 4-1* for the calculation; data points were sampled every ten degrees per subject.) Results show large variation subject to subject, where *Table 4-2* shows a range of values between 2.29° to 15.43°. For reference, Charbonnier et al. calculated an average RMS error of 4° between motion capture and fluoroscopy methods for calculating abduction and flexion shoulder kinematics [29]. Butler et al. calculated RMSD between children with cerebral palsy and typically developing children performing shoulder elevation and found a mean RMSD value of 9-10° [30]. Children with cerebral palsy is a very different patient population than senior citizens with TSA implants, but the results are still useful to put the current study's calculated RMSD values into context. Three out of six subjects present values larger than 10° during abduction. This means that even though on average TSA restores intact elevation motion in abduction, the degree to which it restores can largely vary patient to patient.

It is important to verify if TSA surgery restores motion to that same patient's level of intact motion to deem the surgery successful.

For example, returning to *Figure 4-5* which shows maximum elevation values per subject, both TSA02 and TSA03 reach roughly the same intact elevation but *Table 4-2* shows that the TSA implant in TSA02 restores that individual's motion much better than in TSA03.

Equation 4-1 Root Mean Squared Difference Computed As:

$$RMSD = \sqrt{\frac{\sum_{i=1}^{n}(y_{healthy} - y_{implanted})^2}{n}}$$

Table 4-2 Abduction: Glenohumeral and Scapulothoracic Elevation RMSD

	Abduction		Flexion	
Subject	**Glenohumeral RMSD**	**Scapulothoracic RMSD**	**Glenohumeral RMSD**	**Scapulothoracic RMSD**
TSA01	12.20	12.62	15.43	15.19
TSA02	2.75	2.29	10.09	9.75
TSA05	11.96	12.02	9.95	9.28
TSA03	12.75	12.17	7.70	7.29
TSA04	8.63	9.12	9.18	8.27
TSA06	6.45	6.63	5.56	5.33
Legend:	**ATSA**		**Reverse TSA**	

4.3 Comparison of Shoulder Kinematics During Flexion

Elevation kinematics in forward flexion show similar results as in abduction. The answer to the first research (question 1) Does TSA restore intact shoulder elevation motion in flexion?) is confirmed. *Figure 4-15* and *Figure 4-16* show implanted elevation values remain within intact standard deviation, except for 5° of deviation.

This motion shows more pronounced differences between glenohumeral and scapulothoracic elevation than in abduction. *Figure 4-15* shows implanted shoulders trending lower than the intact mean glenohumeral elevation throughout the entirety of the motion. Conversely *Figure 4-16* shows implanted shoulders trending greater than the intact mean scapulothoracic elevation through the whole motion. In the context of the second research question (2) If subjects achieve intact elevation, are they using compensation as hypothesized with scapula rotation?), flexion shows more scapula compensation than abduction. Maximum glenohumeral (*Figure 4-17*) and scapulothoracic elevation values (*Figure 4-18*) support this statement. Box and whisker plots in *Figure 4-19* show the clear deficit in implanted glenohumeral elevation and that a majority of individuals' implanted sides exceed intact in scapulothoracic elevation. Flexion scapulohumeral rhythm (SH) ratios (*Figure 4-20*) additionally support this finding, with implanted shoulders on average reporting a higher ratio of scapulothoracic to glenohumeral elevation than intact shoulders. Calculated intact SH was found to be 1.95 ± 0.36:1 and 1.69:1 ± 0.33:1 for implanted shoulders.

Scapula compensation shows more strongly in implanted over intact shoulders during flexion than it did in abduction, as seen in *Figure 4-21*. Intact shoulders show a ratio of 2:1 glenohumeral to scapulothoracic elevation throughout the whole motion. This ratio drops to 1.1:1 in ATSA and 0.8:1 in RTSA, showing that scapula compensation presents more strongly in ATSA and even more so in RTSA shoulders.

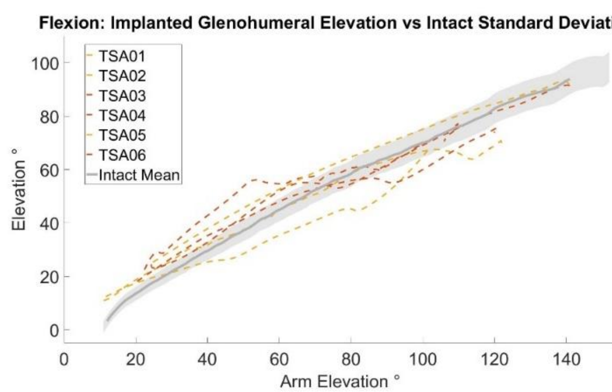

Figure 4-15 Flexion: Implanted Glenohumeral Elevation Trends Plotted Against Intact Mean (Dark Gray) and Standard Deviation (Gray Band)

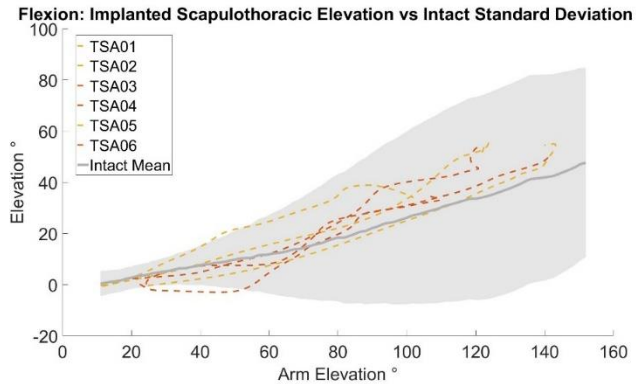

Figure 4-16 Flexion: Implanted Scapulothoracic Elevation Trends Plotted Against Intact Mean (Dark Gray) and Standard Deviation (Gray Band)

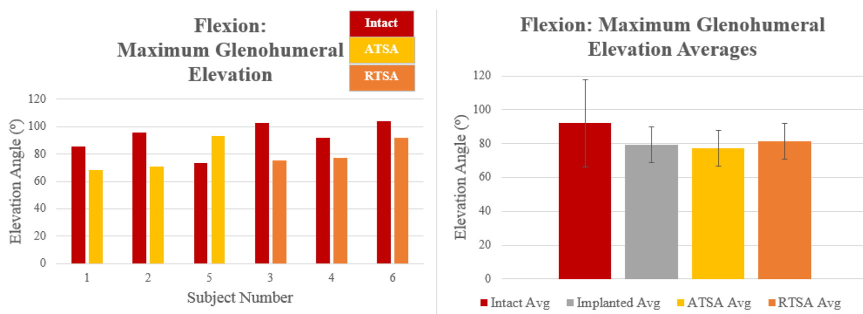

Figure 4-17 Flexion Maximum Glenohumeral Elevation Comparison: In Individuals (left) and on Average (right)

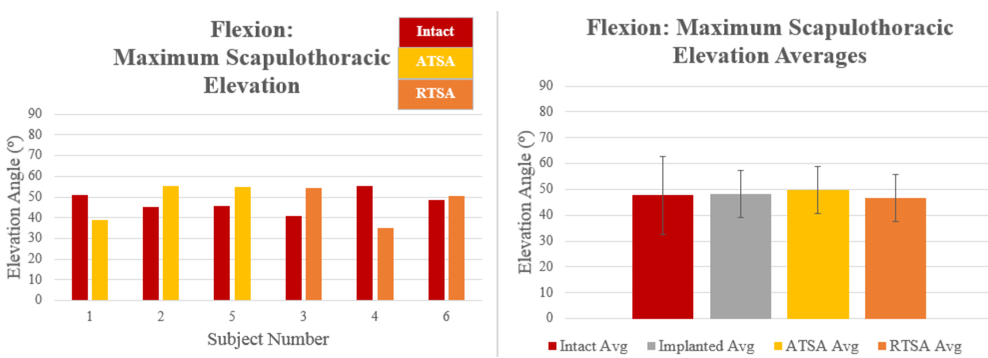

Figure 4-18 Flexion Maximum Scapulothoracic Elevation Comparison: In Individuals (left) and on Average (right)

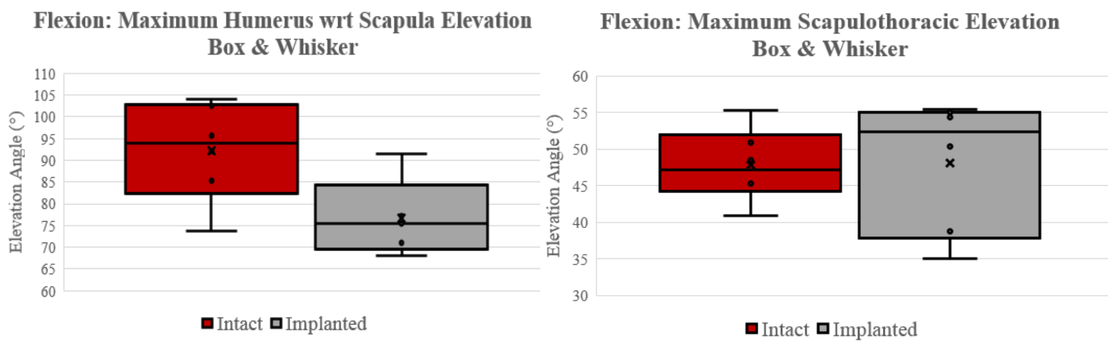

Figure 4-19 Flexion Maximum Glenohumeral (left) and Scapulothoracic (right) Elevation Comparison: Box & Whisker Plots

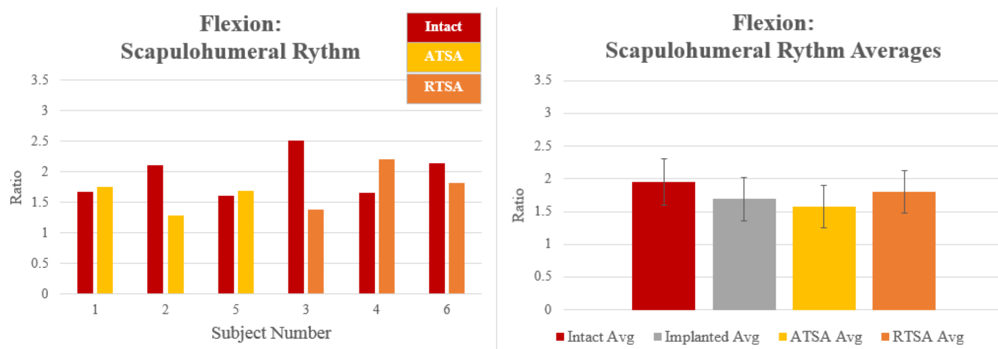

Figure 4-20 Flexion Scapulohumeral Rhythm at Full Extension Pose: In Individuals and on Average

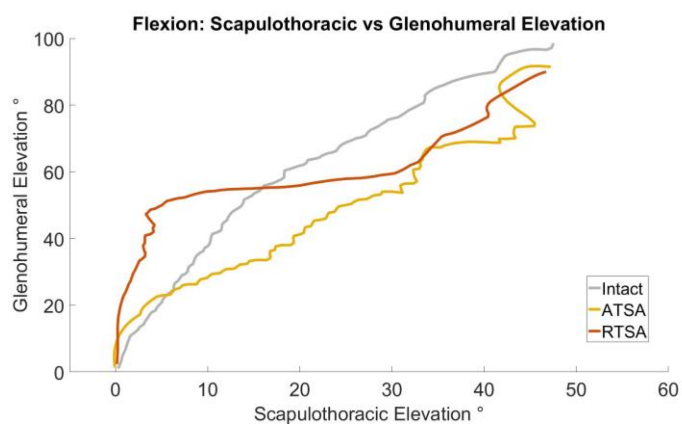

Figure 4-21 Flexion Scapulohumeral Rhythm Trajectory: Relative Contributions of Humerus vs Scapula Elevation

Small differences were found between ATSA and RTSA elevation kinematics in abduction, and there is even less difference in flexion results. Comparing glenohumeral elevation (*Figure 4-22*) and scapulothoracic elevation (*Figure 4-23*) between ATSA and RTSA shows no discernable difference. This answers the third research question, 3) Do any differences present between ATSA and RTSA implant designs in abduction?

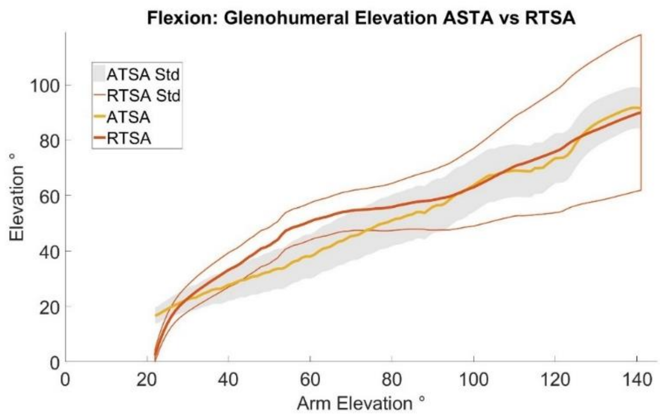

Figure 4-22 Flexion: RTSA Glenohumeral Elevation Mean (Orange)Plotted Against ATSA Mean (Yellow) and Standard Deviation (Gray Band)

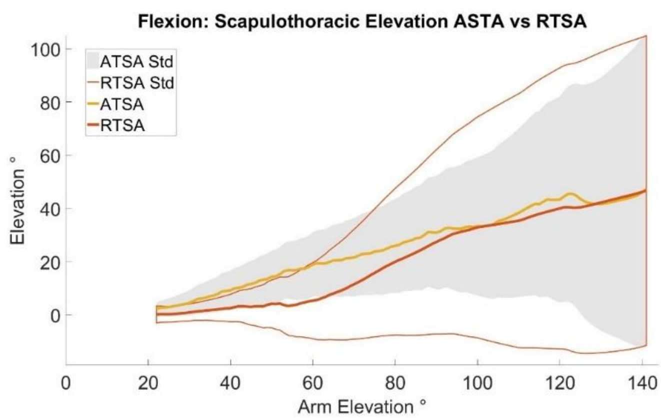

Figure 4-23 Flexion: RTSA Scapulothoracic Elevation Mean (Orange) Plotted Against ATSA Mean (Yellow) and Standard Deviation (Gray Band)

As in abduction, calculating root mean square difference (RMSD) supports the need for comparing TSA kinematics to intact within an individual, answering the fourth research question, 4) Does comparing side-to-side differences in individuals over healthy controls better reveal how TSA changes normal function? See *Table 4-2* for RMSD flexion values. An example visual representation of RMSD is plotted in as $(\text{healthy elevation} - \text{implanted elevation})$ *Figure 4-24.* Any point above the horizontal axis indicates better intact shoulder performance and vice versa. Overall, during flexion individuals show better intact glenohumeral performance over implanted and implanted shoulders show better scapulothoracic performance over intact, but there is a large amount of variability across subjects.

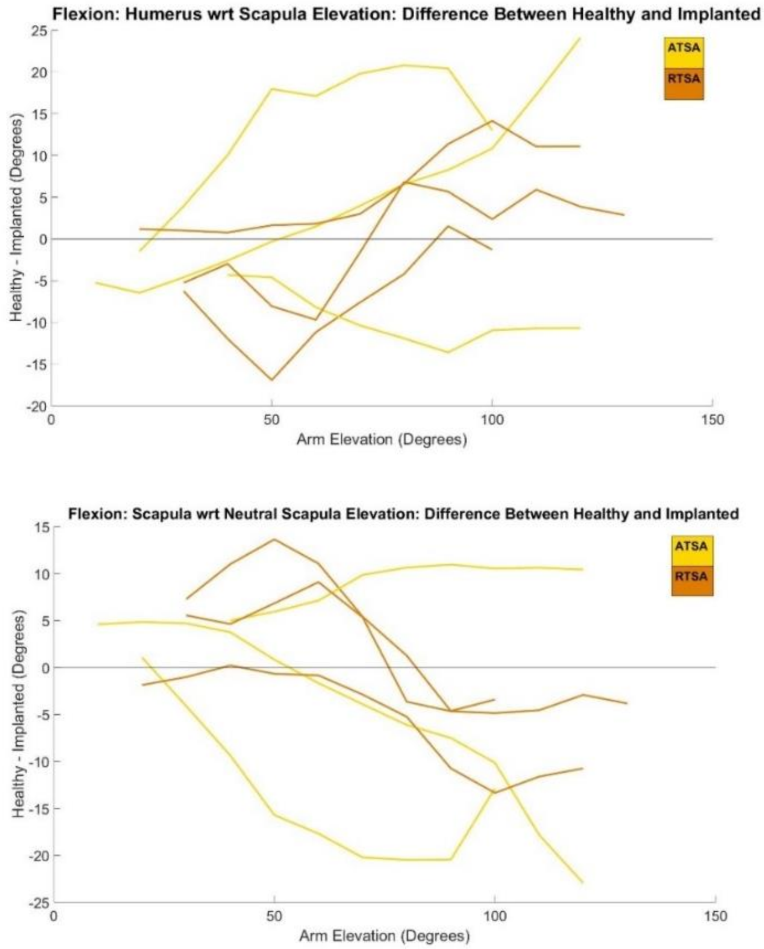

Figure 4-24 Flexion: Glenohumeral (top) and Scapulothoracic (bottom) Plotted Difference Between Intact and Implanted Shoulder Elevation

4.4 <u>Comparison of Shoulder Kinematics During Internal / External Rotation</u>

First this section addresses the question, 1) Does TSA restore intact humerus axial motion during internal / external (I/E) motions?

On average TSA does not restore intact I/E range of motion. Magnitudes of axial glenohumeral change per individual and on average for I/E with arm at the side are shown in *Figure 4-25* for all subjects. *Figure 4-26* shows the same graphs for I/E with the arm abducted to 90°. In all individual subjects except TSA05 (I/E with arm at the side) intact axial rotation exceeds implanted in both trials. This makes it clear that TSA does not restore intact humerus axial motion in these trials. Averages box and whisker plots (*Figure 4-27*) present the same findings.

Participants were instructed to move from maximum internal to maximum external rotation, and results found that both the internal and external rotation deficits of implanted shoulders compared to intact function were substantial. Internal and external rotations were divided by the neutral humeral position as assigned to the bone. *Figure 4-28* shows average comparisons of intact, overall implanted, ATSA, and RTSA internal and external motion. The negative ATSA value during I/E with the arm abducted to 90° shows that most ATSA shoulders had no internal rotation at all.

Next, scapulothoracic I/E rotation can answer the question, 2) Do implanted shoulders use compensation with scapula rotation during I/E motion?

When I/E is performed with the arm at the side, scapula I/E rotation is used as compensation to reach larger internal and external rotations. Scapula I/E rotation presents as a much smaller rotation when the arm is abducted to 90°. *Figure 4-29* and *Figure 4-30* show scapulothoracic I/E axial rotation (retraction) for I/E motions with the arm abducted 0° and 90°. Intact scapulothoracic I/E rotation averages are 23.11° ± 6.40° and 10.48° ± 3.04° for I/E with the arm at the side and I/E with the arm abducted 90°, respectively. Box and whisker plots in *Figure 4-31* support the finding that there is scapula compensation during I/E with arm at the side.

In I/E with arm at the side, intact glenohumeral rotation exceeds implanted on average but implanted scapulothoracic rotation exceeds intact, which shows scapula compensation during this motion. *Figure 4-32* shows implanted scapulothoracic I/E rotation plotted against the intact mean during the entire I/E with the arm at the side motion and supports the finding of scapula compensation.

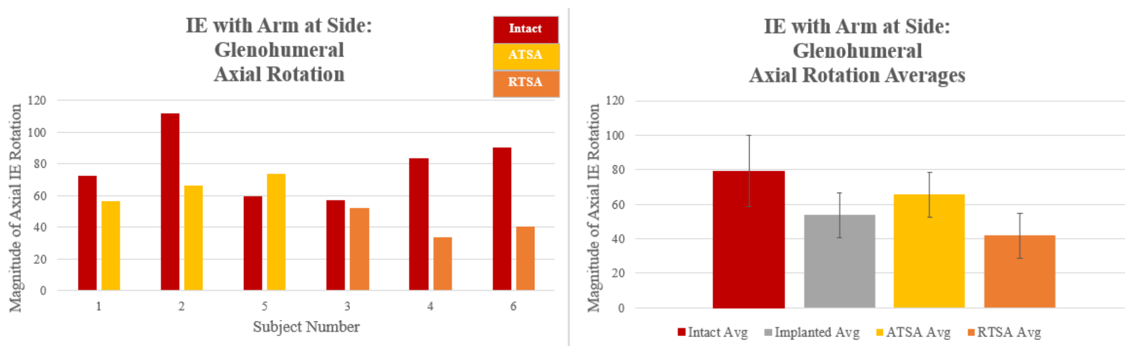

Figure 4-25 I/E with Arm at Side Glenohumeral Axial Rotation: in Individuals (left) and on Average (right)

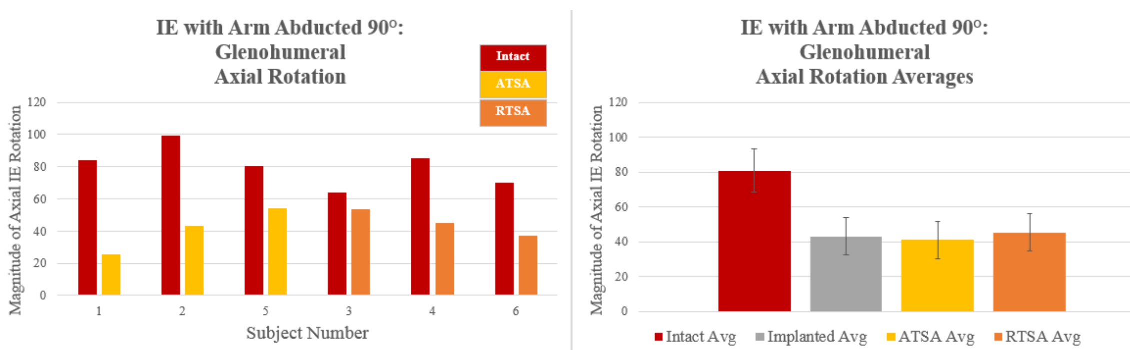

Figure 4-26 I/E with Arm Abducted 90° Glenohumeral Axial Rotation: in Individuals (left) and on Average (right)

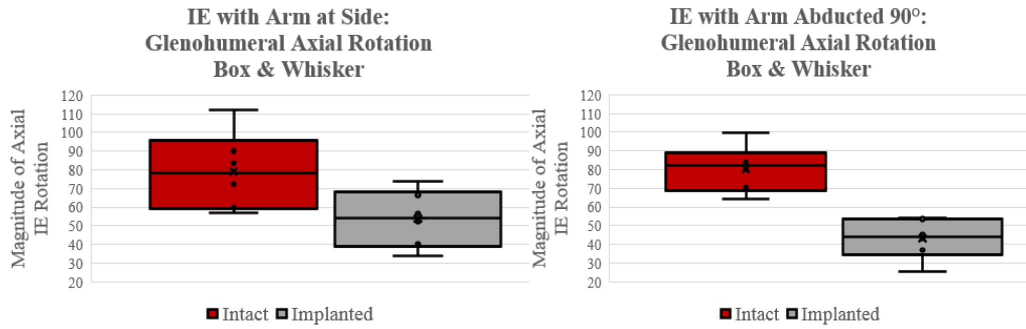

Figure 4-27 I/E with Arm at the Side (left) and with Arm Abducted 90º (right) Glenohumeral Axial Rotation: Box & Whisker Plots

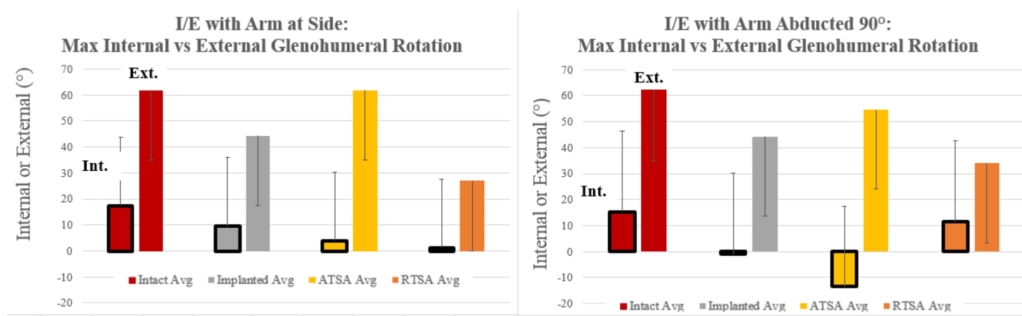

Figure 4-28 I/E with Arm at Side (Left) and I/E with Arm Abducted 90 (right): Maximum Internal vs External Rotation Averages

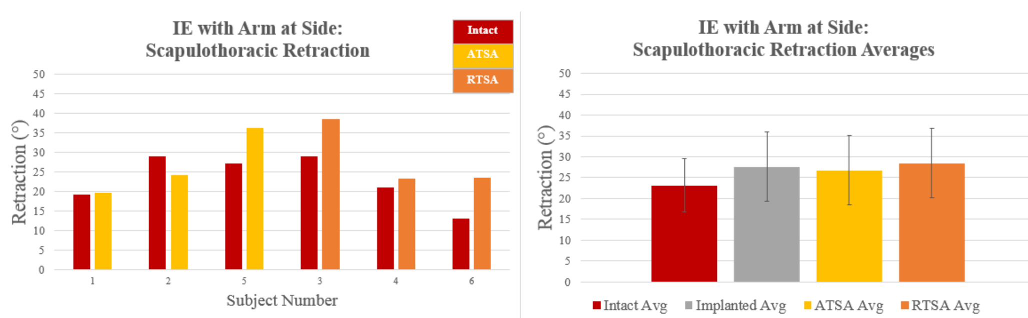

Figure 4-29 I/E with Arm at Side (left) and I/E with Arm Abducted 90° (right): Scapulothoracic Retraction

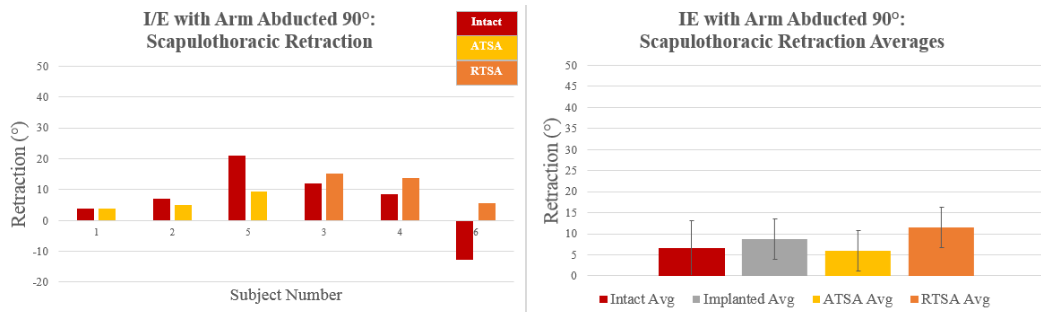

Figure 4-30 I/E with Arm at Side (left) and I/E with Arm Abducted 90° (right): Scapulothoracic Retraction Averages

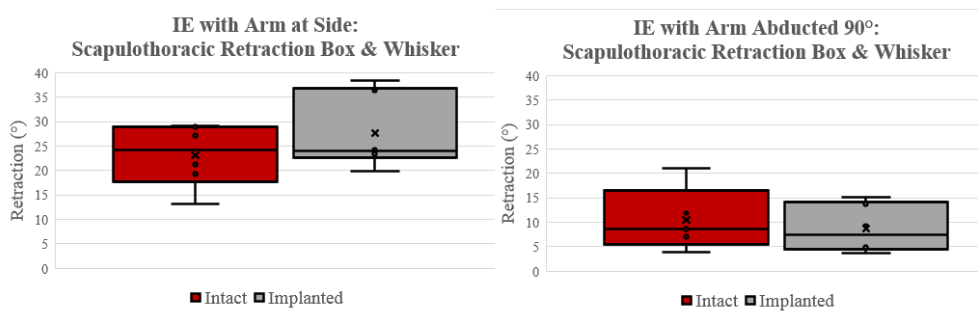

Figure 4-31 I/E with Arm at the Side (left) and with Arm Abducted 90 (right) Scapulothoracic Retraction: Box & Whisker Plots

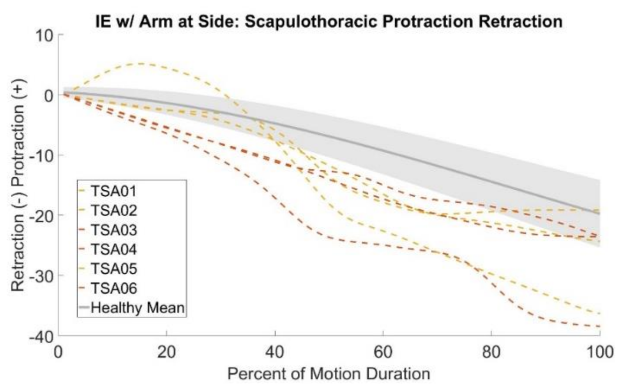

Figure 4-32 I/E with Arm at Side: Implanted Scapulothoracic Retraction Plotted Against Intact Mean (Dark Gray) and Standard Deviation (Gray Band)

Next, the third question will be addressed in the context of I/E motion: 3) Do any differences present between ATSA and RTSA implant designs?

As with abduction and flexion, no notable difference was found between ATSA and RTSA implant designs during I/E. *Figure 4-33* shows RTSA scapulothoracic I/E rotation plotted against ATSA mean. The three RTSA implanted shoulders do not show any clear difference from the ATSA mean and standard deviation, suggesting no notable difference in I/E scapula compensation rotation between the two implant designs.

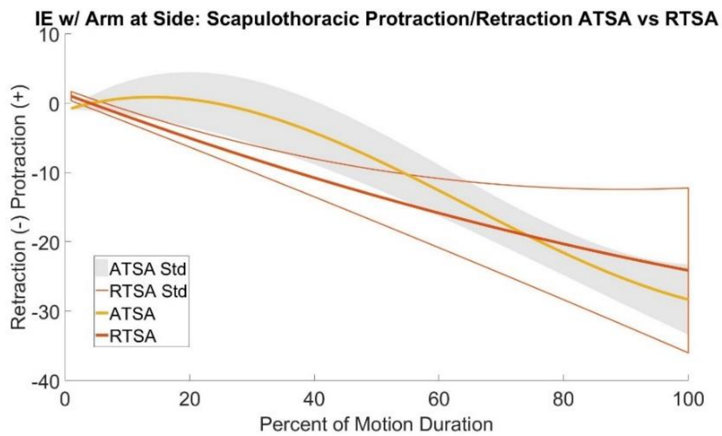

Figure 4-33 I/E with Arm at Side: RTSA (Orange) Scapulothoracic Retraction Plotted Against ATSA (Yellow) Standard Deviation (Gray Band)

The intact TSA06 outlier during I/E with the arm abducted to 90° in *Figure 4-30* reinforces why it is necessary to compare side-to-side in individuals, and addresses the fourth objective, 4) Does comparing side-to-side differences in individuals over healthy controls better reveal how TSA changes normal function? Upon further inspection, the outlier came from the subject performing a motion which involved upward arm elevation, which caused scapulothoracic protraction rather than retraction. When quantifying how TSA restores intact motion in individuals there is value in understanding that persons intact motion, and how it may be different from the norm, to better understand the impact of TSA. In calculating averages, this outlier was not included, but noted as a wholly different method of compensating for a decrease in I/E rotation.

4.5 Translations

Translation is an important part of daily motions such as abduction and flexion, but can be difficult to visualize; *Figure 4-34, Figure 4-35,* and *Figure 4-36* provide visual representations of how much the glenohumeral center of rotation moves superiorly during abduction.

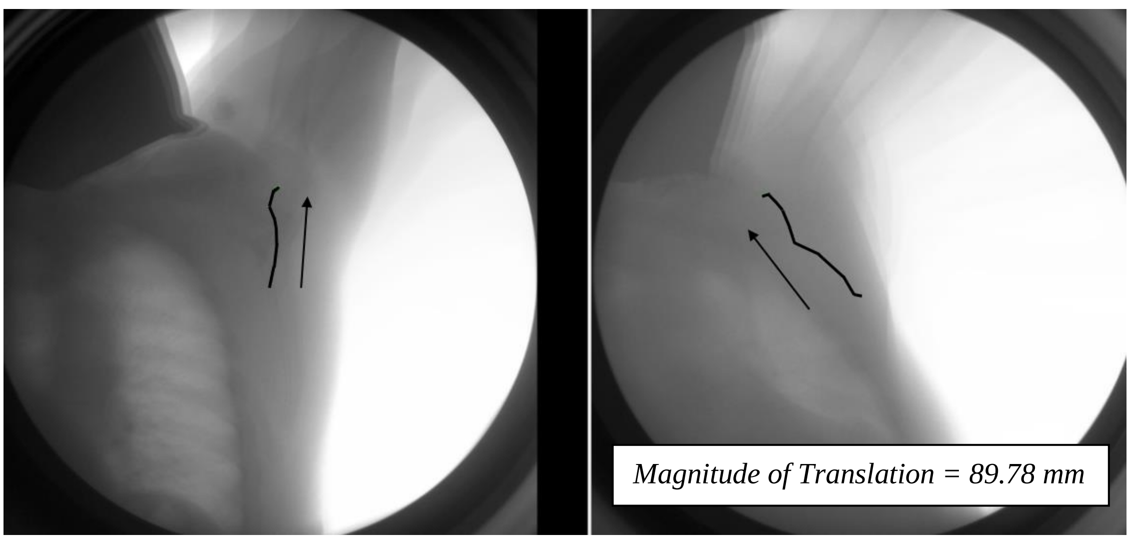

Figure 4-34 Intact Center of Rotation Translation in HSSR System Captured Videos (TSA02 Left Shoulder: Magnitude of Change = 89.78 mm)

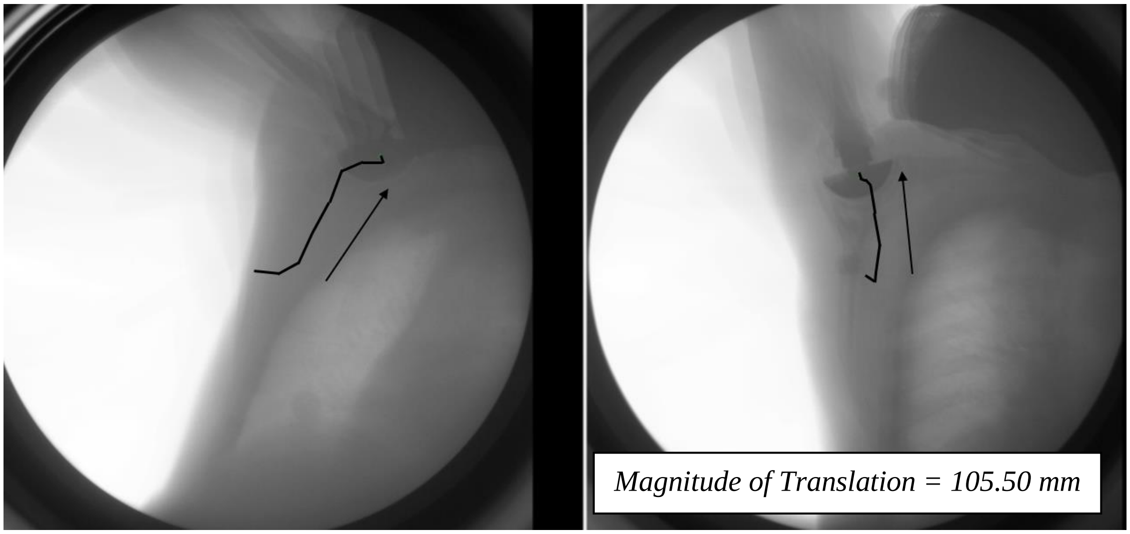

Figure 4-35 ATSA Center of Rotation Translation in HSSR System Captured Videos (TSA02 Right Shoulder: Magnitude of Change = 105.50 mm)

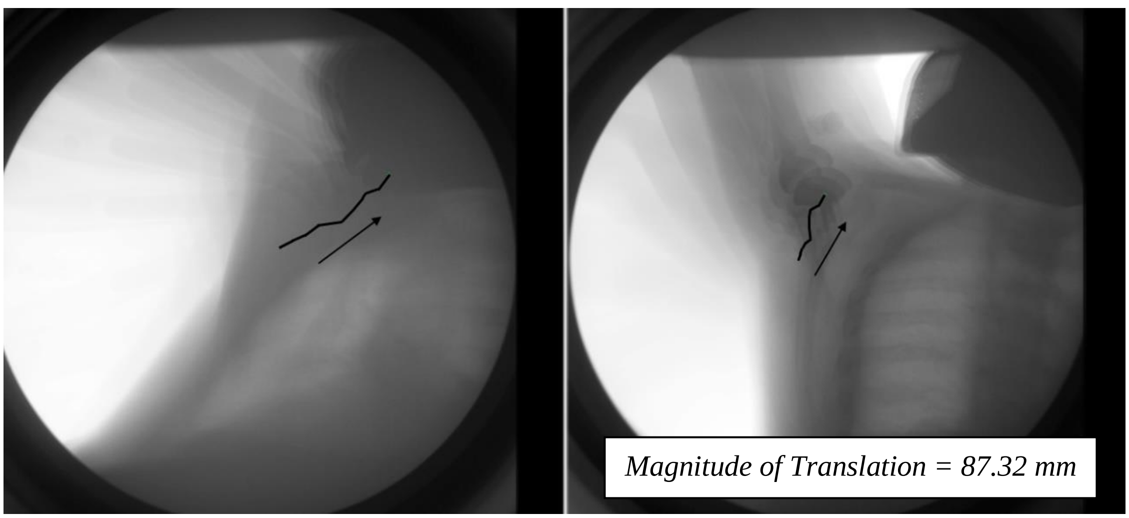

Figure 4-36 RTSA Center of Rotation Translation in HSSR System Captured Videos (TSA03 Right Shoulder: Magnitude of Change = 87.32 mm)

Superior / inferior (S/I) glenohumeral translations have the potential of revealing the differences in joint translation and stability between different shoulders. *Figure 4-37*, *Figure 4-38*, and *Figure 4-39* show S/I translations for intact, ATSA, and RTSA shoulders, respectively. Intact and ATSA translations show similar patterns: overall there is little change, about 5-8 mm; additionally, both intact and ATSA flexion trends show the same change to inferior translation near the end of the motion. RTSA shoulder S/I translation also as expected shows some superior change, but greater than intact or ATSA shoulders. The reason for this is an assigned RTSA humerus coordinate system that does not represent the actual center of rotation (at the center of the glenoid implant) of that joint. The expectation is that if the origin of the humerus coordinate system was relocated to the actual center of rotation, there would be less superior translation and therefore act more like a ball and socket joint. Additionally, there is no inferior dip in the flexion motion as with the other two shoulder types. It is hypothesized that this difference come from the very different geometry and mechanism of RTSA implants.

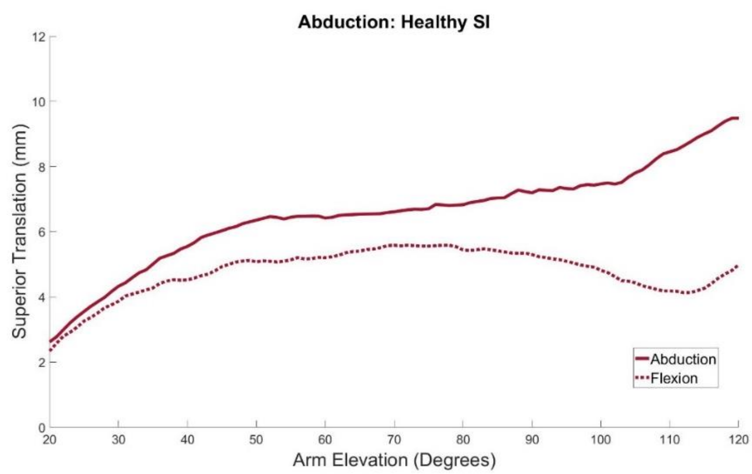

Figure 4-37 Abduction and Flexion Glenohumeral Superior / Inferior Translation for Intact Shoulders

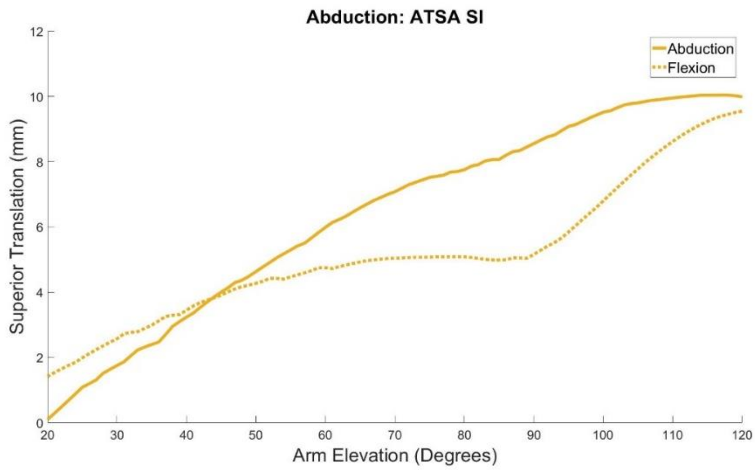

Figure 4-38 Abduction and Flexion Glenohumeral Superior / Inferior Translation for ATSA Shoulders

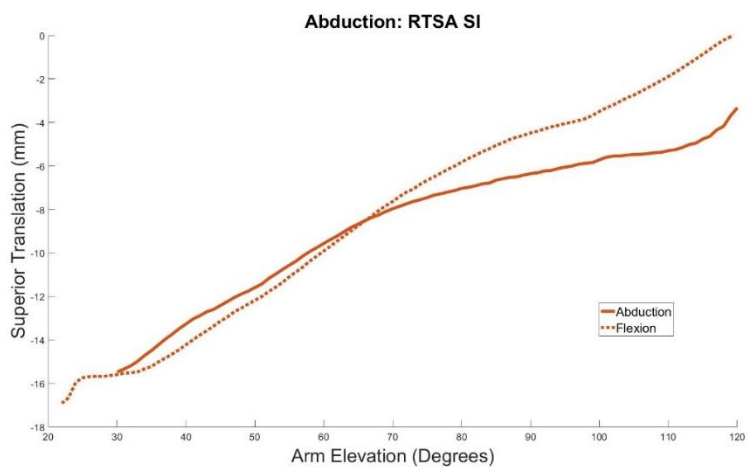

Figure 4-39 Abduction and Flexion Glenohumeral Superior / Inferior Translation for RTSA Shoulders

Chapter 5 Discussion

Comparative analysis of intact and TSA implanted kinematics within the same individual is essential for understanding how to improve current treatments of shoulder pathology and to suggest future research. Results have shown a wide variation in motion among an elderly subject population, which confirms the need to address pathology on an individual basis. Studying a patient's implanted shoulder compared to their own intact shoulder provided insight into how well the surgery restores that person's relative intact motion rather than comparing to a healthy control.

The six participants show that on average TSA restores intact arm elevation motion in abduction and forward flexion, but that patients often compensate for difficulty performing 'normal' glenohumeral elevation by increasing scapulothoracic elevation. This finding agrees with Walker et al. 2015, which reported that "there are greater demands for scapular motion after RTSA, and rehabilitation strategies should increasingly focus on strengthening the periscapular muscles to enhance function and to avoid common complications" [9]. Both ATSA and RTSA show some increase in scapular elevation over the intact average.

No significant differences, within the study's population of six, were found in results between the motion of patients with ATSA and patients with RTSA. In arm elevation during abduction, there is some indication that RTSA shoulders exhibited greater scapula compensation than ATSA and shoulders. A similar lack of differences was found between RTSA and ATSA kinematics during the I/E motions.

It's possible that within an individual the geometry of the implant has less effect compared to the individual shoulder anthropometry, motion, and musculature on the overall motion. The reason for performing TSA surgery is deteriorated glenohumeral bone structure and soft tissue, which means the integrity of those muscles post-surgery may still be a primary limiting factor on a patient's range of motion; the absence of notable differences between RTSA and ATSA style implants in this study suggests that the state of a patient's shoulder musculature has a larger impact on range of motion than implant design does. If both implant designs provide pain relief and reliable functionality and the patient's musculature is reasonably functional, the kinematics will likely be similar.

Within the study population TSA shoulders did not on average achieve the intact range of I/E motion for either the arm abducted to 0° or 90°. The average implanted I/E rotation was not within the range of intact standard deviation in either motion. A deficit was found comparing implanted to intact function for both internal and external rotation. This suggests the possibility for improvement in rehabilitation focusing on strengthening that motion to improve I/E mobility. It also points to studying the depleted use of muscles associated with the I/E humerus motion in a musculoskeletal model.

Results also showed that on average the participants compensated for I/E rotation with the arm at the side with some scapulothoracic retraction to improve the extent of the axial rotation.

Greater scapula compensation during elevation and I/E rotations over intact motion may be necessary to allow patients to achieve a functional range of motion. This would categorize as a negative outcome if compensating with the scapula caused more shoulder and back pain post-surgery. In a survey post-surgery TSA pain by Roberson et al., two papers recorded pain on a visual analog scale and reported a statistically significant decrease in pain 11.4 years post-surgery, and two papers employing the Constant-Murley pain scoring system also reported a statistically significant decrease in pain after 8.8 years [31]. Bjornholdt et al. in a survey of 538 shoulder replacement patients found that “Persistent pain is common 1-2 years after shoulder replacement” and reported that 28% of participants experience back pain during the period 1-2 years after the surgery [32]. This information suggests that rehabilitation after TSA surgery should include strengthening the muscles that aid in scapular rotation to improve patient implanted range of motion. Post-surgery rehabilitation is crucial to maintaining and building muscle strength to achieve better range of motion. Strengthening the deficient implanted glenohumeral joint is the common focus of rehabilitation [33], but more information on scapula-specific shoulder pain is needed to understand if scapular compensation is causing long-term pain.

Scapula compensation presented to a lesser extent in abduction and I/E with the arm abducted to 90°, and therefore these motions are recommended as a test of range of motion during a clinical exam. The reduced scapula rotation allows for a more isolated examination of the range of motion of the glenohumeral joint.

Future work to leverage this study is musculoskeletal modelling to make similar comparisons, between intact and implanted and ATSA and RTSA, but in the context of muscle moment arm and length. Clearer differences between ATSA and RTSA implant designs and the differences they make to primary arm lifting muscles and joint center of rotation can be investigated through this analysis. Musculoskeletal modeling has the potential to show "how theoretical alterations in implant geometry and placement might create more natural muscle function and shoulder articulation" [1].

A notable limit of this study is that its small subject population of six participants did not allow any statistical claims to be made on performance of intact or TSA implanted shoulders. Future work is recommended with a larger population. The population should contain individuals with one intact and one implanted shoulder for comparison to the results found in this study and should have an equal number of males and females to eliminate possible differences of sex. This would clarify the results found in this study and allow for statistical claims; for example, the hypothesis that there is no statistical difference between ATSA and RTSA performance or amount of scapula compensation during elevation or I/E motions could be confirmed or denied.

A sample power analysis was performed on subject TSA03 abduction data and a sample size of 11 participants is recommended for each ATSA and RTSA implant design types. A z-test for normally distributed data with a known standard deviation was chosen with a 5% significance level to detect differences between intact and implanted shoulder kinematics, a power level of 90% (a high standard for counting instances as significant), and an average abduction standard deviation of 17.44°.

Further limitations exist. Transitions were made to make kinematics data more comparable between subjects: 1) Only 'successful' patients with a TSA shoulder were used as subjects; no patients with lower satisfaction due to pain or limited motion were studied. 2) A static torso frame coincident with the neutral scapula frame was used in substitute of a dynamic thorax coordinate system as ISB recommended [15]. In our study as well as others, the neutral scapula frame was found to provide more consistent results in this patient population [21] [22] [9]. A laboratory setting which tested precise, clinical motions such as abduction, flexion, and I/E rotation with the arm limited to specific abduction values in only the coronal plane caused some participants to move in a similarly precise and therefore 'unnatural' way. Conversely, not all patients were able to follow instruction perfectly and therefore performed slightly different variations of the required motion. The decision was made to not use implant geometries from DePuy (DePuy Synthes Raynham, MA, USA) for tracking of the stereo radiography images, and instead to segment the implants along with patient bones to use for tracking; it is unknown if using DePuy implant geometries would further minimized bone measurement error. The method of assigning a humerus local coordinate system based off natural anatomy introduced some error when that same method was used for RTSA joints. Finally, side-to-side symmetry may not be an appropriate goal of TSA if the intact shoulder shows indications of pathology. The condition of a patient's intact side should be evaluated and made note of when used for comparison to the implanted side.

Comparing this study's range of motion to that required for activities of daily living is a useful measure of the success of TSA [34]. Gates et al. reported requirements of 0° - 108° of humeral-thoracic range of motion and -55° internal to 79° external humeral-thoracic range of motion. TSA is found to restore elevation range of motion but not internal or external function. Note that internal range of motion in this population's intact shoulders did not meet the requirement for daily living. Nor was the external range of motion met when the arm was abducted to 90°. This information suggests that improvements might be made on TSA function during I/E rotation.

In conclusion, this study investigated glenohumeral and scapulothoracic kinematics within six individuals with both an intact and an implanted shoulder, with either RTSA or ATSA. The study results found that TSA does restore intact elevation motion in abduction and forward flexion to be within the standard deviation of intact elevation within that same cohort. No notable differences in ATSA compared to RTSA kinematics were found because both the range of motion and how the motion was achieved was similar. Intact I/E humeral rotation was not found to be restored within the bounds of standard deviation for implanted shoulders performing I/E motions with the arm abducted to 0° and 90°. All motions showed some scapula compensation with a deficit in humeral function. A large difference in kinematic measures was found patient-to-patient; with such variation it was valuable to compare each TSA shoulder side-to-side with the intact in the same individual with the same musculature. Including aspects such as investigating the effect of arm dominance, where no statistically significant difference has been found in a young population, but which has not been determined in an elderly population, and including hand-held weights during data collection to enhance differences between intact and implanted shoulders would add valuable information to future work [22] [23]. Further work should be conducted with a similar population with musculoskeletal model analysis to reveal more about the impact TSA has on muscle function and shoulder articulation.

References

[1] K. Shelburne, P. Rullkoetter, B. Davidson, P. Laz and D. Weinstein, "Improving Function and Satisfaction with Total Shoulder Arthroplasty in the Elderly," 2017.

[2] "Human Skeleton Upper Body," Cultua, [Online]. Available: http://cultua.info/human-skeleton-upper-body/.

[3] "Human Shoulder Muscle Diagram and Muscles, Ligaments And Tendons Of The Human Back," Human Anatomy Library, 2018. [Online]. Available: humananatomylib.com.

[4] "Pectoral Muscles: Area, Innervation, & Function," KenHub, 28 December 2014. [Online]. Available: https://www.kenhub.com/en/register?topic=human_anatomy.

[5] C. C. Roberts, A. L. Ekelund, K. J. Renfree, P. T. Liu and F. S. Chew, "Radiologic Assessment of Reverse Shoulder Arthroplasty," *RadioGraphics,* vol. 27, pp. 223-235, 2007.

[6] S. Fealy, J. W. Sperling, R. F. Warren and E. V. Craig, Shoulder Arthroplasty, New York: Thieme Medical Publishers, Inc., 2008.

[7] K. Baumgarten, R. Osborn, W. Schweinle, M. J. Zens and E. Helsper, "Scapular Substitution After Rotator Cuff Repair Correlates with Postoperative Patient Outcome," *International Journal of Sports Physical Therapy,* vol. 13, no. 4, pp. 687-699, 2018.

[8] F. Fayad, A. Roby-Brami, C. Yazbeck, S. Hanneton, M.-M. Lefevre-Colau, V. Gautheron, S. Poiraudeau and M. Revel, "Three-dimensional scapular kinematics and scapulohumeral rhythm in patients with glenohumeral osteoarthritis or frozen shoulder," *Journal of Biomechanics,* vol. 41, no. 2, pp. 326-332, 2008.

[9] D. Walker, K. Matsuki, A. M. Struk, T. W. Wright and S. A. Banks, "Scapulohumeral rhythm in shoulders with reverse shoulder arthroplasty," *Journal of Shoulder and Elbow Surgery,* vol. 24, pp. 1129-1134, 2015.

[10] C. Woon and M. Miller, "Glenohumeral Internal Rotation Deficit (GIRD)," Ortho Bullets, 12 May 2019. [Online]. Available: https://www.orthobullets.com/shoulder-and-elbow/3055/glenohumeral-internal-rotation-deficit-gird.

[11] A. R. Karduna, P. W. McClure, L. A. Michener and B. Sennett, "Dynamic Measurements of Three-Dimensional Scapular Kinematics: A Validation Study," *ASME*, vol. 123, pp. 184-190, 2001.

[12] D. L. Benoit, D. K. Ramsey, M. Lamontagne, L. Xu, P. Wretenberg and P. Renstrom, "Effect of skin movement artifact on knee kinematics during gait and cutting motions measured in vivo," *Gait Posture,* vol. 24, no. 2, pp. 152-164, 2005.

[13] J. D. Mozingo, M. A. Shandiz, F. M. Marquez, B. A. Schueler, D. R. Holmes, C. H. McCollough and K. D. Zhao, "Validation of imagining-based quantification of glenohumeral joint kinematics using an unmodified clinical biplane fluoroscopy system," *Journal of Biomechanics,* vol. 71, pp. 306-312, 2018.

[14] E. Grood and W. J. Suntay, "A Joint Coordinate System for the Clinical Description of Three-Dimensional Motions: Application to the Knee," *Journal of Biomechanical Engineering,* vol. 105, pp. 136-144, 1983.

[15] G. Wu, F. C. van der Helm, H. (. Veeger, M. Makhsous, P. Van Roy, C. Anglin, J. Nagels, A. R. Karduna, K. McQuade, X. Wang, F. W. Werner and B. Buchholz, "ISB recommendation on definitions of joint coordiante systems of various joints for the reporting of human joint motion - Part 2: shoulder, elbow, wrist and hand," *Journal of Biomechanics,* vol. 38, pp. 981-992, 2005.

[16] J. E. Giphart, J. P. Brunkhorst, N. H. Horn, K. B. Shelburne, M. R. Torry and P. J. Millett, "Effect of Plane of Arm Elevation on Glenohumeral Kinematics: A Normative Biplane Fluoroscopy Study," *The Journal of Bone and Joint Surgery,* vol. 95, pp. 238-245, 2013.

[17] W. Sahara, T. Yamazaki, S. Konda, K. Sugamoto and H. Yoshikawa, "Influence of humeral abduction angle on axial rotation and contact area at the glenohumeral joint," *Journal of Shoulder and Elbow Surgery,* vol. 28, pp. 570-577, 2019.

[18] A. R. Karduna, P. W. McClure and L. A. Michener, "Scapular kinematics: effects of altering the Euler angle sequence of rotations," *Journal of Biomechanics,* vol. 33, pp. 1063-1068, 2000.

[19] A. Seth, R. Matias, A. P. Veloso and S. L. Delp, "A Biomechanical Model of the Scapulothoracic Joint to Accuractly Capture Scapular Kinematics during Shoulder Movements," *PLoS ONE,* vol. 11, no. 1, pp. 1-18, 2016.

[20] P. W. McClure, L. A. Michener, B. J. Sennett and A. R. Karduna, "Direct 3-dimensional measurement of scapular kinematics during dynamic movements in vivo," *Journal of Shoulder and Elbow Surgery*, vol. 10, pp. 269-277, 2001.

[21] T. Kijima, K. Matsuki, N. Ochiai, T. Yamaguchi, Y. Sasaki, E. Hashimoto, Y. Sasaki, S. Yamazki, Y. Masuda, H. Umekita, S. A. Banks and K. Takahashi, "In vivo 3-dimensional analysis of scapular and glenohumeral kinematics: comparison of symptomatic or asymptomatic shoulders with rotator cuff tears and healthy shoulders," *Journal of Shoulder and Elbow Surgery,* vol. 24, pp. 1817-1826, 2015.

[22] Y. Kon, N. Nishinaka, K. Gamada, H. Tsutsui and S. A. Banks, "The influence of handheld weight on the scapulohumeral rhythm," *Journal of Shoulder and Elbow Surgery* , vol. 17, pp. 943-946, 2008.

[23] K. Matsuki, K. 0. Matsuki, S. Mu, S. Yamaguchi, N. Ochiai, T. Sasho, H. Sugaya, T. Yoyone, Y. Wada, K. Takahashi and S. A. Banks, "In vivo 3-dimensional analysis of scapular kinematics: comparison of dominant and nondominant shoulders," *Journal of Shoulder and Elbow Surgery,* vol. 20, pp. 659-665, 2011.

[24] D. R. Walker, A. M. Struk, K. Matsuki, T. W. Wright and S. A. Banks, "How do deltoid muscle moment arms change after reverse total shoulder arthroplasty," *Journal of Shoulder and Elbow Surgery,* vol. 25, pp. 581-588, 2016.

[25] D. C. Ackland, P. Pak, M. Richardson and M. G. Pandy, "Moment arms of the muscles crossing the anatomical shoulder," *Journal of Anatomy,* vol. 213, pp. 383-390, 2008.

[26] C. Belvedere, A. Leardini, F. Cantani, S. Piagigiani and B. Innocenti, "In vivo kinematics of knee replacement during daily living activities: Condylar and post-cam contact assessment by three-dimensional fluoroscopy and finite element analyses," *Journal of Orthopaedic Research,* vol. 35, no. 7, pp. 1396-1403, 2016.

[27] V. Kefala, "Assessment of Normal Knee Kinematics using High-Speed Stereo-Radiography System," 2015.

[28] N. Doriot and X. Wang, "Effects of age and gender on maximum voluntary range of motion of the upper body joints," *Ergonomics,* vol. 49, no. 3, pp. 269-281, 2006.

[29] C. Charbonnier, S. Chague, F. Kolo, J. Chow and A. Ladermann, "A patient-specific measurement technique to model shoulder joint kinematics," *Orthopaedics & Traumatology: Surgery & Research,* vol. 100, pp. 715-719, 2014.

[30] E. E. Butler and J. Rose, "The Pediatric Upper Limb Motion Index and a temporal-spatial logistic regression: Quantitative analysis of upper limb movement disorders during the Reach and Grasp Cycle," *Journal of Biomechanics,* vol. 45, pp. 945-951, 2012.

[31] T. A. Roberson, J. C. Bentley, J. T. Griscom, M. J. Kissenberth, S. J. Tolan, R. J. Hawkins and J. M. Tokish, "Outcomes of total shoulder arthroplasty in patients younger than 65 years: a systematic review," *Journal of Shoulder and Elbow Surgery,* vol. 26, pp. 1298-1306, 2017.

[32] K. T. Bjornhold, B. Brandsborg, K. Soballe and L. Nikolajsen, "Persistent pain is common 1-2 years after shoulder replacement: A nationwide registry-based questionnaire study of 538 patients," *Acta Orthopaedica,* vol. 86, no. 1, pp. 71-77, 2015.

[33] M. Kraus, G. Krischak and L. Tepohl, "Postoperative Rehabilitation of Patients with Shoulder Arthroplasty - A Review of the Standard Care," *International Journal of Physical Medicine and Rehabilitation,* vol. 5, no. 1, pp. 1-7, 2014.

[34] D. H. Gates, L. S. Walters, J. Cowley, J. M. Wilken and L. Resnik, "Range of Motion Requirements for Upper-Limb Activities of Daily Living," *The American Journal of Occupational Therapy,* vol. 70, no. 1, pp. 1-50, 2016.

Appendices

Appendix A: Standard Deviations

Subject	Implant Side	Motion	Left Shoulder							Right Shoulder						
			Scapulothoracic			Glenohumeral				Scapulothoracic			Glenohumeral			
			Elev.	I/E	Ant. / Post.	Elev.	Plane of Elev.	I/E	S/I Translation	Elev.	I/E	Ant. / Post.	Elev.	Plane of Elev.	I/E	S/I Translation
TSA01	Right ATSA	Abduction	12.69	1.30	9.85	23.32	7.32	24.55	2.37	16.29	8.72	8.99	19.95	18.79	7.47	4.18
		Flexion	18.10	12.60	19.88	25.81	4.90	13.06	8.23	14.20	14.53	17.83	16.78	27.88	22.47	3.07
		IE with Arm at Side	4.99	7.06	4.35	1.70	25.13	6.95		4.66	7.82	4.65	2.31	19.47	12.58	
		IE with Arm Abducted 90°	1.01	1.09	2.25	4.94	25.63	1.52		1.07	1.84	1.54	0.85	9.85	1.24	
TSA02	Right ATSA	Abduction	17.63	6.04	12.92	27.72	23.50	20.33	5.70	14.77	5.73	9.74	28.48	24.38	19.22	1.61
		Flexion	12.92	8.93	16.67	28.57	10.89	19.95	3.57	19.74	15.14	12.59	18.34	14.08	7.30	1.47
		IE with Arm at Side	12.20	8.84	5.76	6.59	34.62	9.01		7.81	8.50	3.59	8.12	26.98	9.28	
		IE with Arm Abducted 90°	3.68	2.18	1.07	1.99	33.75	4.40		3.93	1.47	2.43	1.14	14.92	2.76	
TSA03	Right RTSA	Abduction	22.89	14.52	20.92	12.04	26.05	18.79	2.98	22.89	14.52	20.92	12.04	26.05	18.79	3.40
		Flexion	16.90	10.59	22.88	15.14	13.31	8.74	2.12	16.90	10.59	22.88	15.14	13.31	8.74	3.18
		IE with Arm at Side	4.65	11.95	3.39	4.22	23.98	13.01		4.65	11.95	3.39	4.22	23.98	13.01	
		IE with Arm Abducted 90°	8.96	5.10	5.39	2.90	7.75	6.84		8.96	5.10	5.39	2.90	7.75	6.84	
TSA04	Right RTSA	Abduction	16.18	13.29	23.21	26.71	15.53	16.31	1.80	16.13	2.24	9.30	18.10	14.89	10.83	5.05
		Flexion	17.28	9.60	20.16	24.75	15.37	14.05	1.06	13.26	6.92	21.62	13.05	9.67	9.26	6.53
		IE with Arm at Side	5.16	7.33	1.75	3.95	19.25	2.90		2.55	4.50	0.72	2.25	4.06	2.91	
		IE with Arm Abducted 90°	3.85	3.01	3.80	3.46	33.62	8.24		8.80	4.52	4.02	4.22	5.69	9.38	
TSA05	Left ASTA	Abduction	17.32	9.63	20.20	18.15	9.18	13.74	1.73	14.09	4.22	10.07	20.51	12.04	13.22	2.50
		Flexion	17.16	8.86	17.11	17.57	21.18	8.31	1.81	14.19	4.71	14.20	17.22	6.66	17.84	4.43
		IE with Arm at Side	14.88	14.62	1.28	5.53	22.33	5.53		8.80	10.36	6.98	3.57	12.47	6.73	
		IE with Arm Abducted 90°	1.18	4.07	1.53	2.38	17.37	6.10		4.61	7.67	1.26	2.00	45.33	26.06	
TSA06	Left RTSA	Abduction	17.03	23.62	3.90	9.59	17.63	15.93	5.06	21.33	4.73	5.00	36.29	20.87	17.31	3.01
		Flexion	15.92	11.91	22.87	22.27	15.00	11.34	6.16	12.47	10.99	17.55	29.07	9.79	15.67	2.96
		IE with Arm at Side	3.43	7.62	0.96	1.35	13.17	1.82		4.49	5.36	2.14	4.43	26.78	8.86	
		IE with Arm Abducted 90°	9.77	2.11	9.94	2.80	12.23	3.85		6.62	3.20	8.86	6.52	27.10	5.46	
Average			Left and Right Shoulders													
		Abduction	17.44	9.05	12.92	21.08	18.02	16.37	3.28							
		Flexion	15.75	10.45	18.85	20.31	13.50	13.06	3.71							
		IE with Arm at Side	6.52	8.83	3.24	4.02	21.02	7.72								
		IE with Arm Abducted 90°	5.20	3.45	3.96	3.01	20.08	6.89								

Appendix B: Confidence Levels

	Glenohumeral		Scapulothoracic	
	Abduction			
	Intact	Implanted	Intact	Implanted
Standard Deviation	16.0	14.5	9.9	11.1
95% Confidence	[10.0, 39.2]	[9.0, 35.5]	[6.2, 24.3]	[6.9, 27.2]
	Flexion			
	Intact	Implanted	Intact	Implanted
Standard Deviation	11.4	10.6	5.0	8.9
95% Confidence	[7.1, 27.9]	[6.6, 25.9]	[3.1, 12.3]	[5.6, 21.9]
	I/E with Arm at Side			
	Intact	Implanted	Intact	Implanted
Standard Deviation	23.9	15.3	6.4	7.7
95% Confidence	[15.2, 52.6]	[9.5, 37.5]	[4.0, 15.7]	[4.8, 18.9]
	I/E with Arm Abducted 90°			
	Intact	Implanted	Intact	Implanted
Standard Deviation	12.4	10.7	6.6	8.7
95% Confidence	[7.7, 30.4]	[6.7, 26.3]	[7.0, 27.4]	[3.0, 11.9]

Appendix C: Raw Kinematics Data

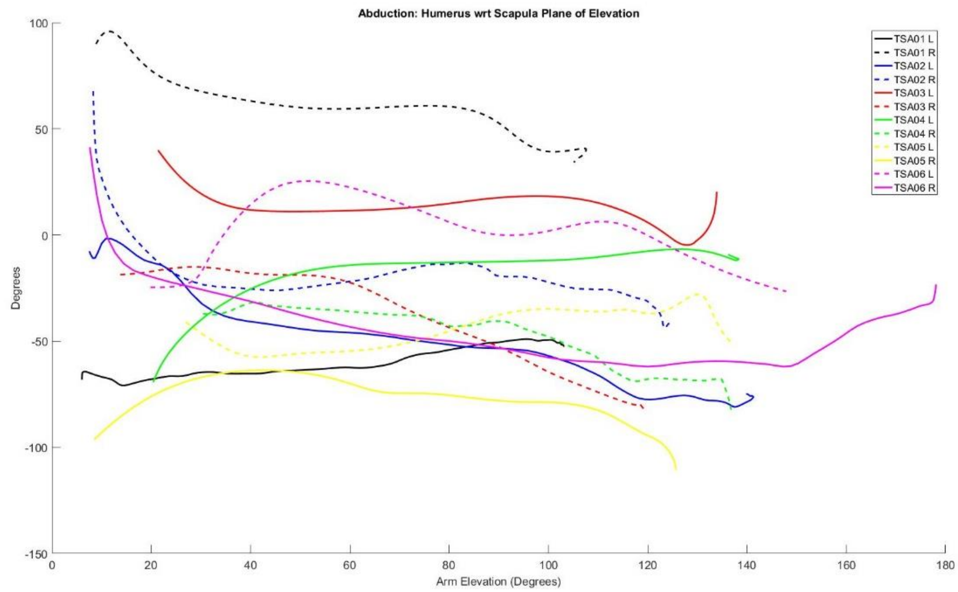

Figure C. 1 Abduction: Plane of Elevation

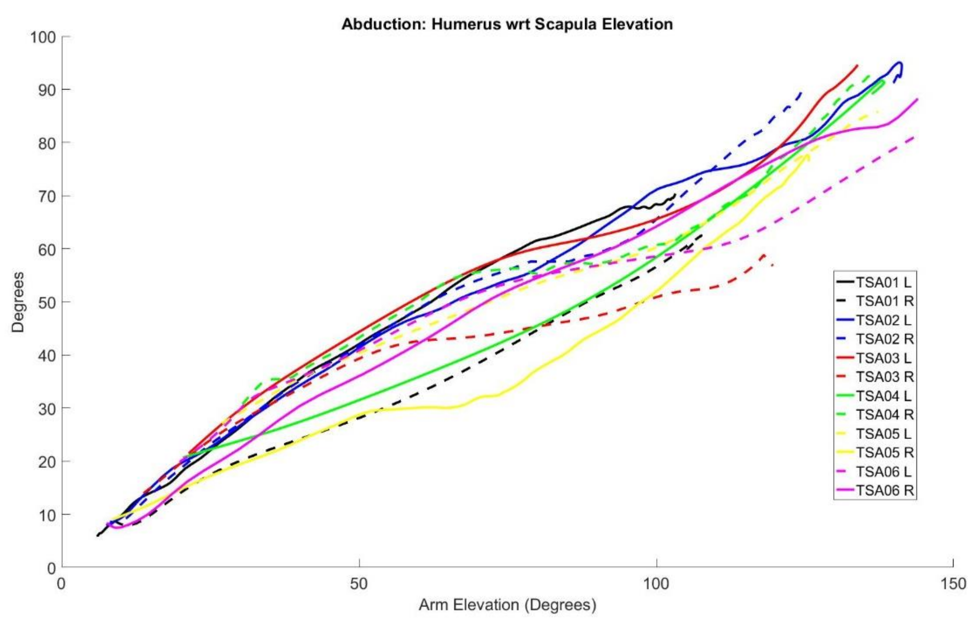

Figure C. 2 Abduction: Glenohumeral Elevation

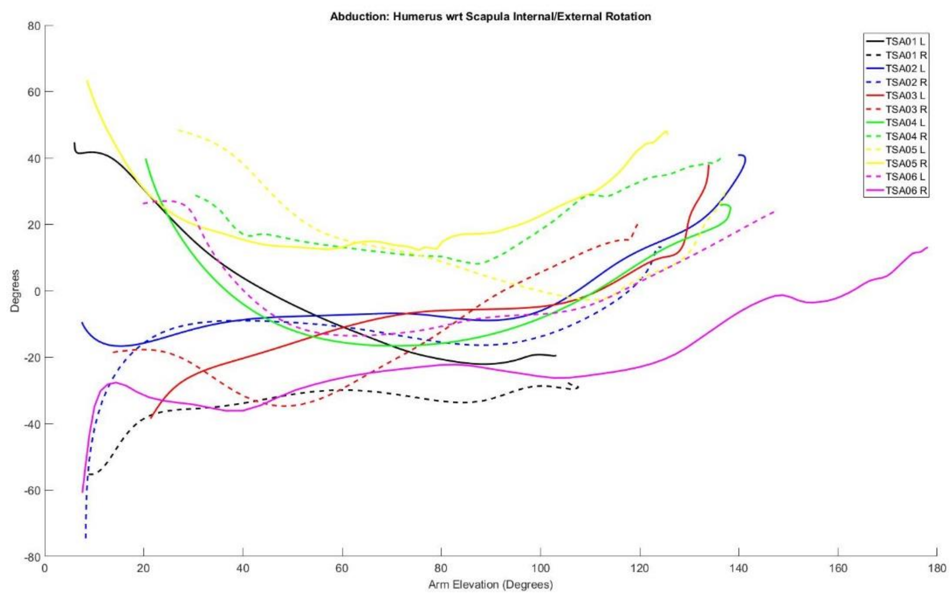

Figure C. 3 Abduction: Glenohumeral I/E Rotation

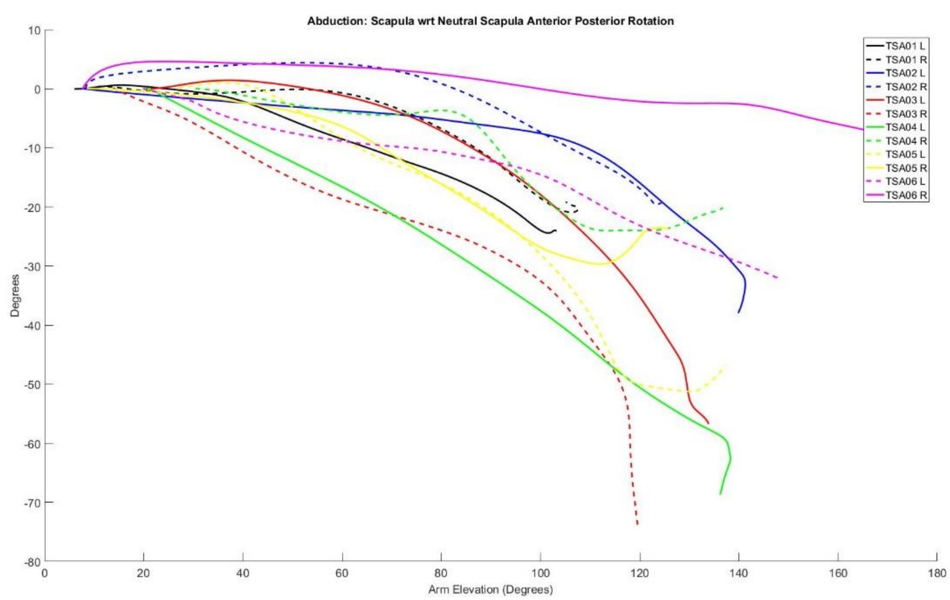

Figure C. 4 Abduction: Scapulothoracic Anterior / Posterior Rotation

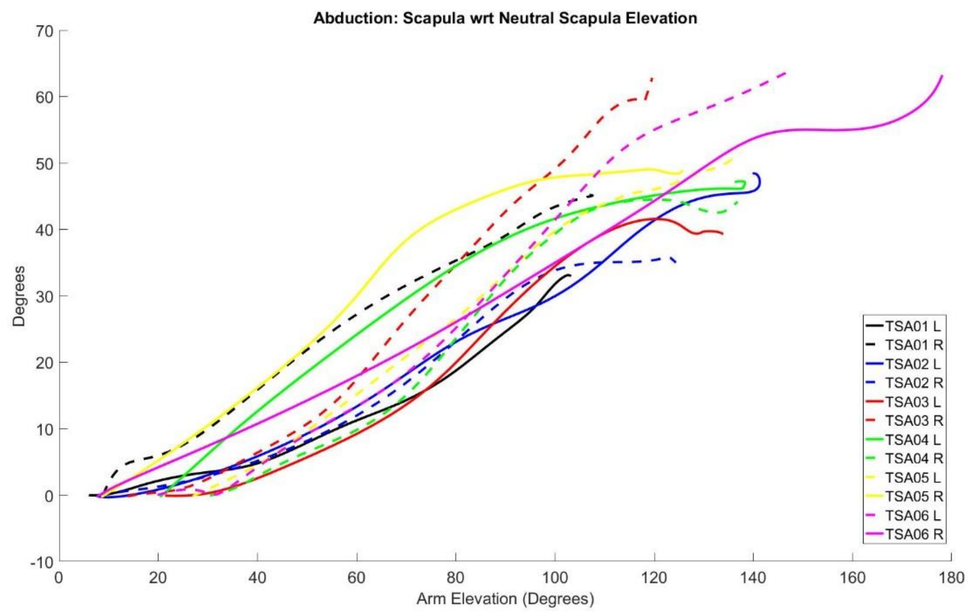

Figure C. 5 Abduction: Scapulothoracic Upward Tilting

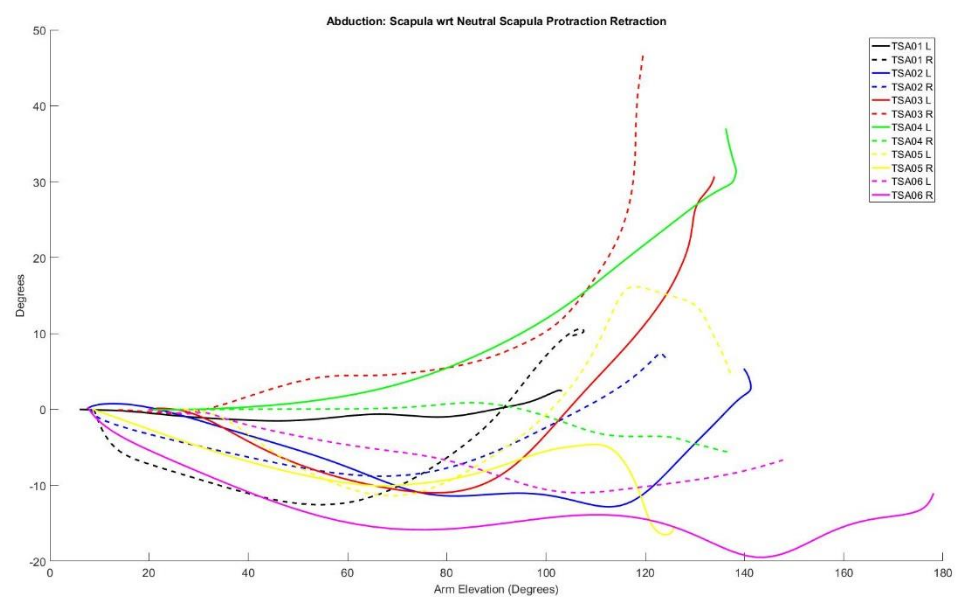

Figure C. 6 Abduction: Scapulothoracic Protraction / Retraction

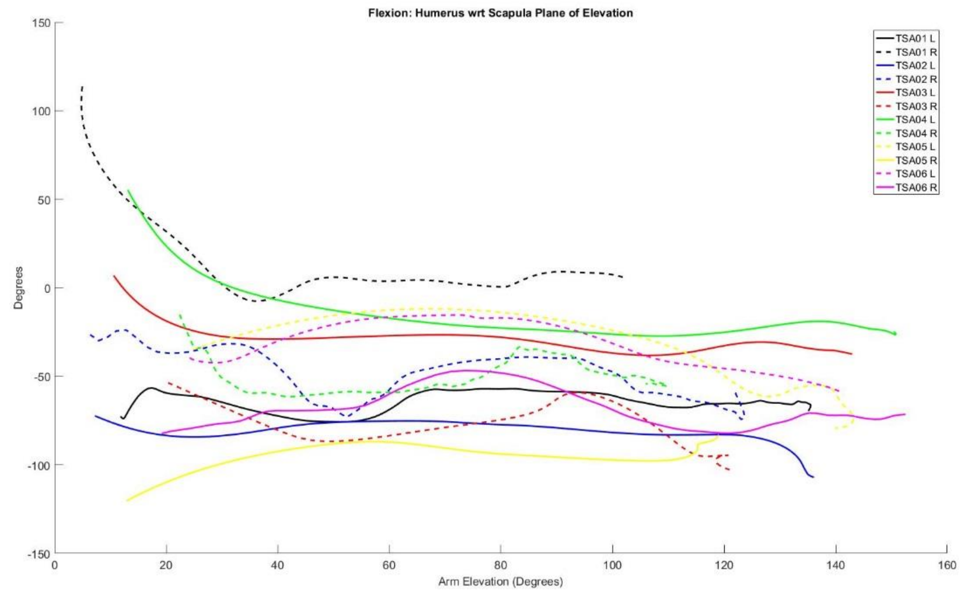

Figure C. 7 Flexion: Glenohumeral Plane of Elevation

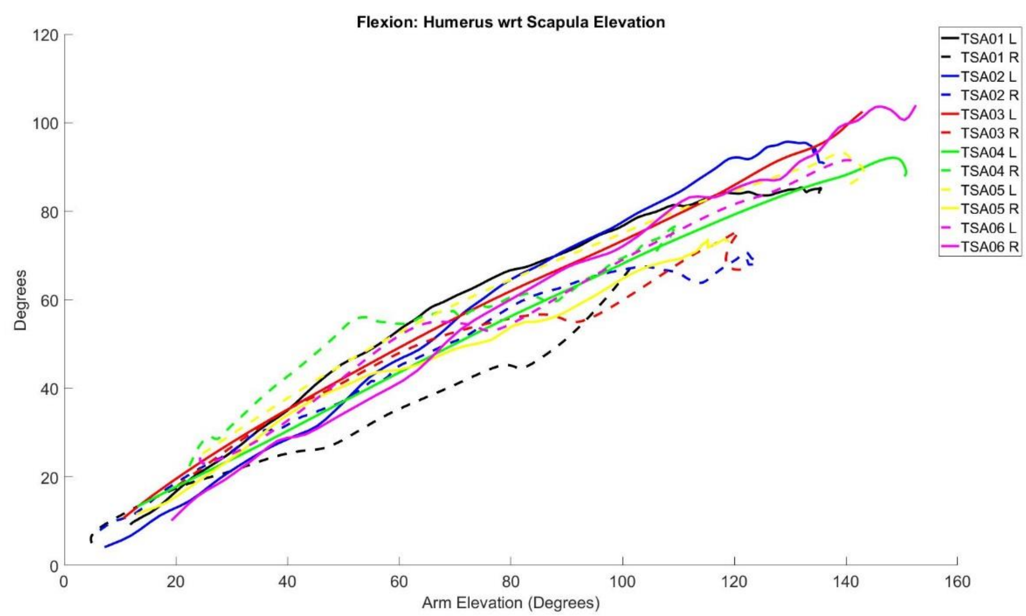

Figure C. 8 Flexion: Glenohumeral Elevation

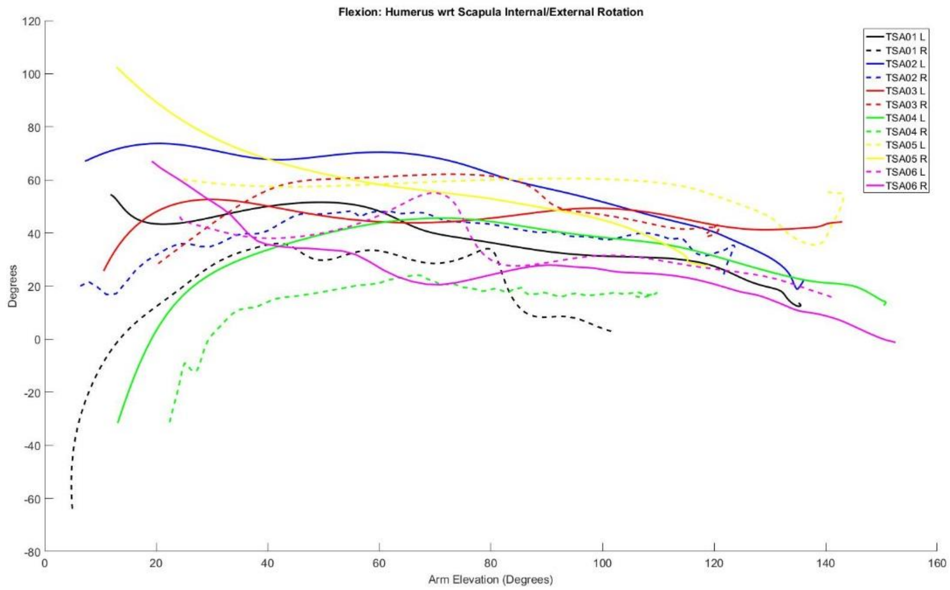

Figure C. 9 Flexion: Glenohumeral I/E Rotation

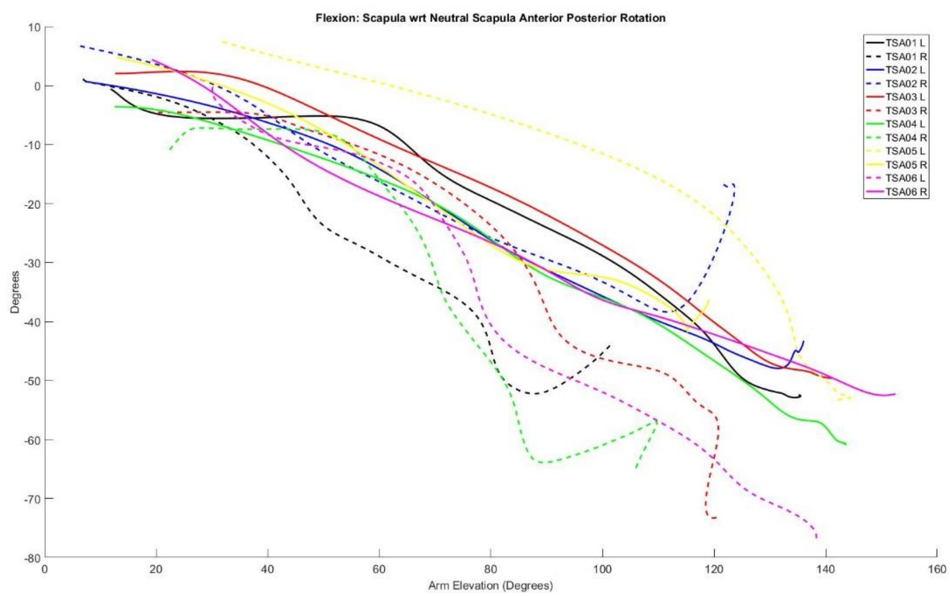

Figure C. 10 Flexion: Scapulothoracic Anterior / Posterior Rotation

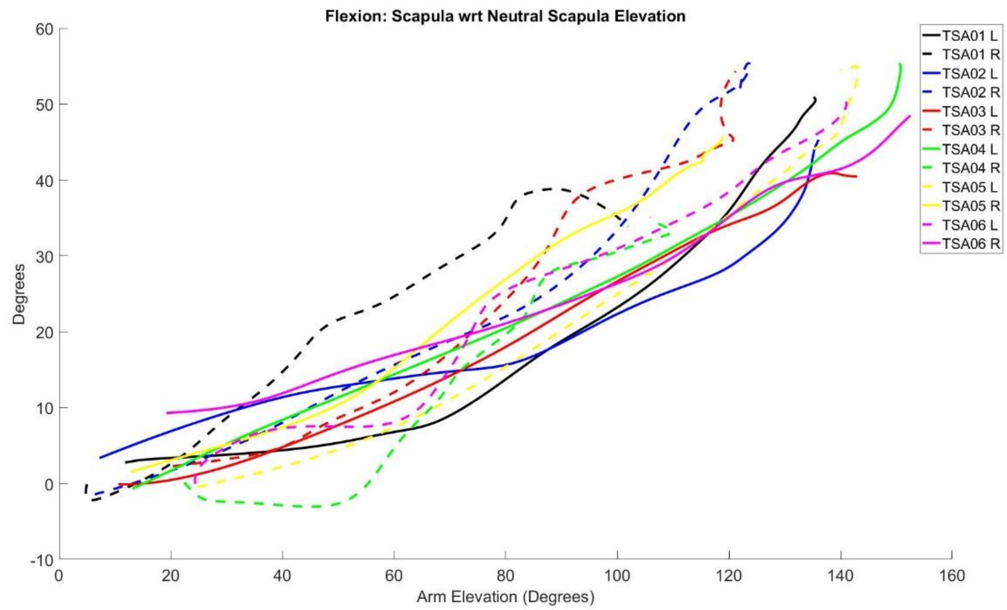

Figure C. 11 Flexion: Scapulothoracic Upward Tilting

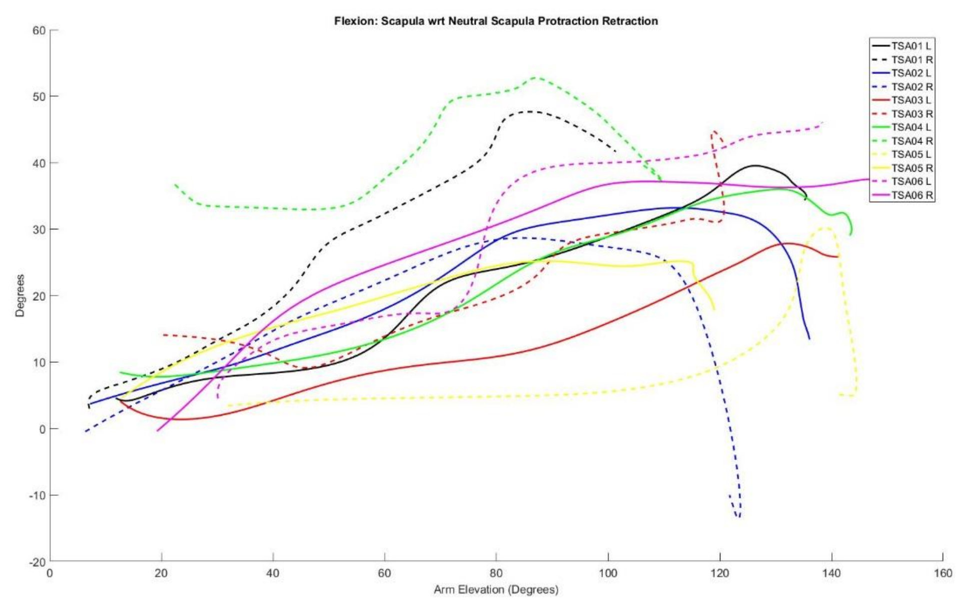

Figure C. 12 Flexion: Scapulothoracic Retraction / Protraction

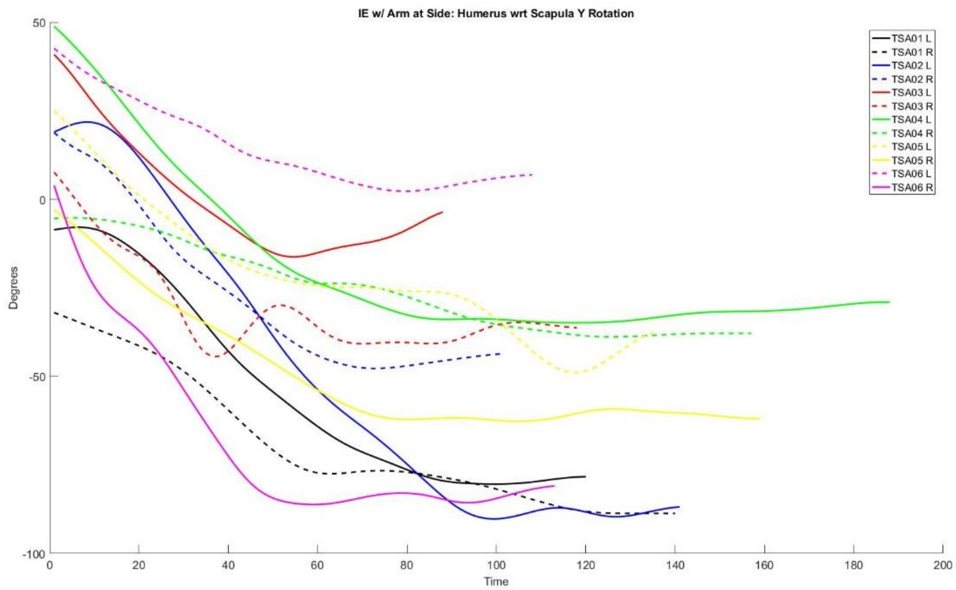

Figure C. 13 I/E with Arm at Side: Glenohumeral Y Rotation

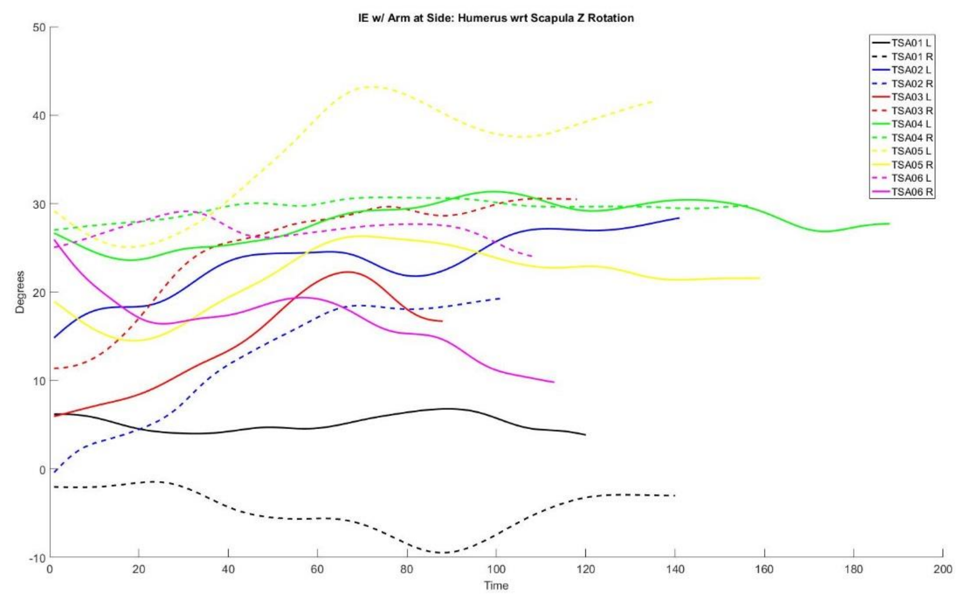

Figure C. 14 I/E with Arm at Side: Glenohumeral Z Rotation

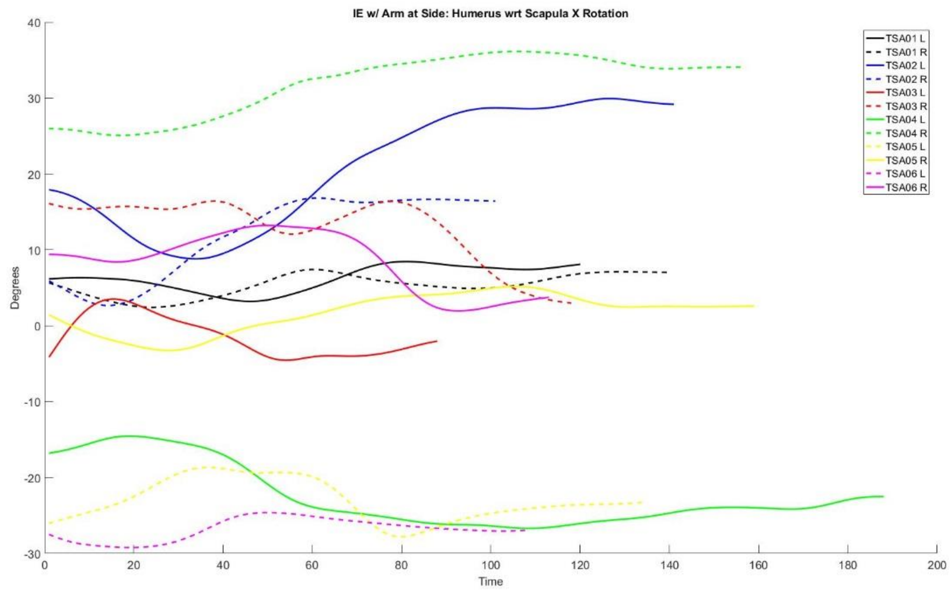

Figure C. 15 I/E with Arm at Side: Glenohumeral X Rotation

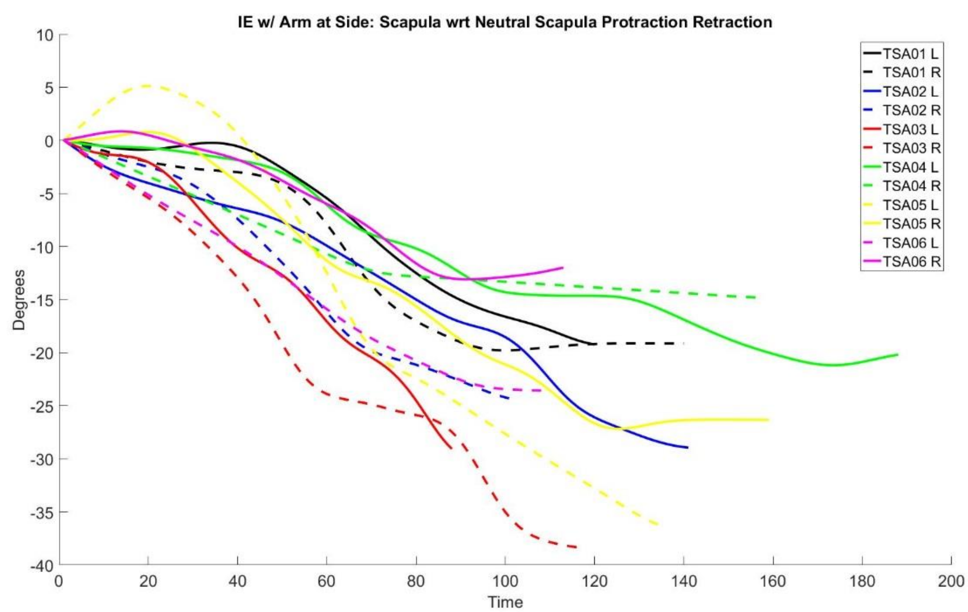

Figure C. 16 I/E with Arm at Side: Scapulothoracic Retraction / Protraction

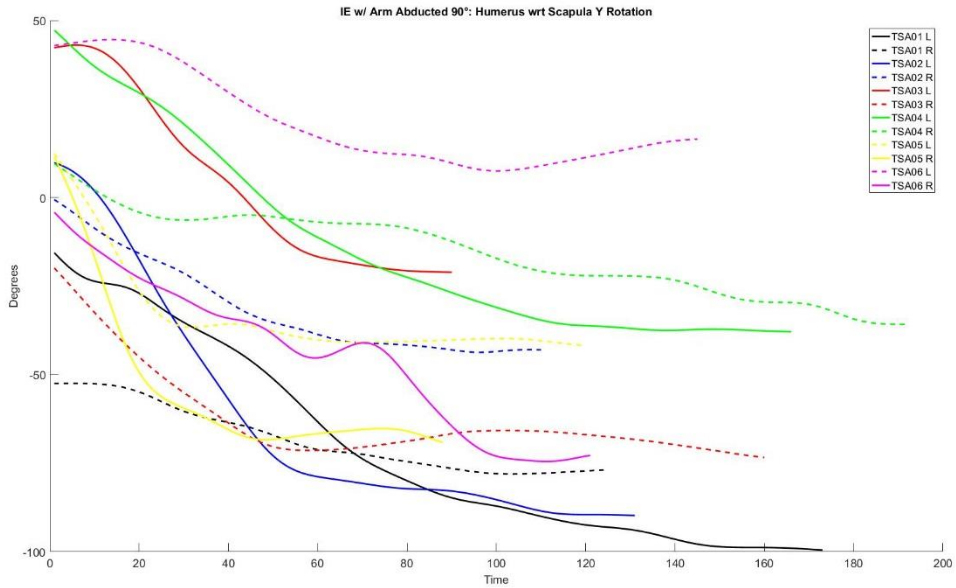

Figure C. 17 I/E with Arm Abducted 90°: Glenohumeral Y Rotation

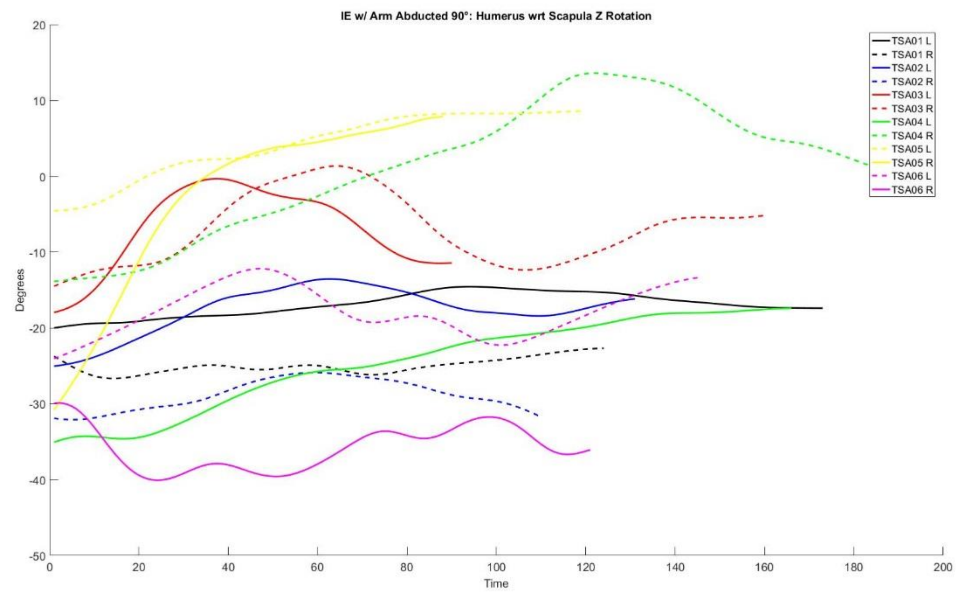

Figure C. 18 I/E with Arm Abducted 90°: Glenohumeral Z Rotation

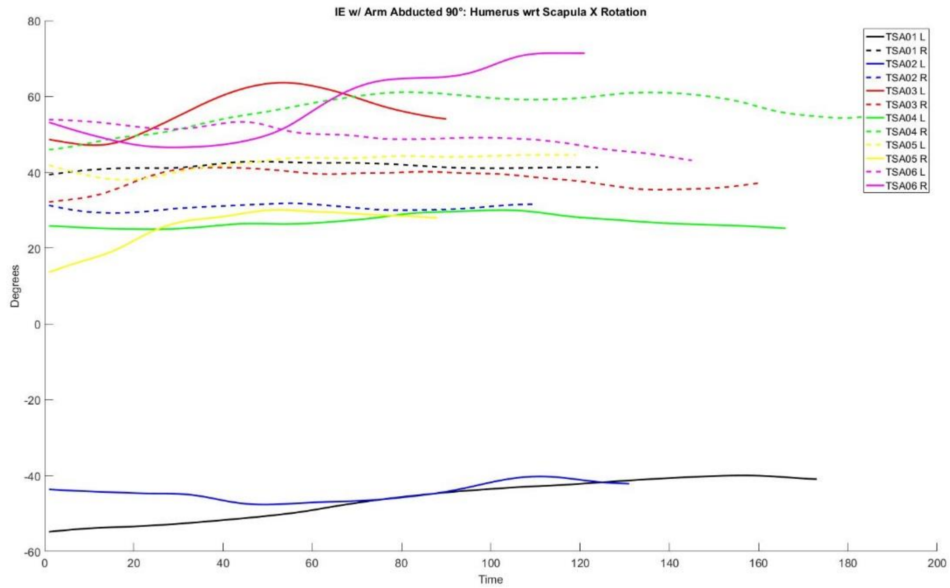

Figure C. 19 I/E with Arm Abducted 90°: Glenohumeral X Rotation

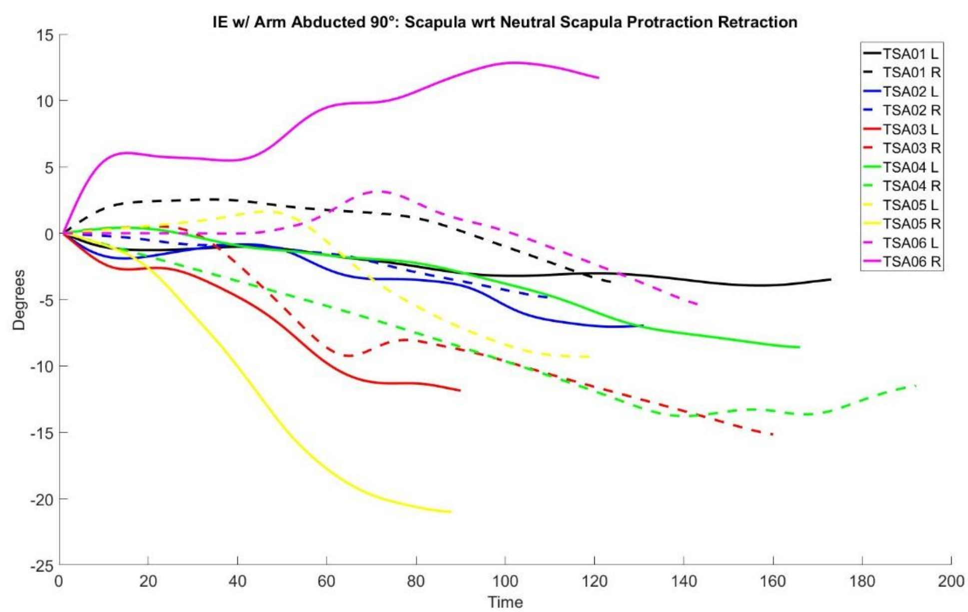

Figure C. 20 I/E with Arm Abducted 90°: Scapulothoracic Retraction / Protraction

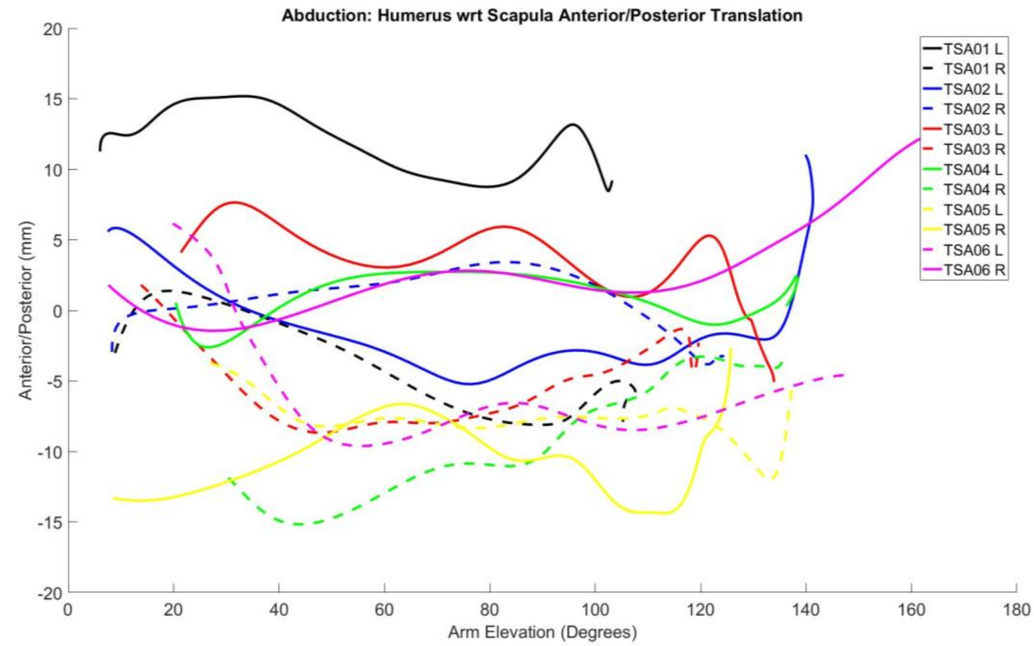

Figure C. 21 Abduction Anterior / Posterior Translation

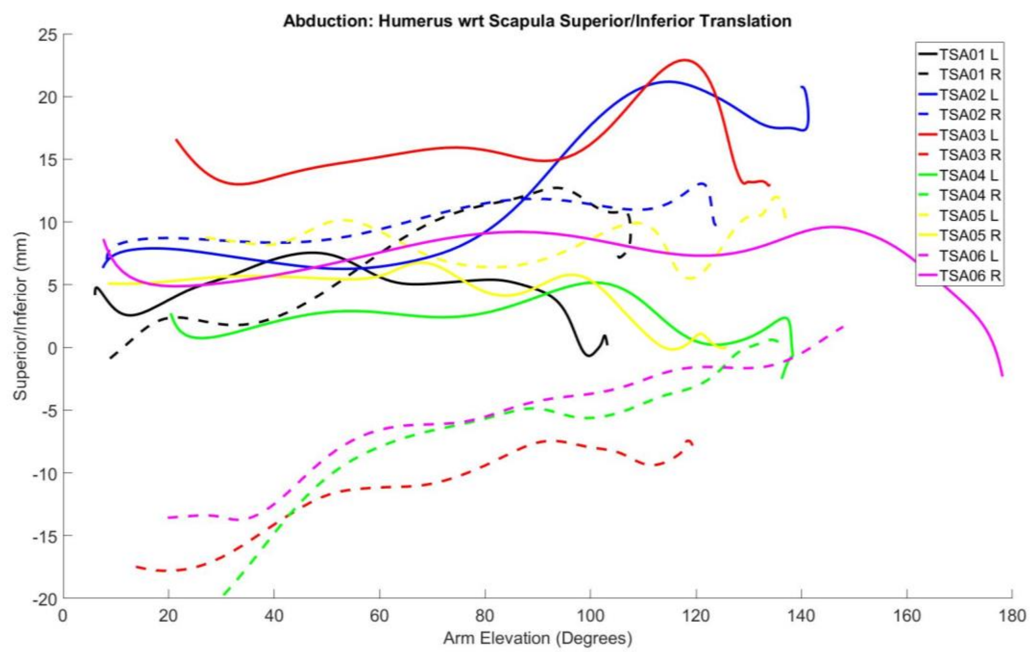

Figure C. 22 Abduction Superior / Inferior Translation

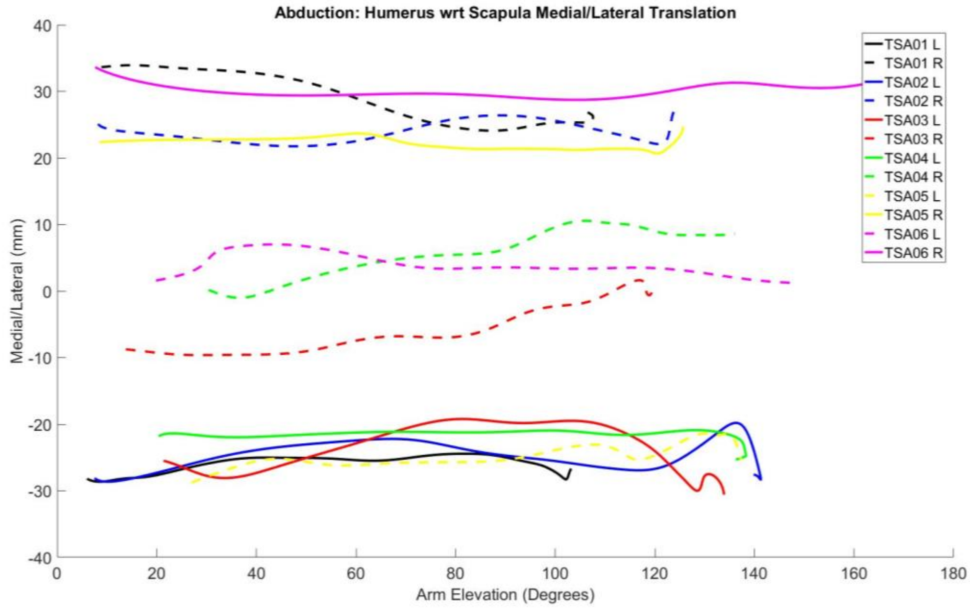

Figure C. 23 Abduction Medial / Lateral Translation

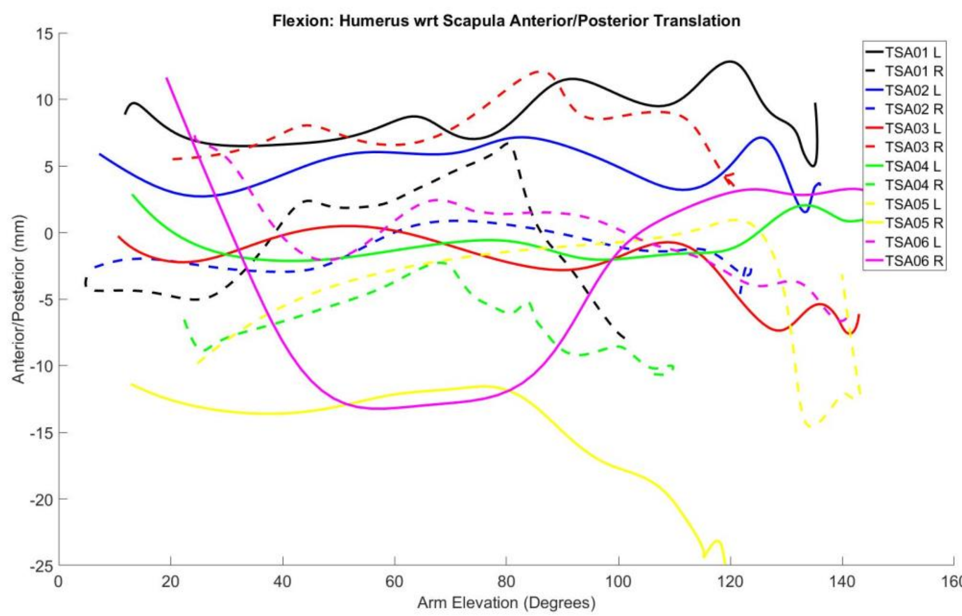

Figure C. 24 Flexion Anterior / Posterior Translation

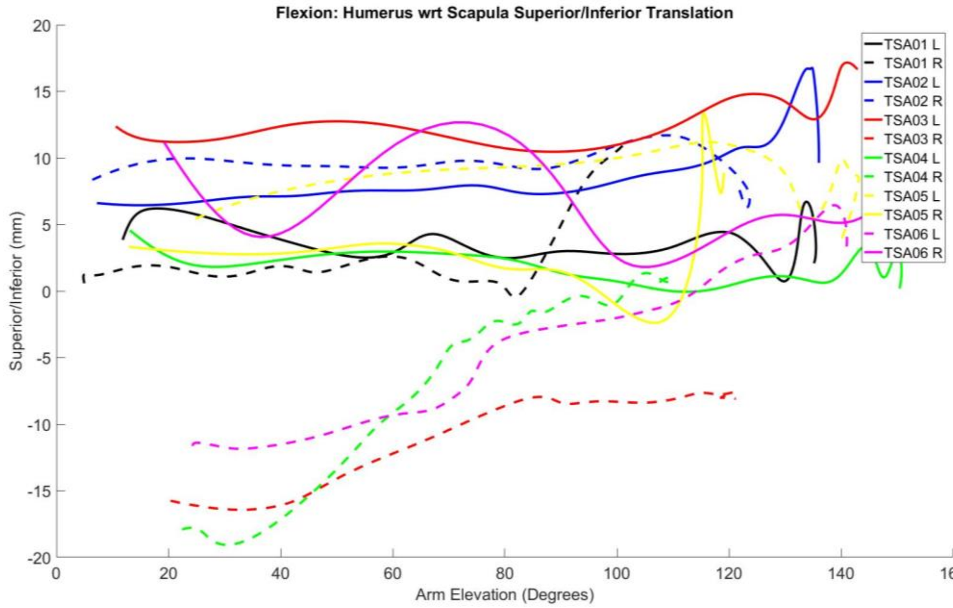

Figure C. 25 Flexion Superior / Inferior Translation

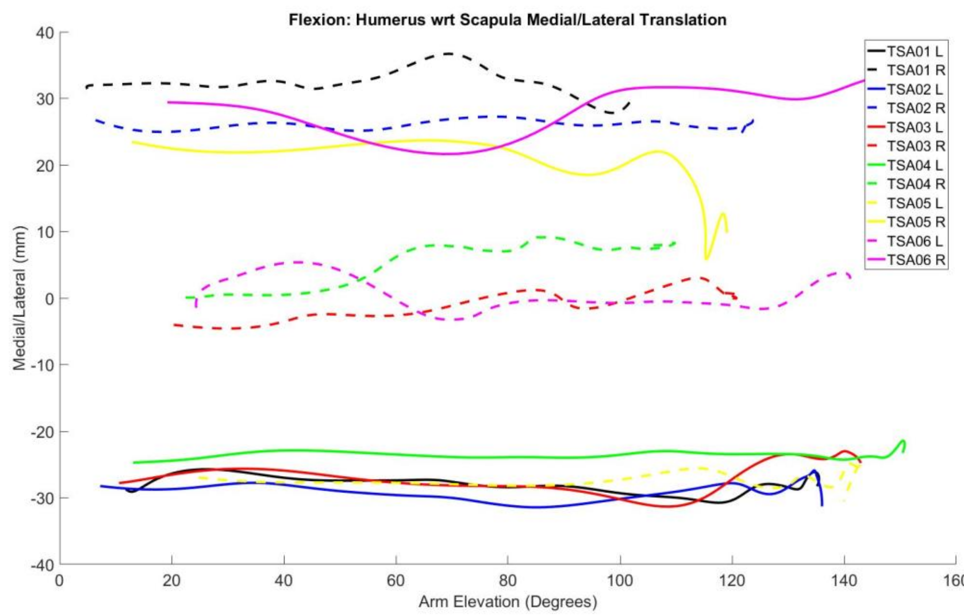

Figure C. 26 Flexion Medial / Lateral Translation

Appendix D: Shoulder Kinematics Matlab Script

(Matlab, Simulink software Natick, MA, USA)

```
% Shoulder Tracking Kinematics for Processing Full TSA Subjects

% Written by Sarah Walden 2018-2019

clear; clc
close all

% Initialize

SUBJ = 'TSA01'

RL = 'L';

%Vicon's global coordinate system (Y axis is gravity vector)
   % 1st method for calculating scapula kinematics (very rudimentary)
   gravityVector=[1        0        0        0
   0      0.013924687      -0.022215014      0.99933147
   0      0.936702564      0.34637455        -0.005321098
   0      -0.346143853     0.936694177       0.02545421]*[1 0 0 0;0 -1 0 0;0 0 1 0;0 0 0 1];

% Associated trial , data ranges, and thorax coordinate systems(globe)
   % 2nd method (thorax CS)for calculating scapula kinematics
      % There is a thorax CS for each subject and each shoulder
% Also includes the origin of the glenoid CS, "glenoidMP"
%TSA01
if SUBJ == 'TSA01'
   if RL == 'R'
      TRIALS = ['05';'09';'07';'08'];
      DataRanges = [[10 130];[9 178];[5 144];[1 124]];
      globe=[1     0        0        0
      127.7340426        0.034377854     -0.196865231     0.979496317
      -214.3692321       -0.926084015    -0.371495293     -0.042130522
```

```
    -137.2376964	0.372297268	-0.906134551	-0.19538266];
  elseif RL == 'L'
    TRIALS = ['12';'13';'14';'15'];
    DataRanges = [[10 162];[15 187];[6 125];[4 176]];
    globe=[1	0	0	0
    -145.5595388	0.133754225	-0.075262656	0.987823937
    -220.6179076	-0.963717374	-0.236664667	0.112489978
    -125.9293768	0.225339328	-0.967562512	-0.104424314];
  end

%TSA02
elseif SUBJ == 'TSA02'
  if RL == 'R'
    TRIALS = ['04';'05';'06';'07'];
    DataRanges = [[9 108];[9 133];[9 109];[12 121]];
    globe=[1	0	0	0
    147.70705	-0.089432971	0.068393792	0.993641803
    -236.489722	-0.960424026	-0.270152377	-0.067848222
    -103.4257876	0.263794298	-0.96038533	0.089847571];
  elseif RL == 'L'
    TRIALS = ['13';'14';'15';'16'];
    DataRanges = [[14 137];[7 154];[8 148];[8 138]];
    globe=[1	0	0	0
    -142.7925725	0.150257624	0.068393792	0.986278325
    -245.9797946	-0.9488695	-0.270152377	0.163292265
    -112.1174764	0.277613612	-0.96038533	0.024304329];
  end

%TSA03
elseif SUBJ == 'TSA03'
  if RL == 'R'
    TRIALS = ['05';'06';'07';'08'];
    DataRanges = [[1 124];[1 119];[1 118];[1 160]];
    globe=[1	0	0	0
    111.9345117	-0.078020806	-0.283957091	0.955657431
```

```
        -193.1508566         -0.924173226     -0.338928473     -0.176157144
        -126.067872 0.373920584      -0.896936932     -0.235982067];
    elseif RL == 'L'
        TRIALS = ['14';'15';'16';'17'];
        DataRanges = [[2 127];[6 128];[1 88];[1 90]];
        globe=[1     0          0          0
        -144.2762936         0.08918969       -0.283957091     0.954679826
        -190.2038585         -0.94072337      -0.338928473     -0.012924037
        -137.1820677         0.327238048      -0.896936932     -0.297353997];
    end

%TSA04
elseif SUBJ == 'TSA04'
    if RL == 'R'
        TRIALS = ['04';'05';'06';'08'];
        DataRanges = [[16 150];[16 222];[12 168];[9 200]];
        globe=[1     0          0          0
        131.9132767          -0.146024112     -0.081100798     0.985951124
        -201.7267312         -0.987975604     -0.039227586     -0.149550668
        -144.694576 0.050805161      -0.995933661     -0.074397436];
    elseif RL == 'L'
        TRIALS = ['14';'15';'16';'17'];
        DataRanges = [[9 125];[18 176];[10 197];[10 175]];
        globe=[1     0          0          0
        -110.2845245         0.140182873      -0.059492976     0.988336657
        -219.1509751         -0.989465367     -0.04486516      0.137642305
        -148.650079 0.036153133      -0.997219987     -0.065155566];
    end

%TSA05
elseif SUBJ == 'TSA05'
    if RL == 'R'
        TRIALS = ['04';'05';'06';'08'];
        DataRanges = [[15 137];[21 143];[9 167];[27 114]];
        globe=[1     0          0          0
```

```
        180.6942799     -0.092484984    0.039881562     0.994915066
        -250.0497289    -0.995324731    -0.031642831    -0.091254651
        -165.5864395    0.027842551     -0.998703255    0.042621592];
    elseif RL == 'L'
        TRIALS = ['13';'14';'15';'17'];
        DataRanges = [[18 150];[11 123];[11 145];[9 127]];
        globe=[1    0       0       0
        -152.9366931    -0.064098964    0.023043639     0.99767746
        -280.8447971    -0.996956614    0.042972457     -0.065045198
        -166.8736665    -0.04437153     -0.998810471    0.020219019];
    end

%TSA06
elseif SUBJ == 'TSA06'
    if RL == 'R'
        TRIALS = ['04';'05';'06';'07'];
        DataRanges = [[1 84];[1 88];[1 113];[1 121]];
        globe=[1    0       0       0
        153.6818748     0.00153028      0.057703372     0.9983326
        -185.7286486    -0.965547112    -0.259705262    0.016490924
        -163.6155834    0.260223812     -0.963962394    0.055317903];
    elseif RL == 'L'
        TRIALS = ['10';'14';'12';'13'];
        DataRanges = [[1 107];[1 156];[1 108];[1 145]];
        globe=[1    0       0       0
        -163.6261958    -0.099954897    -0.041000539    0.994146858
        -198.1076722    -0.974523879    -0.197584124    -0.106130688
        -160.1648506    0.200779052     -0.979428134    -0.020206503];
    end
end


% Loop through trials for selected subject
for n=1:2%length(TRIALS)
```

```
    clear HS S H kinhs kins kinh scap_raw hum_raw kinhs_f kins_f kinh_f prevRow row

TRIAL = TRIALS(n,:);

subjpath = ['R:\Research Common\HDL\Projects\HSSR\Data\Shoulder TSA\',SUBJ,'\'];

%LOAD motion tracking files
% Scapula
 scap_track=dlmread([subjpath 'Autoscoper\Tracking\',SUBJ,'_',TRIAL,'_',RL,'_Scapula_Interpolate.tra']);
    % Replace the tracking file upload with the below line to switch to glenoid CS tracking for translations
%scap_track=dlmread([subjpath 'Autoscoper\Tracking\',SUBJ,'_',TRIAL,'_',RL,'_Scapula_Glenoid.tra']);
% Humerus
hum_track=dlmread([subjpath 'Autoscoper\Tracking\',SUBJ,'_',TRIAL,'_',RL,'_Humerus_Interpolate.tra']);

%Specify what range for tracking data
DataRange = DataRanges(n,:);

METHOD = 1;

% Transform original STL into Autoscoper space

% Slicing into a Tiff stack changes the origin of the coordinate system, which must be corrected

%Read in the transformed STL from completing the Shoulder Preprocess code
disp('Reading scapula...')
scapscan = stlread([subjpath 'Local Coord System STLs\',RL,'\transf_',SUBJ,'_scap.stl']);
    % Replace the STL file upload with the below line to switch to glenoid CS tracking for translations
%scapscan = stlread([subjpath 'Local Coord System STLs\',RL,'\transf_',SUBJ,'_scap_glenoidBinary.stl']);
disp('Reading humerus...')
humscan = stlread([subjpath 'Local Coord System STLs\',RL,'\transf_',SUBJ,'_hum.stl']);

scapscan = reducepatch(scapscan,0.5);

humscan = reducepatch(humscan,0.5);

sn(:,2:4) = scapscan.vertices; sn(:,1) = 1;
```

```
hn(:,2:4) = humscan.vertices; hn(:,1) = 1;

    %Some coordinate assignment fixes, SPECIFIC to the TSA study
      %NOTE: these throw off translation calculations - comment out if you are calculating translations
      if SUBJ == 'TSA01'
        if RL == 'R'
          hn(:,2:4) = hn(:,2:4)*[cos(pi/2) 0 sin(pi/2);0 1 0;-sin(pi/2) 0 cos(pi/2)]; % Rotate 90 deg to fix
axes switch
        end
      end
      if SUBJ == 'TSA03'
        if RL == 'R'
          hn(:,2:4) = hn(:,2:4)*[cos(pi/2) 0 sin(pi/2);0 1 0;-sin(pi/2) 0 cos(pi/2)]; % Rotate 90 deg to fix
axes switch
        end
  %       if RL == 'L'
  %         hn(:,2:4) = hn(:,2:4)*[cos(-0.70) 0 sin(-0.70);0 1 0;-sin(-0.70) 0 cos(-0.70)]; % Rotate -40
deg to fix misalignment
  %       end
      end
      if SUBJ == 'TSA04'
        if RL == 'L'
          hn(:,2:4) = hn(:,2:4)*[cos(-pi/2) 0 sin(-pi/2);0 1 0;-sin(-pi/2) 0 cos(-pi/2)]; % Rotate -90 deg to
fix axes switch
          hn(:,2:4) = hn(:,2:4)*[cos(0.44) 0 sin(0.44);0 1 0;-sin(0.44) 0 cos(0.44)]; % Rotate 25 deg to
fix misalignment
        end
        if RL == 'R'
          hn(:,2:4) = hn(:,2:4)*[cos(pi/2) 0 sin(pi/2);0 1 0;-sin(pi/2) 0 cos(pi/2)]; % Rotate 90 deg to fix
axes switch
        end
      end
      if SUBJ == 'TSA05' & RL == 'L'
          hn(:,2:4) = hn(:,2:4)*[cos(-pi/2) 0 sin(-pi/2);0 1 0;-sin(-pi/2) 0 cos(-pi/2)]; % Rotate -90 deg to
fix axes switch
```

```
        hn(:,2:4) = hn(:,2:4)*[cos(0.61) 0 sin(0.61);0 1 0;-sin(0.61) 0 cos(0.61)]; % Rotate 35 deg to
fix misalignment
    end
    if SUBJ == 'TSA06' & RL == 'L'
        hn(:,2:4) = hn(:,2:4)*[cos(-pi/2) 0 sin(-pi/2);0 1 0;-sin(-pi/2) 0 cos(-pi/2)]; % Rotate -90 deg to
fix axes switch
        hn(:,2:4) = hn(:,2:4)*[cos(0.79) 0 sin(0.79);0 1 0;-sin(0.79) 0 cos(0.79)]; % Rotate 45 deg to
fix misalignment
    end



S=[1 0 0 0;0 1 0 0;0 0 1 0;0 0 0 1]; % NEW Scapula

H=[1 0 0 0;0 1 0 0;0 0 1 0;0 0 0 1]; %NEW humerus

snT = (inv(S)*sn')'; % Transform Scapula into local CS
hnT = (inv(H)*hn')'; % Transform Humerus into local CS

stifforigin = [min(snT(:,2)) min(-snT(:,3)) min(snT(:,4))]; %
htifforigin = [min(hnT(:,2)) min(-hnT(:,3)) min(hnT(:,4))]; %

%origin of the two tiff stack bones as x y z coordinates
  % These origins were incorrectly assigned in tiff stack generation
  % They must be 'subtracted out' from tracking files

stifforigin = [min(snT(:,2)) min(-snT(:,3)) min(snT(:,4))]; %
htifforigin = [min(hnT(:,2)) min(-hnT(:,3)) min(hnT(:,4))]; %

  % Not used in this code - can be used to flip along Z axis
  scaptiff = [1 0 0 0;-stifforigin(1,1) 1 0 0;-stifforigin(1,2) 0 1 0;-stifforigin(1,3) 0 0 1];
  humtiff = [1 0 0 0;-htifforigin(1,1) 1 0 0;-htifforigin(1,2) 0 1 0;-htifforigin(1,3) 0 0 1];
%format the origin of the two bones as a 4x4 matrix
sTtiff = [1 0 0 0;-stifforigin(1,1) 1 0 0;-stifforigin(1,2) 0 -1 0;-stifforigin(1,3) 0 0 1];
hTtiff = [1 0 0 0;-htifforigin(1,1) 1 0 0;-htifforigin(1,2) 0 -1 0;-htifforigin(1,3) 0 0 1];
```

```
% Calculate Humeral/Scapula Kinematics

% Autoscoper flips the z-axis of the TIFF stack
ZFlip = [1 0 0 0;0 1 0 0;0 0 1 0;0 0 0 -1];


scap_track_filt = scap_track;
hum_track_filt = hum_track;


% % % Get scap and hum transformations at each frame
for i=DataRange(1):DataRange(2)
   % Convert tracking data to 4x4 transforms
	scapTcube=[1 0 0 0;scap_track_filt(i,13:15)' scap_track_filt(i,1:3)' scap_track_filt(i,5:7)'
scap_track_filt(i,9:11)'];
	humTcube=[1 0 0 0;hum_track_filt(i,13:15)' hum_track_filt(i,1:3)' hum_track_filt(i,5:7)'
hum_track_filt(i,9:11)'];


		% Some coordinate assignment fixes, SPECIFIC to the TSA study
		    %NOTE: these throw off translation calculations - comment out if you are calculating
translations
		if SUBJ == 'TSA01'
		    if RL == 'R'
		     humTcube=humTcube*[1 0 0 0;0 cos(-pi/2) 0 sin(-pi/2);0 0 1 0;0 -sin(-pi/2) 0 cos(-pi/2)];
% Rotate -90 deg
		    end
		end
		 clear tempx
		 if SUBJ == 'TSA03'
		    if RL == 'R'
		       humTcube=humTcube*[1 0 0 0;0 cos(-pi/2) 0 sin(-pi/2);0 0 1 0;0 -sin(-pi/2) 0 cos(-
pi/2)]; % Rotate -90 deg
		    end
%		      if RL == 'L'
%		         humTcube=humTcube*[1 0 0 0;0 cos(0.70) 0 sin(0.70);0 0 1 0;0 -sin(0.70) 0
cos(0.70)]; % Rotate 40 deg to fix misalignment
%		      end
```

```
                end
                if SUBJ == 'TSA04'
                  if RL == 'L'
                    humTcube=humTcube*[1 0 0 0;0 cos(pi/2) 0 sin(pi/2);0 0 1 0;0 -sin(pi/2) 0 cos(pi/2)];
% Rotate +90 deg
                    humTcube=humTcube*[1 0 0 0;0 cos(-0.44) 0 sin(-0.44);0 0 1 0;0 -sin(-0.44) 0 cos(-
0.44)]; % Rotate -25 deg to fix misalignment
                  end
                  if RL == 'R'
                    humTcube=humTcube*[1 0 0 0;0 cos(-pi/2) 0 sin(-pi/2);0 0 1 0;0 -sin(-pi/2) 0 cos(-
pi/2)]; % Rotate -90 deg
                  end
                end
                if SUBJ == 'TSA05' & RL == 'L'
                   humTcube=humTcube*[1 0 0 0;0 cos(pi/2) 0 sin(pi/2);0 0 1 0;0 -sin(pi/2) 0 cos(pi/2)]; %
Rotate +90 deg
                   humTcube=humTcube*[1 0 0 0;0 cos(-0.61) 0 sin(-0.61);0 0 1 0;0 -sin(-0.61) 0 cos(-
0.61)]; % Rotate -35 deg to fix misalignment
                end
                if SUBJ == 'TSA06' & RL == 'L'
                   humTcube=humTcube*[1 0 0 0;0 cos(pi/2) 0 sin(pi/2);0 0 1 0;0 -sin(pi/2) 0 cos(pi/2)]; %
Rotate +90 deg
                   humTcube=humTcube*[1 0 0 0;0 cos(-0.79) 0 sin(-0.79);0 0 1 0;0 -sin(-0.79) 0 cos(-
0.79)]; % Rotate -45 deg to fix misalignment
                end

        scap_raw(:,:,i-[DataRange(1)-1])=scapTcube;
        hum_raw(:,:,i-[DataRange(1)-1])=humTcube;
end

% 3rd Method for calculating scapual kinematics: save neutral scap pose from abduction trial
  % Set the coordinate system origin to the thorax origin
  % Choose which 'neutral' pose you want to caluclate with respect to
  if n == 1
    neutralScap = scap_raw(:,:,1);
```

```
      neutralScap(:,1) = globe(:,1);
    end
    if n == 3
      neutralScap = scap_raw(:,:,1);
      neutralScap(:,1) = globe(:,1);
    end
    if n == 4
      neutralScap = scap_raw(:,:,1);
      neutralScap(:,1) = globe(:,1);
    end

% Loop through kinematics calculations

row=1; prevRow=1;
for i=1:size(hum_raw,3)
    if METHOD == 1
        % Humerus with respect to Scapula Kinematics
        HS(:,:,row)= (inv(sTtiff)*ZFlip*inv(scap_raw(:,:,i))*hum_raw(:,:,i)*ZFlip*hTtiff);

        % Scapula with respect to Thorax (Neutral Scapula) Kinematics
        S(:,:,row)= (inv(neutralScap)*scap_raw(:,:,i)*ZFlip*sTtiff);

        % Humerus with respect to Thorax (Neutral Scapula) Kinematics
        H(:,:,row)= (inv(neutralScap)*hum_raw(:,:,i)*ZFlip*hTtiff);
    end

% A note on tangent sign flips: qualitatively decide which side of the flip is 'best'
    % 1) Use either this method which is more automatic but only corrects flips looking ahead in the motion
        %                   %if kinhs(row,2)>0 %To flip sign when goes past 90 degrees
                        %  %Note: the boundary # above will change based on whether flips from + to - or -to +)
                        %kinhs(row,2)=kinhs(row,2)-pi;
                        %end
    % 2) Or use this method to manually + pi or - pi for values under or over a decided value:
                        %if abs((kins(row,2)-kins(prevRow,2))) > 1
                        %kins(row,2)=kins(row,2)+pi;
                        %end
```

```
% YXY Humerus wrt Scapula Kinematics:
   kinhs(row,1)=acos(HS(3,3,row)); % Rotation Angle 2 - X
   kinhs(row,2)=atan(HS(3,2,row)/-HS(3,4,row)); % Rotation Angle 1 - Y
%                 if kinhs(row,2)>0 %To flip sign when goes past 90 degrees
%                    %Note: the boundary # above will change based on whether flips from + to - or -to +)
%                 kinhs(row,2)=kinhs(row,2)-pi;
%                 end
   kinhs(row,3)=atan(HS(2,3,row)/HS(4,3,row)); % Rotation Angle 3 - Y
%                 if kinhs(row,3)> 0 %To flip sign when goes past 90 degrees
%                    %Note: the boundary # above will change based on whether flips from + to - or -to +)
%                 kinhs(row,3)=kinhs(row,3)-pi;
%                 end
   kinhs(row,4)=HS(2,1,row);% - glenoidMP(1); % AP translation
   kinhs(row,5)=HS(3,1,row);% - glenoidMP(2); % SI translation
   kinhs(row,6)=HS(4,1,row);% - glenoidMP(3); % ML translation

% YZX Humerus wrt Scapula Kinematics for IE Rotations:
   % The Euler sequence best for I/E motions; uncomment when necessary.
%    kinhs(row,1)=asin(-HS(2,3,row)); % Rotation Angle 2 - Z
%    kinhs(row,2)=atan(HS(2,4,row)/HS(2,2,row)); % Rotation Angle 1 - Y
%    kinhs(row,3)=atan(HS(4,3,row)/HS(3,3,row)); % Rotation Angle 3 - X


% YXZ Scapula wrt Thorax (Neutral Scapula) Kinematics:
   kins(row,1)=asin(S(4,3,row)); % Rotation Angle 2 - X
   kins(row,2)=atan(-S(4,2,row)/S(4,4,row)); % Rotation Angle 1 - Y
              %To flip sign when goes past 90 degrees
%                 if abs((kins(row,2)-kins(prevRow,2))) > 1
%                 kins(row,2)=kins(row,2)+pi;
%                 end
   kins(row,3)=atan(-S(2,3,row)/S(3,3,row)); % Rotation Angle 3 - Z
              %To flip sign when goes past 90 degrees
%                 if abs((kins(row,3)-kins(prevRow,3))) > 1
%                 kins(row,3)=kins(row,3)+pi;
```

```
%                    end

   %Arm Elevation = humerus elevation w/ respect to scap + scap elevation (upward rotation w/ respect to
gravitational vector)
   if RL == 'L' % left shoulder scapula elevation needs to be flipped to match right shoulder
      kinhs(row,7)= kinhs(row,1) + kins(row,1).*-1;
   elseif RL == 'R'
      kinhs(row,7)= kinhs(row,1) + kins(row,1);
   end


   % YXY Humerus wrt Thorax (Neutral Scapula) Kinematics:
   kinh(row,1)=acos(H(3,3,row)); % Rotation Angle 2 - X
   kinh(row,2)=atan(H(3,2,row)/-H(3,4,row)); % Rotation Angle 1 - Y
%                    %To flip sign when goes past 90 degrees
%                    if abs((kinh(row,2)-kinh(prevRow,2))) > 1
%                    kinh(row,2)=kinh(row,2)+pi;
%                    end
%                    if kinh(row,2)<-0.8 %To flip sign when goes past 90 degrees
%                       %Note: the boundary # above will change based on whether flips from + to - or -to +)
%                    kinh(row,2)=kinh(row,2)+pi;
%                    end
   kinh(row,3)=atan(H(2,3,row)/H(4,3,row)); % Rotation Angle 3 - Y
                  %To flip sign when goes past 90 degrees
%                    if abs((kinh(row,3)-kinh(prevRow,3))) > 1
%                    kinh(row,3)=kinh(row,3)+pi;
%                    end
%                    if kinh(row,3)<0 %To flip sign when goes past 90 degrees
%                       %Note: the boundary # above will change based on whether flips from + to - or -to +)
%                    kinh(row,3)=kinh(row,3)+pi;
%                    end


 % Iterate
   prevRow=row;
```

```
    row=row+1;
end



% % %  Account for left shoulder
    %Whichever rotations switch ML direction from R to L
if RL=='L'
        kins(:,3)=kins(:,3)*-1;
end

% % %  Convert to decimal from radian
kinhs(:,1:3)=kinhs(:,1:3)*180/pi;
kinhs(:,7)=kinhs(:,7)*180/pi;
kins(:,1:3)=kins(:,1:3)*180/pi;
kinh(:,1:3)=kinh(:,1:3)*180/pi;

% Filter:
        [B3,A3] = butter(2, 4/50,'low');

        kinhs_f = filtfilt(B3,A3,kinhs);
        kins_f = filtfilt(B3,A3,kins);
        kinh_f = filtfilt(B3,A3,kinh);

  % One method of saving:
% kinhs_f_save{n} = kinhs_f;
% kins_f_save{n} = kins_f;
% kinh_f_save{n} = kinh_f;

  % Preferred method of exporting to Excel files:
  % Uncomment as necessary

% % % SAVE KINEMATICS (ROTATIONS) TO CSV FILE
% saveFile = [SUBJ,'_',RL,'_Kinematics.xlsx'];
% xlswrite(saveFile,{'H Arm Elev','H Plane of Elev','H I/E','S Elevation','S I/E','S Up/Down Rot','HS Arm Elev','HS Plane of Elev','HS I/E'},TRIAL,'A1');
```

```
% xlswrite(saveFile,[kinh_f(:,1:3),kins_f(:,1:3),kinhs_f(:,1:3)],TRIAL,'A2');

% % % SAVE KINEMATICS (IE ROTATIONS) TO CSV FILE
% saveFile = [SUBJ,'_',RL,'_Kinematics.xlsx'];
% xlswrite(saveFile,{'HS Z Rot','HS Y Rot','HS X Rot'},TRIAL,'A1');
% xlswrite(saveFile,[kinhs_f(:,1:3)],TRIAL,'A2');


% % % SAVE ARM ELEVATION (X AXIS DATA)
% saveFile = [SUBJ,'_',RL,'_ArmElevation.xlsx'];
% xlswrite(saveFile,{'Arm Elevation = HS Elevation + S Elevation'},TRIAL,'A1');
% xlswrite(saveFile,[kinhs_f(:,7)],TRIAL,'A2');

% % % SAVE TRANSLATIONS TO CSV FILE
% saveFile = [SUBJ,'_',RL,'_Translations.xlsx'];
% xlswrite(saveFile,{'HS AP','HS SI','HS ML'},TRIAL,'A1');
% xlswrite(saveFile,[kinhs_f(:,4:6)],TRIAL,'A2');

%Plot kinematics; choose whether or not to plot wrt Arm Elevation
  % For abduction and flexion this makes sense, for I/E it does not

% % PLOT KINEMATICS - YXY Humerus wrt Scapula
        titles = {'HS Rotation 2, X','HS Rotation 1, Y','HS Rotation 3, Y','HS AP','HS SI','HS ML'};
        %titles = {'HS Rotation 2, Z','HS Rotation 1, Y','HS Rotation 3, X','HS AP','HS SI','HS ML'};
        ylabels = {'X Rotation','Y Rotation','Y Rotation','Anterior(+)/Posterior(-)','Superior(+)/Inferior(-
)','Medial(-)/Lateral(+)'};
        %ylabels = {'Z Rotation','Y Rotation','X Rotation','Anterior(+)/Posterior(-)','Superior(+)/Inferior(-
)','Medial(-)/Lateral(+)'};
        xlabels = {'Arm Elevation (deg)','Arm Elevation (deg)','Arm Elevation (deg)','Arm Elevation
(deg)','Arm Elevation (deg)','Arm Elevation (deg)'};

%         for i=4:6 % 1:3 to plot rotations; 4:6 to plot translations
%           figure; hold on; set(gca,'FontSize',14);
%           title(titles{i},'FontSize',14);
%           plot(kinhs_f(:,i),'Color',[0.7 0 0],'LineWidth',3);
```

```
%                %plot(kinhs_f(:,7),kinhs_f(:,i),'Color',[0.7 0 0],'LineWidth',3);
%                ylabel(ylabels{i},'FontSize',14);
%                %xlabel(xlabels{i},'FontSize',14);
%                legend(TRIAL)
%                save = [SUBJ,'_',TRIAL,'_',titles{i},'.jpg'];
%                saveas(gcf,save)
%              end

% PLOT KINEMATICS - YXZ Scapula wrt Thorax
%              titles = {'S Rotation 2, X','S Rotation 1, Y','S Rotation 3, Z','S ML','S AP','S SI'};
%              ylabels = {'X Rotation','Y Rotation','Z Rotation','Medial(-)/Lateral(+)','Anterior(+)/Posterior(-
)','Superior(+)/Inferior(-)'};
%
%              for i=1:3
%                figure; hold on; set(gca,'FontSize',14);
%                title(titles{i},'FontSize',14);
%                plot(kins_f(:,i),'Color',[0.7 0 0],'LineWidth',3);
%                %plot(kinhs_f(:,7),kins_f(:,i),'Color',[0.7 0 0],'LineWidth',3);
%                ylabel(ylabels{i},'FontSize',14);
%                %xlabel(xlabels{i},'FontSize',14);
%                legend(TRIAL)
%                save = [SUBJ,'_',TRIAL,'_',titles{i},'.jpg'];
%                saveas(gcf,save)
%              end


% PLOT KINEMATICS - YXY Humerus wrt Thorax
%              titles = {'H Rotation 2, X','H Rotation 1, Y','H Rotation 3, Y','H ML','H AP','H SI'};
%              ylabels = {'X Rotation','Y Rotation','Y Rotation','Medial(-)/Lateral(+)','Anterior(+)/Posterior(-
)','Superior(+)/Inferior(-)'};
%
%              for i=1:3
%                figure; hold on; set(gca,'FontSize',14);
%                title(titles{i},'FontSize',14);
%                %plot(kinh_f(:,i),'Color',[0.7 0 0],'LineWidth',3);
```

```
%               plot(kinhs_f(:,7),kinh_f(:,i),'Color',[0.7 0 0],'LineWidth',3);
%               ylabel(ylabels{i},'FontSize',14);
%               xlabel(xlabels{i},'FontSize',14);
%               legend(TRIAL)
%               save = [SUBJ,'_',TRIAL,'_',titles{i},'.jpg'];
%               saveas(gcf,save)
%             end
%

end
```

Published with MATLAB® R2016a